Title
SOME EXPERIMENTS IN LOW-TEMPERATURE THERMOMETRY

Author
Fogle, W.E.

Publication Date
1982-11-01

LBL-14399

Lawrence Berkeley Laboratory
UNIVERSITY OF CALIFORNIA

Materials & Molecular Research Division

SOME EXPERIMENTS IN LOW-TEMPERATURE THERMOMETRY

William E. Fogle
(Ph.D. thesis)

November 1982

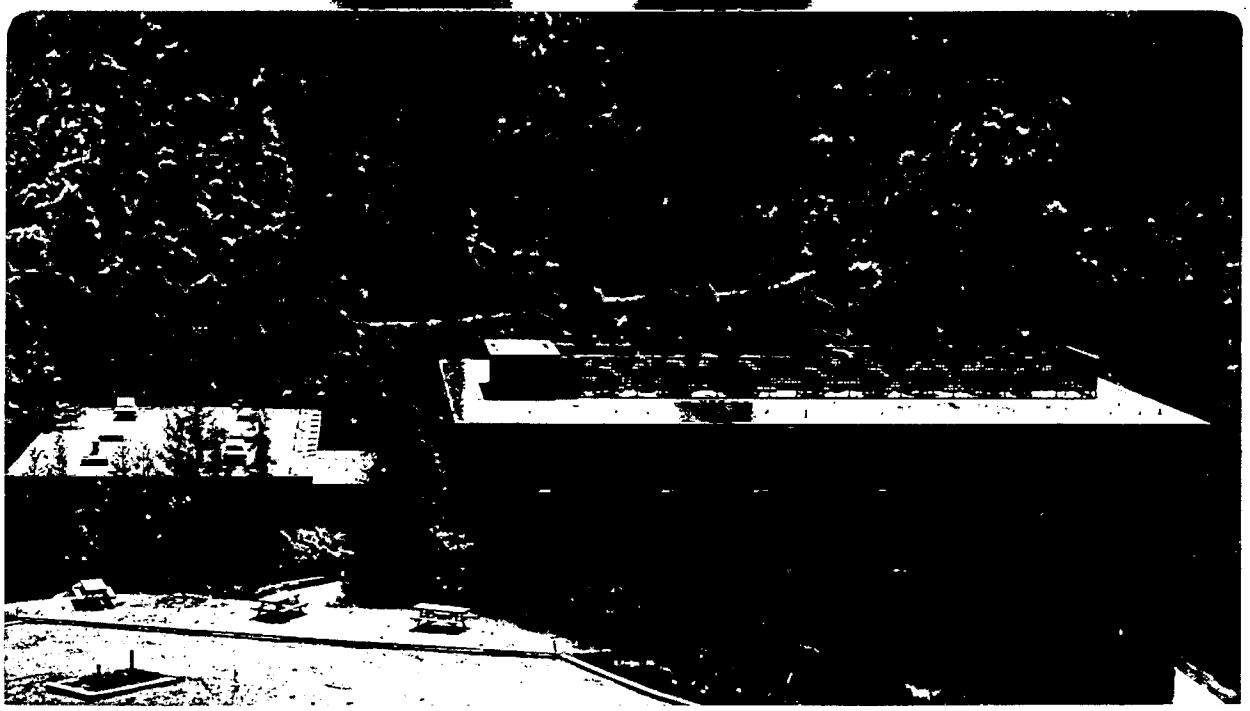

Prepared for the U.S. Department of Energy under Contract DE-AC03-76SF00098

DISCLAIMER

LBL-14399

SOME EXPERIMENTS IN LOW-TEMPERATURE THERMOMETRY

William E. Fogle

(Ph.D. Thesis)

Lawrence Berkeley Laboratory

University of California

Berkeley, California 94720

This work was supported by the Director, Office of Energy Research, Office of Basic Energy Sciences, Materials and Molecular Research Division of the U. S. Department of Energy under Contract No. DE-AC03-76SF00098.

CONTENTS

SOME EXPERIMENTS IN LOW-TEMPERATURE THERMOMETRY

William E. Fogle
(Ph.D. Thesis)

Materials and Molecular Research Division
Lawrence Berkeley Laboratory and Department of Chemistry
University of California
Berkeley, California

ABSTRACT

A powdered cerous magnesium nitrate (CMN) temperature scale has been developed in the 0.016-3.8 K region which represents an interpolation between the $^3He/^4He$ (T_{62}/T_{58}) vapor pressure scale and absolute temperatures in the millikelvin region as determined with a ^{60}Co in hcp Co nuclear orientation thermometer (NOT). Both ac and dc susceptibility thermometers were used in these experiments. The ac susceptibility of a 13 mg CMN-oil slurry was measured with a mutual inductance bridge employing a SQUID null detector while the dc susceptibility of a 3 mg slurry was measured with a SQUID/flux transformer combination. To check the internal consistency of the NOT, γ-ray intensities were measured both parallel and perpendicular to the Co crystal c-axis. The independent temperatures determined in this fashion were found to agree to within experimental error. For the CMN thermometers employed in these experiments, the susceptibility was found to obey a Curie-Weiss law with a Weiss constant of $\Delta = 1.05 \pm 0.1$ mK. The powdered CMN scale in the 0.05-1.0 K region was transferred to two germanium resistance thermometers for use in

low-temperature specific heat measurements. The integrity of the scale was checked by examining the temperature dependence of the specific heat of high purity copper in the 0.1-1 K region. In more recent experiments in this laboratory, the scale was also checked by a comparison with the National Bureau of Standards cryogenic temperature scale (NBS-CTS-1). The agreement between the two scales in the 99-206 mK region was found to be on the order of the stated accuracy of the NBS scale.

1. INTRODUCTION

The two objectives of this work are to improve significantly the existing laboratory temperature scale for use with germanium resistance thermometers (GRT) in the 0.05–1.0 K region and to initiate efforts to establish a laboratory temperature scale for $T < 0.05$ K. This work was motivated by the fact that in a number of cases the interpretation of low-temperature specific heat data is limited by the accuracy of the temperature scale on which the measurements are made. Several examples of interest in the $T > 50$ mK region are the comparison of calorimetrically determined 0-K Debye temperatures, θ_0, with values derived from elastic constants measurements, the measurement of entropies of magnetization of magnetic substances, and the identification of various predicted anomalies in the electronic specific heat of metals associated with charge-density waves, electron-phonon interactions, and spin fluctuations. To elaborate on the charge-density-wave example, the identification of a "phason" anomaly in the specific heat of an alkali metal would constitute perhaps the best experimental evidence of a charge-density-wave ground state in these metals. Although such an anomaly has been reported, it may equally well be explained on the basis of temperature scale errors.[1] The answer to the question of the existence of phason anomalies in alkali metals will require additional measurements for $T > 50$ mK on a temperature scale that is more accurate than those used in previous measurements. In the $T < 50$ mK region, a topic of current interest concerns the magnitude and temperature dependence of the specific heat of the normal phase of liquid ^{3}He. Various measurements to date differ in magnitude by as much as

40 percent for $5 < T < 10$ mK and, in addition, exhibit different temperature dependences in the low-temperature limit.[2] As a result, the degree to which the Landau theory of normal Fermi liquids accurately describes the properties of liquid ^{3}He at low temperatures remains uncertain. A definative resolution of this question will certainly require an accurate temperature scale in the millikelvin region.

The existing temperature scale in this laboratory, and indeed in many laboratories for temperatures below 1 K, relies upon the extrapolation of the ^{3}He and ^{4}He vapor pressure scales from the 1-4 K range to lower temperatures via a suitable magnetic thermometer. Several excellent discussions on magnetic thermometry are available in the literature.[3,4] "Ideal" magnetic thermometers, in which there are no interactions between magnetic ions and which have only one crystal field multiplet, are useful for extrapolation purposes as they come close to being primary thermometers and have increasing sensitivities at lower temperatures (since they follow a Curie law $\chi = C/T$ where χ is the magnetic susceptibility, T is the absolute temperature and C is the Curie constant which may, in principle, be calculated). To the next higher order of approximation, one must use the Curie-Weiss susceptibility relation $\chi = C/(T-\Delta)$ where Δ, which must be determined experimentally at low temperatures, is a parameter which accounts for the interactions between the magnetic ions and the shape of the thermometric material.[5] Thus, the magnetic thermometer is degraded to the status of an extremely useful secondary thermometer. The usual arrangement for this type of calibration consists of measuring the magnetic susceptibility of the paramagnetic salt cerous

magnesium nitrate (CMN) with a mutual inductance bridge technique. The bridge is calibrated in the 1-4 K range using a Curie law and an extrapolation to lower temperatures is used to define magnetic temperatures via the relation $T^* = C/\chi$. The GRT being calibrated (and assumed to be in equilibrium with the CMN) is monitored simultaneously and a R vs T^* relation is established for each resistance thermometer.

There are several practical difficulties with this procedure. If, for example, there is a temperature gradient between the CMN and the thermometer being calibrated, it may well go undetected and an erroneous calibration will result. A detailed example of this difficulty will be presented in this thesis. Another problem concerns the possibility of dehydrating CMN powder and thus affecting the temperature dependence of the susceptibility. Butterworth et al.[6] have observed that 16 of the 24 waters of hydration of the salt may be removed by substantial pumping resulting in a twofold increase in the Curie constant for $1.4\ K < T < 4.2\ K$. More ominous is the observation by Graebner[7] that partial dehydration of the CMN results in substantial deviations from a Curie law for $T < 0.2\ K$. Finally, the question of the relation between T and T^* must be addressed. This relation has been investigated for single crystal CMN[8] by fundamental thermodynamic measurements. However, for most low-temperature experiments where the CMN must be in equilibrium with other materials, the CMN is used in powdered form along with a suitable thermal contact agent (such as ^3He or oil). There is, at present, considerable experimental evidence that the T, T^* relationship for powdered CMN varies by

a significant amount from one thermometer to another. Specifically, Wheatley[9] has examined many properties of normal liquid ^{3}He to ~2 mK in considerable detail and has found the ^{3}He to behave as an ideal normal Fermi liquid if his powdered CMN thermometer's susceptibility obeys the $\chi = C/(T-\Delta)$ relationship with $0.0\ \text{mK} < \Delta < 0.5\ \text{mK}$. The value of Δ varied from run to run by several tenths of a millikelvin as might be expected since Δ depends upon salt geometry, packing fraction, etc. In later work by Webb et al.,[10] a direct comparison of a powdered CMN thermometer and a Johnson noise thermometer was made. For 0.01–4.2 K, the CMN susceptibility followed a Curie-Weiss law with $\Delta = 0.0 \pm 0.12$ mK while for T < 5 mK, evidence was presented that Δ became temperature dependent. In two recent experiments at the National Bureau of Standards (NBS), Soulen[11] has examined the susceptibility of a spherical powdered CMN thermometer using a Johnson noise thermometer and a nuclear orientation thermometer (NOT).[12] In the first experiment, which covered the 10–50 mK range and employed the NOT, Curie-Weiss behavior was observed with $\Delta = 0.48$ mK. The second experiment utilized the Johnson noise thermometer in the 0.01–0.20 K region and, as before, found Curie-Weiss behavior but with $\Delta = 0.15$ mK. (Note the primary coil of the CMN thermometer was changed between the two runs.) Finally, Greywall and Busch[13] have reported recently the results of a magnetic thermometer–^{3}He melting curve thermometer study in which a powdered CMN thermometer was calibrated in the 100–200 mK region with an NBS fixed point device (see Sec. X) and in the 0.3–1.0 K region versus the ^{3}He vapor pressure scale. After assuming a Curie-Weiss law to be valid, the low-temperature extrapolation of the tem-

perature scale was made so as to agree with the Cornell ^{3}He melting pressure scale at ~10 mK. A rather large Δ = 0.7 mK resulted from this procedure.

For the above reasons, as has been emphasized by Hudson et al.,[4] blind extrapolations from high temperatures to generate temperature scales may be dangerous. This does not mean that magnetic thermometers employing CMN are not useful but rather that one must take precautions to eliminate the difficulties described above. With this in mind, a calibration experiment was devised which employed two CMN thermometers, an NOT and several GRT. To minimize systematic errors, the two magnetic thermometers were fabricated with different materials and were physically separated as a test for thermal gradient problems. While one CMN thermometer was monitored using an ac bridge technique, the second CMN thermometer utilized a dc susceptibility measurement. The CMN was calibrated in the 1.3-3.7 K region against a GRT which carried the laboratory representation of the ^{3}He/^{4}He vapor pressure scale and was then extrapolated to lower temperatures where the NOT, by providing independent and absolute temperatures, assisted in the defining of an accurate magnetic temperature scale. The major objective then was to use the CMN scale to calibrate two low resistance GRT in the 0.05-1.0 K region for use with low-temperature heat capacity experiments. Details concerning the construction of the thermometers and experimental results will be discussed separately.

II. DC SUSCEPTIBILITY THERMOMETRY

Previously, the magnetic thermometry in this laboratory employed a mutual inductance bridge technique[14] in which a sphere of single crystal CMN formed the core of an unknown mutual inductance and bridge balance was achieved with a variable mutual inductor and a resistive network. There were a number of undesirable effects associated with the bridge including day-to-day reproducibility problems, helium bath level influences on the bridge null point and an asymmetry associated with switching a given mutual inductance element into the circuit in a positive or negative sense. To avoid these and other problems, the use of a high sensitivity superconducting quantum interference device (SQUID) was introduced for the purpose of measuring the susceptibility of powdered CMN. Since detailed reviews of the design and operating principles of SQUID magnetometers are available in the literature,[15] only a few remarks will be made here to illustrate the advantages this device has over our conventional bridge system.

The operation of a SQUID magnetometer is based on several important principles. First of all, the microscopic theory of superconductivity by Bardeen, Cooper and Schrieffer[16] indicates that all superconducting pairs in a superconductor are described by a single macroscopic wave function and have an identical quantum mechanical phase ψ. Second, the flux threading a superconducting ring is not arbitrary but is quantized in units of the flux quantum $\phi_0 = h/2e = 2 \times 10^{-7}$G-cm^2. Finally, the Josephson effect[17] demonstrates that superconducting pairs may

tunnel through a thin insulating barrier connecting two bulk superconductors according to the relation $J_s = J_c \sin(\Delta\psi)$ where J_s is the supercurrent, J_c is the critical current and $\Delta\psi$ is the phase difference generated by the supercurrent across the barrier. In the dc Josephson effect, $J_s < J_c$ and no voltage appears across the junction and $\Delta\psi$ is time independent. At finite voltages, the ac Josephson effect occurs and the supercurrent oscillates with time since $\Delta\psi$ then obeys the relation $d(\Delta\psi)/dt = \omega = 2eV/\hbar$ where V is the voltage across the junction. Note that this expression may be written $V = h\nu/2e = \phi_0\nu$ which indicates that the Josephson voltage-frequency relation and flux quantization are related.

Practical SQUID magnetometers are constructed with an insulating or weak link section in an otherwise superconducting ring. If the weak link is in the finite voltage state, the rigorous flux conservation in a bulk superconductor then gives way to a situation where flux is admitted to the ring, approximately in units of ϕ_0 (if $2\pi LJ_c/\phi_0 > 1$ where L is the ring inductance) as the ring moves through quantum states $n = 0,1,2,3\cdots$. One way to monitor the state of the ring is to couple it to an LC resonant circuit which is driven at its resonant frequency ω_0 (generally 20-30 MHz) and to monitor the voltage appearing across the resonant circuit as in Fig. 1. The drive level of the resonant circuit must be adjusted to bias the weak link into the finite voltage state for at least part of the duty cycle. At this point, the number of transitions between ring quantum states depends directly upon the dc flux applied to the ring. Hence, changes

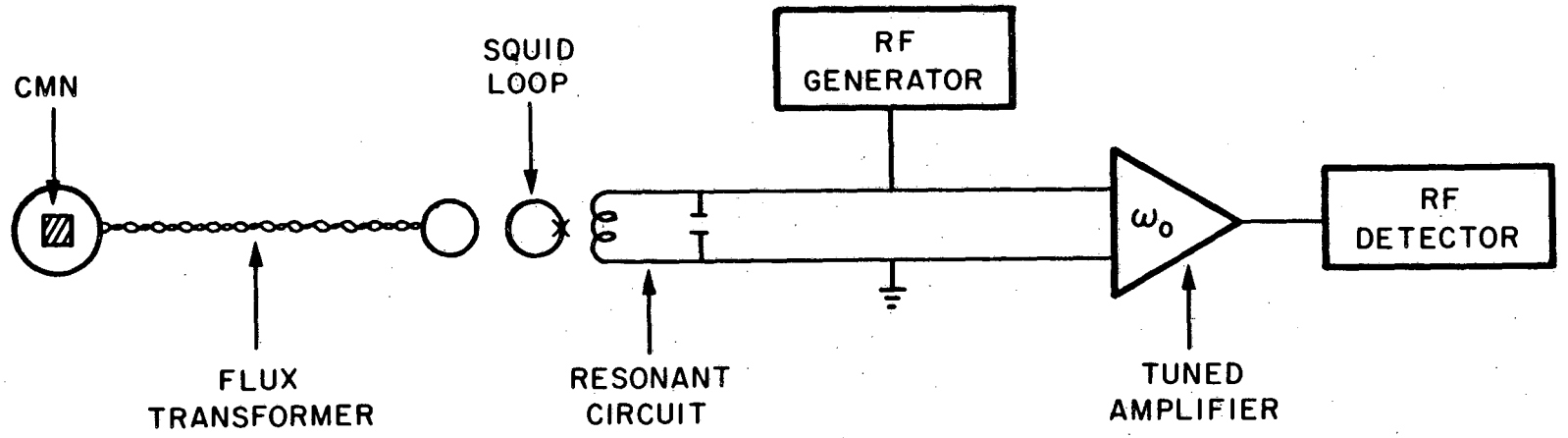

Fig. 1. Schematic representation of the dc susceptibility thermometer electronics. The detected rf voltage is a periodic function of the flux applied to the SQUID loop.

in the applied flux result in a periodic voltage output across the resonant circuit since the flux changes in the ring directly modulate the resonant circuit. The degree of modulation is determined by passing the resonant circuit voltage through an rf amplifier tuned to ω_o to an rf detector. One can then easily use the device to count applied flux in units of ϕ_o (as the output is periodic in ϕ_o) and in fact, using negative feedback techniques (which essentially make the ring a flux null detector), one can resolve $\sim 10^{-4}\phi_o/\sqrt{Hz}$. For a ring with a 2 mm diameter, this corresponds to a field sensitivity of 6×10^{-10} G.

This technique has several substantial advantages over conventional mutual inductance bridge measurements. First of all, the sensitivity of the SQUID magnetometer allows one to work with milligram quantities of CMN whereas conventional measurements require ~20 grams to achieve similar sensitivities. Hence, the new thermometers are much more compact, have faster thermal relaxation times and have substantially smaller heat capacities. Additionally, the use of the powdered form of CMN results in enhanced thermal contact which in turn allows for the use of these susceptibility thermometers to substantially lower temperatures. Second, the method of detection described above for the SQUID magnetometer results in the initial amplification of the CMN signal taking place in the resonant circuit which is at helium temperatures (the SQUID is a parametric amplifier which mixes the low-frequency CMN signal with the rf signal such that the CMN signal appears at a greatly increased power level in the form of sidebands of the rf signal due to parametric up-conversion). With our conventional

bridge arrangement, all signal amplification and detection is done with room temperature electronics. This allows lead impedances to the cryostat, for example, to adversely affect the bridge performance.

From a practical point of view, the CMN signal is coupled to the SQUID indirectly using a flux transformer. This device is simply a closed superconducting loop made with superconducting wire whose operation exploits the principle of flux conservation. The CMN forms the core of a superconducting inductor at one end of the transformer while the other end is tightly coupled to the SQUID ring as in Fig. 1. This design has the advantage that the SQUID may be located remotely at some fixed temperature (usually 4.2 K) thus allowing stable operation while the CMN stage is maintained at the temperature of interest in the experiment. As the temperature of the CMN changes, the flux threading the CMN coil of the transformer will also change if a static measuring field has been impressed upon the CMN. Since the total flux through the flux transformer must remain constant, a supercurrent is spontaneously generated in the transformer in such a way as to maintain flux conservation. This dictates that

$$N_{tr}\phi_{CMN} \times 10^{-8} + (L_{CMN} + L_{sg} + L_{ld})\, J_{tr} = 0 \qquad (1)$$

where N_{tr} is the number of turns in the CMN coil, ϕ_{CMN} is the flux coupled into a single turn of the CMN coil, L_{CMN} is the inductance of the CMN coil, L_{sg} is the inductance of the transformer coil directly coupled to the SQUID ring, L_{ld} is the stray inductance of the twisted leads of the transformer and J_{tr} is the spontaneous current generated in the transformer. In Eq. (1), flux is in units of

$G\text{-}cm^2$, inductance is in units of henries and current is in units of amperes. The actual flux coupled to the SQUID is given by $\phi_{sq} = M_{sg} J_{tr} \times 10^8$ where M_{sg} is the mutual inductance between the transformer signal coil and the SQUID ring. Combining these equations, the basic flux transformer equation is

$$|\phi_{sq}| = M_{sg} N_{tr} (L_{CMN}+L_{sg}+L_{ld})^{-1} \phi_{CMN} = f\phi_{CMN} \quad . \qquad (2)$$

In order to minimize the pickup of stray signals and to maximize the flux transfer factor f, L_{ld} must be minimized by tightly twisting the wire of the transformer between the CMN coil and the SQUID signal coil. It then turns out[18] that to maximize the flux transfer factor f, the transformer should be designed to have $L_{sg} = L_{CMN}$. Typical flux transfer factors range from 0.005 to 0.05.[19]

The design of the dc susceptibility thermometer was similar to that of Giffard et al.[18] and a cross section of the thermometer is shown in Fig. 2. The body of the thermometer was machined from high purity copper[20] (99.9999%) to minimize the effects of magnetic impurities. This portion of the thermometer was in two parts, the first which held the pickup coils of the flux transformer and the second which held the CMN powder. Note that the flux transformer actually formed an astatic pair of coils rather than a single coil. This arrangement tended to cancel low-frequency magnetic disturbances and also substantially compensated for weak magnetism in the construction materials (note the construction was designed to leave the same amount of copper in each coil). For this reason, the two coil grooves were machined to be as nearly identical as possible. In our case, the groove widths were the

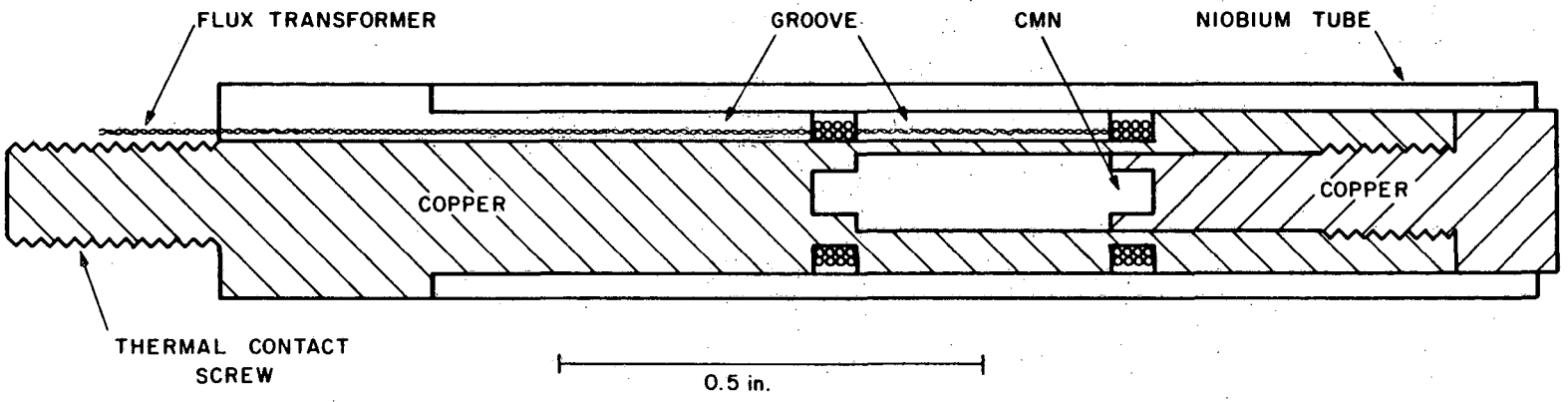

Fig. 2. Cross section of the gold-plated copper dc susceptibility thermometer sensor. The teflon sleeve-copper coil assembly used for trapping the static measuring field, which slips over the niobium tube, has been omitted for clarity.

same as the cutting tool width and the radii of the coil forms were estimated to be within 0.001 in. of each other. All machining of the copper was done with clean tools and clean oil to avoid contamination. The copper was degreased and lightly etched in dilute HNO_3 after machining to further remove any contamination. Finally, the two copper parts were gold plated to avoid long term oxidation. The CMN sample space was a right circular cylinder with diameter equal to height with this dimension being 0.053 in. The CMN was positioned inside one of the two flux transformer coils which were wound on a 0.125 in. diameter in a groove 0.053 in. wide. A channel 0.04 in. wide was cut in the copper to allow passage of the twisted flux transformer leads between the coils and out of the thermometer. The flux transformer was made with 0.003 in. NbTi solid core wire[21] with formvar insulation and was sufficiently long to wind the pickup coils and provide tightly twisted leads to reach the SQUID probe at 4.2 K. This avoided any spot welds in the transformer and enhanced its reliability. Early experiments indicated that the formvar insulation on the NbTi wire was not always continuous. The gold-plated copper surface was therefore insulated by coating with GE7031 varnish diluted 50/50 by volume with a methanol/ toluene solution (also 50/50 by volume) and subsequently heating to ~100°C for 1 hour. Each coil was then wound in two layers with 12 turns per layer and with a coating of GE7031 varnish applied to the top of each layer to provide rigidity. The NbTi was tightly twisted between the two members of the astatic pair and all the way to the SQUID probe. Because of the insulation problem mentioned above, after

twisting the NbTi wires, several applications of dilute GE7031 were made to the twisted pair to insure adequate insulation.

The high purity CMN used in the various calibration experiments was grown by R. A. Fisher and came from the same batch as the spherical single crystal used in his magnetothermodynamic study.[8] Reference 22 may be consulted for sample preparation details and for the results of extensive impurity analyses. For our purposes, a small piece of single crystal CMN was ground to a powder fine enough to pass through an NBS 400 sieve which yielded a particle size < 37μ. The powder was then made into a slurry by combining it with an equal weight of Dow Corning 704 Fluid.[23] The method of thermal contact used by Giffard et al.[18] (which was suggested by W. A. Steyert--see Ref. 18) was to mix the CMN powder with fine gold powder and to press the mixture into the sample space. Although this method of thermal contact may result in a somewhat faster thermal response time, the Dow Corning fluid was chosen as the thermal contact agent for our thermometer because the fluid is believed to be quite free of any paramagnetic impurities which might interfere with measuring the CMN susceptibility and it is believed that the submersion of the CMN in the oil thwarts the tendency of the CMN to dehydrate under room-temperature vacuum conditions.

The magnetic field necessary to measure the dc susceptibility of CMN was obtained by trapping a static field in a Nb cylinder. The attractive feature of a solid Nb tube is the inherent stability of the trapped magnetic field. On the other hand, the actual field trapped was rather uncertain and changing the field in the tube required

heating the assembly above the Nb superconducting transition temperature of 9.2 K. The Nb tube used in the experiments[24] was 1.375 in. long and had a 0.25 in. outer diameter with a 0.03 in. wall thickness. The inner diameter of the tube was a slide fit on the gold-plated thermometer base.

The flux-trapping coil, which was used to generate the field trapped by the Nb tube, was wound on a teflon sleeve 2.25 in. long with a 0.28 in. outer diameter and a 0.015 in. wall thickness. The procedure for winding the coil was to first insert the Nb tube inside the teflon sleeve to the desired position with a snug fit and then to insert temporary brass end caps to define the ends of the coil. The coil was then wound using formvar-insulated number 40 copper wire in 4 layers with 450 turns/cm using small amounts of GE7031 varnish between each layer for rigidity. Four number 28 formvar-insulated copper wires were epoxied with Stycast 1266 lengthwise to the surface of the coil. These wires were subsequently soldered to the thermometer bus to assist in cooling the thermometer assembly and to minimize the thermal response time. Note that the flux trapping coil was considerably longer than the Nb tube. This design was chosen to make the applied field uniform over the length of the Nb tube to ~1 percent. It is believed that this uniformity was an important aspect of minimizing variations in the trapped field from run to run. Calculations indicate that $H = 562\ I$ at the center of the coil where H is the field in gauss and I is the coil current in amperes. For all the experiments reported here, a current of 8.9×10^{-3} A was used which resulted in a nominal field of 5 G.

Assembly of the dc susceptibility thermometer proceeded by first inserting a fresh batch of the CMN slurry into the right circular cylinder sample space, care being taken to remove all air bubbles. The two gold-plated copper pieces were then screwed together snugly to ensure good thermal contact. The Nb tube and flux trapping coil assembly were slid onto the gold-plated copper pieces using a small amount of Apiezon N grease to enhance thermal contact and rigidity. This method of assembly made the thermometer relatively immune to vibration which might have otherwise manifested itself as noise in the SQUID output. Finally, the whole assembly was screwed into the thermometer bus (to be described in detail in Sec. VI). The tightly twisted leads of the flux transformer were pulled into sections of superconducting PbSn tubing (0.035 in. outer diameter and 0.013 in. inner diameter) with Apiezon N grease being continuously applied to the wire as it entered the tubing. The PbSn tubing acted as a shield against external magnetic disturbances while the frozen grease at low temperatures assisted thermal contact of the transformer wire to the tubes and prevented mechanical vibrations of the wire in the magnetic field trapped in the PbSn tubing. The PbSn tubing was broken into sections ~3 in. long, each one thermally lagged to successively lower temperatures between 4.2 K and the thermometer bus. This design helped to eliminate any heat leak that might otherwise flow directly into the thermometer assembly. The joints between the sections of PbSn tubing were shielded with soft-solder coated CuNi tubing, each piece being ~1 in. long with 0.031 in. outer diameter and 0.004 in. walls. At the high temperature end of the flux transformer, the connection to the SQUID was made. The

SQUID is a commercial instrument[25] and the signal coil inductor which couples to the SQUID loop is provided in the probe housing. The flux transformer leads were attached to the Nb terminals in the probe to complete the flux transformer connection.

As was shown in Eq. (2), the flux coupled into the SQUID (ϕ_{sq}) may be estimated if the circuit parameters and the factor representing the CMN flux coupled into a single turn of the CMN transformer coil (ϕ_{CMN}) are known. Giffard et al.[18] have made measurements of the inductance of superconducting coils inside Nb tubes with dimensions similar to ours. For our transformer, $L_{CMN} \sim 2 \times 1.75 \times 10^{-6}$ H (there were two coils in the astatic pair). The stray lead inductance was estimated to be[18] $\sim 1 \times 10^{-7}$ H. The parameters L_{sg} and M_{sg} are estimated by the manufacturer to be $\sim 2 \times 10^{-6}$ H and $\sim 20 \times 10^{-9}$ H, respectively. Following Eq. (2), $f = 0.086$, which is a very efficient flux transfer factor. The term ϕ_{CMN} is difficult to calculate accurately for as Giffard et al.[18] state, "The precise calculation of the flux ϕ_{CMN} produced by a sample in the field trapped in a tube of comparable dimensions is complicated." Clearly the flux picked up by the sensing coil depends upon the relative size and shape of the CMN slurry and the sensing coil. In addition, the field each cerium ion sees is not the same since the slurry is not an ellipsoid of revolution. In any case, Giffard et al.[18] give an approximate expression for ϕ_{CMN} which is appropriate for our geometry. They estimate, for a short sample, $\phi_{CMN} = 4\pi f' \chi H_a V/D$ where f' is the powdered CMN packing fraction, χ is the volume susceptibility of powdered CMN, H_a

is the applied field, V is the volume of the CMN slurry and D is the diameter of the pickup coil. For single crystal CMN,[3] $\chi_\perp = 8.65 \times 10^{-4}/T$. Due to the anisotropy of the CMN, the Curie constant must be multiplied by a factor of 2/3 to allow for the random orientation of the crystallites in a powdered specimen. Hence, $\chi = 5.76 \times 10^{-4}/T$. The CMN packing fraction, which is required to account for dilution of the CMN density in fabricating the slurry, was 0.373. Then,

$$\phi_{CMN} = (7.72 \times 10^{-5}/T)\ G\text{-}cm^2 \qquad (3)$$

or, putting the flux in units of the flux quantum, $\phi_{CMN} = 386\phi_o/T$. Finally,

$$\phi_{sq} = f\phi_{CMN} = (0.086)(386\phi_o/T) = 33.2\phi_o/T \quad . \qquad (4)$$

Note that since a well shielded SQUID system can easily resolve $10^{-3}\phi_o$, a sensitivity of ~8 nK may in principle be obtained at 16 mK which corresponds to a fractional sensitivity of 5×10^{-7}. This serves to illustrate the enormous sensitivity of this thermometer even though only milligram quantities of CMN are used. Since the SQUID output is a known linear function of the input flux, experimental results may be compared quantitatively with Eq. (4). A word of caution, however, is in order here. The self inductance and mutual inductance parameters used in the flux transformer factor f are not easily determined. In addition, the field trapped in the Nb tube is not simply related to the applied field of the copper solenoid. For these reasons, and perhaps others, it turns out to be difficult to

predict accurately the output sensitivity. In Sec. IX A it will become apparent that these predictions are typically in error by as much as 20-50 percent.

Although the SQUID is assumed to have an output which is linear in T^{-1}, in principle deviations from this dependence should be seen due to the effect of the magnetization of the CMN on the measuring field. This complication arises from the fact that both the flux transformer and the Nb tube trap a constant flux. As the magnetization of the CMN increases, an ever larger current flows in the flux transformer which in turn generates a magnetic field on the CMN in opposition to the field trapped in the Nb tube. The tube will respond to the changing CMN magnetization by generating surface currents (over and above those necessary for the initial trapped field) to maintain flux conservation through cross sections of the tube. As with the flux transformer, the field generated by these currents opposes the initial field trapped in the tube. When cooling to low temperatures, these effects result in somewhat smaller flux changes than predicted and temperature determinations which are correspondingly high. Fortunately, for samples with small susceptibilities like CMN, the quantitative effect of this complication is not too serious as may be seen by the following estimates: (1) The current flowing in the flux transformer, which may be determined by combining Eqs. (1) and (3), is

$$J_{tr} = N_{tr}\phi_{CMN} \times 10^{-8} (L_{CMN}+L_{sg}+L_{ld})^{-1} = (3.31\times10^{-6}/T)\ A. \qquad (5)$$

The resulting field generated at the center of the CMN slurry by this current is given by

$$H_1 = \frac{4\pi}{10} \frac{N_{tr}}{2b} J_{tr} \frac{b}{(r^2 + b^2)^{1/2}} \qquad (6)$$

where $r = 0.17$ cm and $2b = 0.12$ cm are the pickup coil radius and length, respectively. Then, $H_1 = (2.78\times10^{-4}/T)$ G. In cooling to 16 mK the anomalous magnetic field induced in the flux transformer is 0.017 G which is 0.3 percent of the 5 G measuring field. Due to the shape of the pickup coil, this effect is essentially the same (to within ~10 percent) over the whole sample volume. (2) To estimate the effect of the changing sample magnetization on the applied field in the Nb tube, assume the CMN may be represented by a point dipole moment $\underset{\sim}{M}$ and that the tube will generate surface currents to compensate all flux lines from the dipole outside the boundary of the tube. For a CMN slurry volume susceptibility of $f'\chi = 2.15 \times 10^{-4}/T$, a sample volume of 1.92×10^{-3} cm^3 and a nominal field of 5 G, the moment is

$$M = (2.15\times10^{-4}/T)(5\ G)(1.92\times10^{-3}cm^3) = (2.06\times10^{-6}/T)\ G\text{-}cm^3. \qquad (7)$$

The dipolar field distribution in a plane perpendicular to and through the midpoint of $\underset{\sim}{M}$ is given by $B = M/r^3$ and integration from the tube radius ($r_0 = 0.32$ cm) to infinity over the plane surface yields the amount of dipolar flux to be compensated by the tube. Thus,

$$\phi = \int_S B\,dS = \int_{r_0}^{\infty} \int_0^{2\pi} (2.06\times10^{-6}/T) r^{-2}\, dr d\theta = (4.04\times10^{-5}/T)\ G\text{-}cm^2. \qquad (8)$$

If the tube compensates this flux uniformly over its cross section, the compensating field generated by the surface currents is

$$H_2 = \phi/A = (4.04\times10^{-5}/T)\,G\text{-}cm^2/0.32cm^2 = (1.26\times10^{-4}/T)\ G \qquad (9)$$

where A is the cross sectional area of the tube. In cooling to 16 mK, $H_2 = 7.9\times10^{-3}$ G which corresponds to a 0.16 percent reduction in the measuring field.

If CMN follows a Curie law, $M = CH_a/T$ and errors will be made in determining extrapolated temperatures due to the anomalous fields generated in the flux transformer and the Nb tube. Quantitative estimates of the errors may be made by recognizing that the anomalous fields are proportional to the CMN magnetization, i.e., $H_1 = \lambda_1 M$ and $H_2 = \lambda_2 M$. Modifying the Curie law expression to account for the induced fields results in $M = C(H_a - \lambda M)/T$ where $\lambda = \lambda_1 + \lambda_2$. Then, the magnetization is $M = CH_a/(T+C\lambda)$ and the effect of the induced magnetic fields thus manifests itself in a form exactly like the Δ in the Curie-Weiss law discussed in Sec. I. The sum of the two induced fields is $H_1 + H_2 = \lambda M = (4.04\times10^{-4}/T)$ G and using the modified Curie law expression with $H_a = 5$ G yields $C\lambda = 8.1\times10^{-5}$ K. This constant corresponds to 0.5 percent of the temperature at 16 mK and will be taken into account in defining the powdered CMN temperature scale for the dc susceptibility thermometer (see Sec. IX C). Note that many paramagnetic salts have Curie constants which are at least an order of magnitude larger than CMN. A similar number of moles of spins as used here will then lead to complications which are comparably larger. These complications highlight earlier statements as to the

desirability of having other independent thermometers in the calibration experiments. The NOT, for example, does not suffer from the above complications.

When considering the operational convenience of this thermometer, it must be realized that random flux jumps in the SQUID can be a problem. This phenomenon simply amounts to the SQUID sensor jumping into a different quantum state, usually under the influence of magnetic noise at the SQUID input, without any real change of input flux from the thermometer. At best, when all of the above shielding precautions have been taken, flux jumps are infrequent (depending upon environmental conditions) and may be compensated by returning the thermometer to a known temperature and checking the SQUID output for flux changes in some multiple of $n\phi_0$. At its worst, the flux jumping is too frequent to allow proper corrections to be made and one must improve the rigidity and the shielding of the thermometer or reduce the environmental noise or both before proceeding.

III. AC SUSCEPTIBILITY THERMOMETRY

The second magnetic thermometer measured the ac susceptibility of CMN using a mutual inductance bridge technique. The bridge used in this work is a commercial instrument[25] and differs from our conventional bridge described in the last section in two very important ways. First, this bridge does not use a variable mutual inductance but rather employs a fixed mutual inductance in conjunction with three ratio transformers. Second, a SQUID is used in the null detection circuitry of the bridge in order to give good sensitivity with low power dissipation for small samples of CMN. Figure 3 shows the bridge circuit and the inset illustrates how the CMN was used as the core of the unknown mutual inductance.

The ratio transformers used in this bridge are manufactured by Electro Scientific Industries[26] and are five decade devices. The three most significant decades utilize discrete step switches while the two least significant decades employ an interpolating rheostat. The transformers are specified to be linear to ±10 ppm for frequencies between 50 Hz and 1 kHz. The bridge oscillator, which may be run up to 5 volts in ten discrete steps (1-2-5 sequence), was used to drive the unknown mutual inductance and the first of the three ratio transformers. Since a fraction of the drive voltage across the first ratio transformer was tapped off to drive the in-phase and out-of-phase ratio transformers, a high precision of adjustment could be maintained for the latter two transformers with a broad variation in the unknown mutual inductance. According to the manufacturer, the bridge should

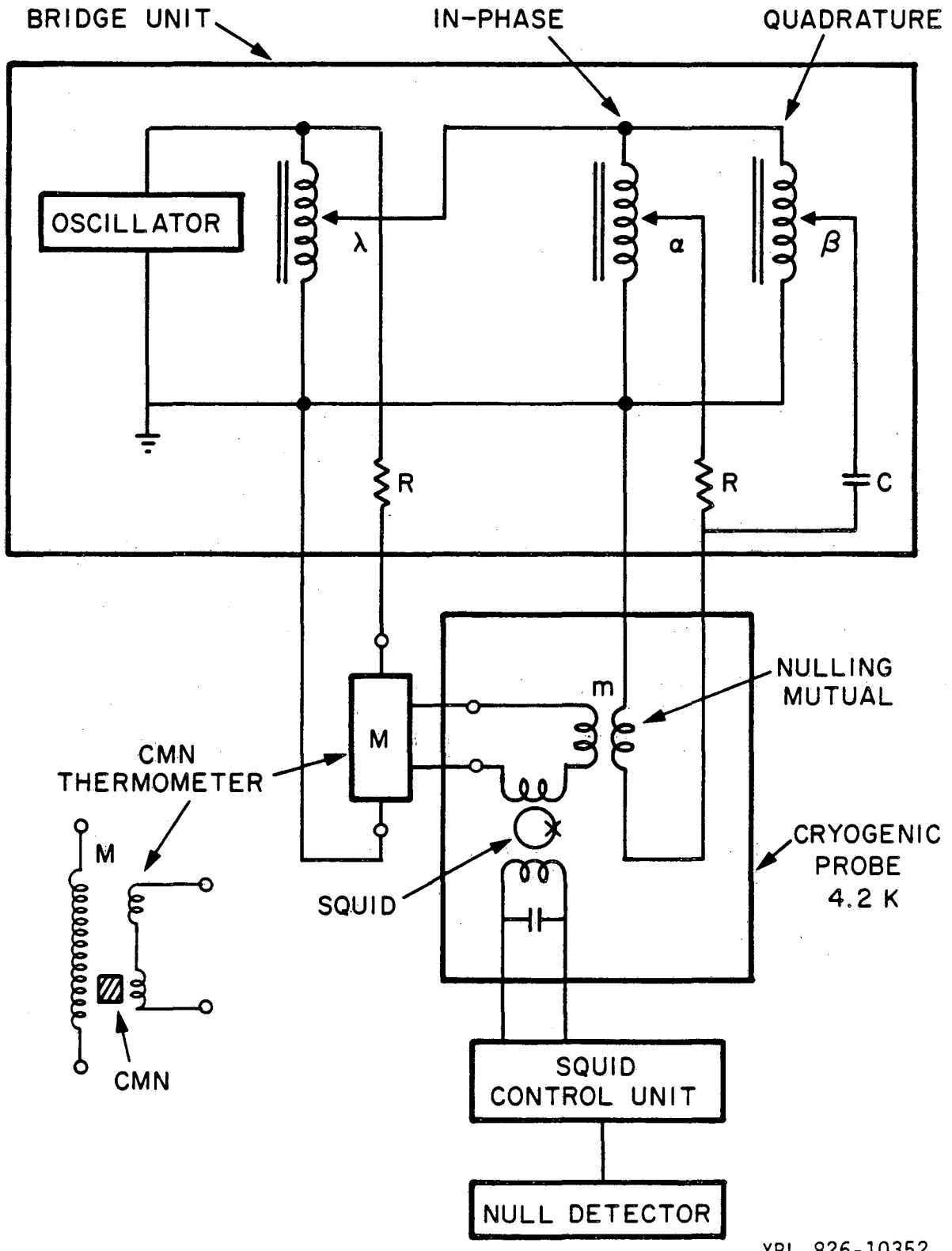

XBL 826-10352

Fig. 3. Schematic diagram of the mutual inductance bridge (R=10KΩ, C=0.1μF and m=1.02μH) and the SQUID detection circuit used with the ac susceptibility thermometer. The inset illustrates how the CMN was incorporated into the unknown mutual inductance M.

have a resolution of 0.001 percent if $M > 6 \times 10^{-7}$ H, a stability of 0.01 percent, an absolute inaccuracy of < 2 percent, and a departure from linearity in the in-phase component of < 0.02 percent of the reading plus 0.04 percent of the quadrature dial setting. Since the bridge can operate at 16, 32, 80, and 160 Hz, the frequency dependence of the CMN susceptibility may be examined if desired. In addition, inspection of Fig. 3 indicates that if the secondary of the bridge circuit is completely superconducting, the bridge may be turned off and the secondary used simply as a flux transformer between the CMN and the SQUID. The thermometer then operates at essentially dc as described in the previous section. As will be described later, this feature turned out to be particularly useful.

The off-null signal current in the secondary was detected by the SQUID which in turn was connected to a Princeton Applied Research[27] (PAR) Model 113 low noise preamplifier that, in addition to providing a gain of 50, had variable low-pass and high-pass filters which enhanced the signal to noise ratio. The in-phase and out-of-phase components of the off-null signal were then detected with a PAR Model 129A lock-in amplifier (the in-phase signal contains the temperature dependent portion of the CMN susceptibility). At low temperatures, where the CMN sensitivity is high, the bridge was balanced using the two rheostats. Since the CMN has a much lower sensitivity at high temperatures (the sensitivity temperature dependence is T^{-2}), a more complex arrangement was used in this region. Although the out-of-phase signal was nulled with a rheostat, the in-phase rheostat was set to zero and the bridge run off null. The output voltage of the in-phase

channel of the lock-in amplifier was measured with a Hewlett-Packard[28] (HP) Model 2401C integrating digital voltmeter. This voltage was carefully calibrated in units of the in-phase ratio transformer dial settings. The advantage of this technique lies in the significant improvement of the signal to noise ratio afforded by the long integration times of the HP 2401C voltmeter. In this manner, the resolution of the bridge was enhanced substantially when necessary.

Considering the specifications stated above, several typical examples will serve to illustrate the bridge performance. First, with respect to resolution, approximately 10 ten-second integration time integrals were generally taken with the HP 2401C voltmeter (at constant temperature) to measure the off-null voltage at high temperatures (~1 K). With this 100 second signal to noise averaging, the uncertainty in the off-null voltage was found to be ~1 mV. When translated into ratio transformer units or, equivalently, mutual inductance units, this corresponds to a fractional uncertainty of 0.00012 percent which is fully eight times better than the specified figure of 0.001 percent. This illustrates that if the SQUID system is carefully tuned and care is taken with respect to signal to noise considerations, extremely high precision measurements may be made. Second, with respect to the stability of the bridge, the repeatability of the in-phase null reading was monitored at 0.500 K over a period of three weeks in one experiment. The maximum variation in five independent determinations was found to be 0.0017 percent which is six times better than the stated stability specification of 0.01 percent.

A number of considerations were reviewed in deciding how to fabricate the ac CMN susceptibility thermometer. Insofar as construction materials were concerned, high purity copper and epoxy were considered. Both were believed to be suitably free of paramagnetic impurities but the copper was favored due to its higher thermal conductivity. However, since the measuring field is no longer static (as with the dc susceptibility thermometer), eddy current heating and skin depth considerations become important with pure copper. For high purity copper with a conductivity of ~5 x 10^{10} $(\Omega\text{-m})^{-1}$, the skin depth at 16 Hz is only ~0.5 mm and is correspondingly shorter at higher frequencies. In this case the measuring field would not fully penetrate the copper former and, to the extent the conductivity is temperature dependent, the amplitude of the measuring field would also be temperature dependent. Therefore, the thermometer was fabricated from Epibond 100A[29] and Stycast 1266,[30] both of which have been demonstrated to have very weak susceptibilities.[31,13] Although the response time of the thermometer was somewhat longer due to the use of epoxies, it should be emphasized that this thermometer was designed to be a calibration device, not a fast secondary thermometer.

Epibond 100A is supplied as a powder with a self-contained catalyst. The powder melts and the catalyst is activated at elevated temperatures. Details are available in the literature for fabricating bubble-free pieces of this epoxy.[31,32] Stycast 1266 is a low-viscosity epoxy which begins curing at room temperature after adding a liquid catalyst. Pieces may be fabricated very simply using this epoxy

by pouring the epoxy "laced" with catalyst into a properly designed mold. The epoxy components of this thermometer are shown in Fig. 4.

The coil former was machined from Epibond 100A using clean tools and oil to avoid contamination. Extra care was taken in machining the two grooves for the secondary coils to make them as identical as possible. Each groove was 0.060 ± 0.001 in. wide and had a diameter of 0.240 ± 0.001 in. The center bore of the former was 1.500 ± 0.002 in. deep and, along with the two inserts, allowed the CMN to be located symmetrically and reproducibly inside one coil of the secondaries. The secondaries were wound from solid core 0.003 in. NbTi wire[21] (with an additional 0.001 in. formvar insulation) in two layers with 13 turns/layer using small amounts of GE7031 varnish between layers for stability. The wire was tightly twisted between the coils and as it left the thermometer assembly to minimize the stray inductance. A 0.04 in. channel in the Epibond 100A was provided for this purpose. A piece of 0.002 in. mylar was wrapped around the 0.4 in. diameter body of the thermometer to provide a base upon which to wind the primary. The primary was wound in six layers yielding an average of 360 turns/layer with a 0.001 in. piece of mylar placed between adjacent layers and the usual GE7031 varnish used to ensure the rigidity of each layer. Note that in the first version of this thermometer, the primary layers were wound from wall to wall on the epoxy former. With this configuration, the primary circuit was found to be open at low temperatures and subsequent examination of the coil revealed one or more breaks in the wire near the ends of the coil. A rough calculation indicates that the Epibond 100A former contracts lengthwise upon cooling by an amount

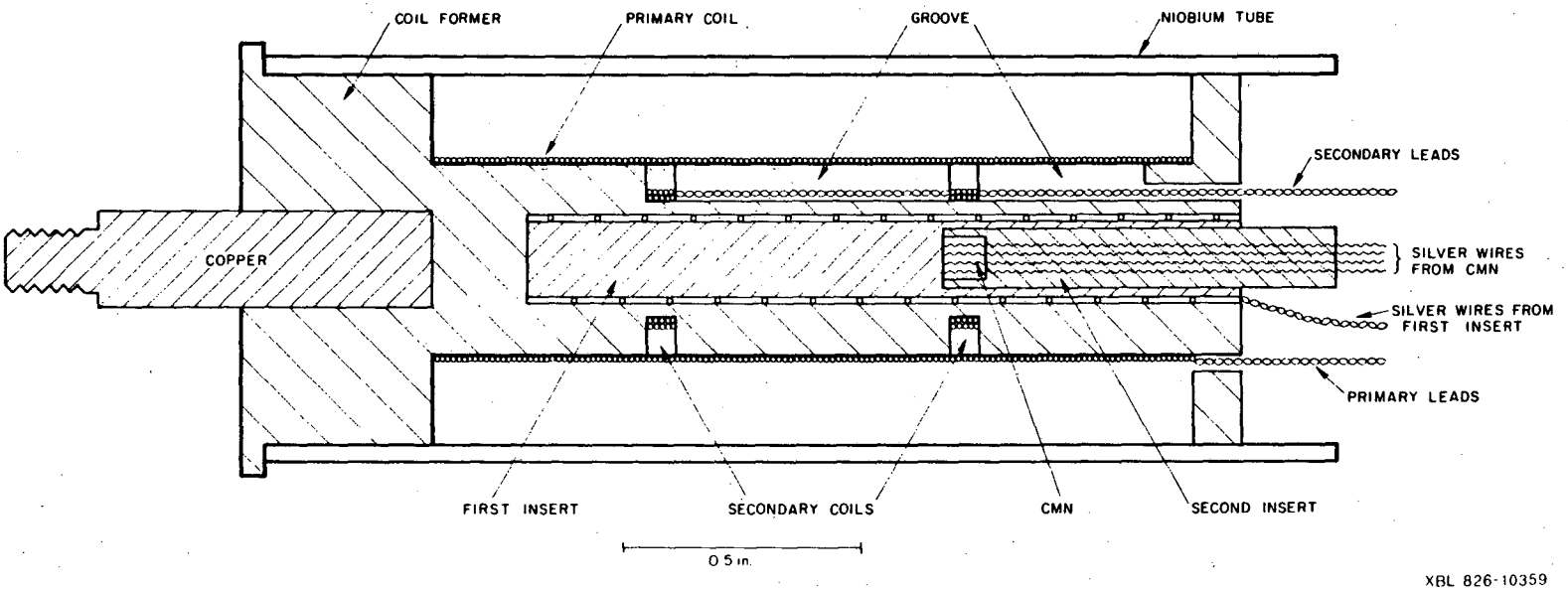

Fig. 4. Cross section of the ac susceptibility thermometer sensor.

which is large compared with the contraction of the wire itself. In the subsequent winding of primary coils, gaps equivalent to two or three wire diameters were left at each end of the coil and no further difficulties with breakage occurred.

The first insert of this thermometer was also fabricated from Epibond 100A. Although its initial outer diameter was 0.17 in., after epoxying six 0.005 in. silver wires around the outer diameter, it fit snugly in the 0.18 in. diameter bore of the former. The silver wires, which were later soldered to the thermometer bus, enhanced the thermal contact of the thermometer assembly. The second insert was made with Stycast 1266 since its very low viscosity facilitated filling a mold of small dimensions. The mold cast four 0.005 in. silver wires into the right circular cylinder CMN sample space to improve the thermal response time of the CMN slurry.

The thermometer was assembled by first charging the sample space with the CMN slurry mentioned in the dc susceptibility thermometer discussion. The second insert was then snugly placed in the first insert, a little silicone oil being used for lubrication. This combination was inserted into the coil former, again using silicone oil for lubrication. A 0.77 in. inner diameter Nb tube with 0.035 in. walls and 2.25 in. in length was then placed over the coils and attached to the base end of the former with two 2-56 nylon screws and a little Apiezon N grease. Six insulated number 28 copper wires were epoxied to the outer surface of the Nb tube and subsequently attached to the thermometer bus to enhance thermal contact. Note that the aspect ratio of this tube is not nearly so favorable as that for the dc susceptibil-

ity thermometer. The ramifications of this comparison will become evident in Secs. VIII and IX B. Finally, a threaded copper stud was epoxied into the base of the epoxy former such that the thermometer assembly could then be screwed into the thermometer bus. The primary and secondary leads were each shielded in their own PbSn tubing as they were routed from the thermometer to a SQUID probe housing. As described in Sec. II, the leads were greased in the tubes, had no spot welds and were thermally lagged at various temperatures.

The right circular cylinder sample space for the CMN had a diameter of 0.088 in. which yielded a volume that was 4.6 times larger than that for the dc susceptibility thermometer. This volume enhancement was designed to improve the magnetic thermometer sensitivity in the high temperature region, i.e., for 1 K < T < 4 K where calibrations versus the vapor pressure temperature scale were conducted.

Given the geometry of the primary coil, the field profile may be calculated along with the maximum amplitude of the measuring field. When the bridge oscillator drive was 5 V, the primary current was 1.77×10^{-4} A and the maximum primary field was 0.12 G. Note that the diamagnetic response of the Nb tube acted to reduce the amplitude of the measuring field by a factor of $f_{sh} = (1-d_p^2/d_{sh}^2) \sim 0.74$ where d_p is the diameter of the primary coil and d_{sh} is the diameter of the Nb shielding tube. The measuring field uniformity over the volume of the CMN was ~1.1 percent. Since the various coil geometries and the CMN slurry susceptibility are known, the expected mutual inductance of this thermometer may be calculated. From Giffard et al.,[18] the in-phase component of the mutual inductance is

$M = 16\pi^2 n_s n_p f_s f_p f_{sh} f' \chi V \times 10^{-9}$ H where n_s and n_p are the number of turns per unit length of the secondary and the primary, respectively, f_s and f_p are coil geometry factors,[33] f_{sh} is the shielding factor for the Nb tube, f' is the packing fraction of the powdered CMN, χ is the susceptibility of powdered CMN and V is the volume of the CMN slurry. For our thermometer, n_s = 170.6 turns/cm, n_p = 532 turns/cm, f_s = 0.231, f_p = 0.950, f_{sh} = 0.738, f' = 0.373, $\chi = 5.76 \times 10^{-4}/T$, and $V = 8.67 \times 10^{-3}$ cm^3. The predicted mutual inductance is then

$$M = (4.32 \times 10^{-9}/T)\ H. \qquad (10)$$

As will be discussed in Sec. IX A, agreement with this expression is good to a few percent which is on the order of the uncertainty in the amount of CMN used in the thermometer. The agreement with theory is much better than with the dc susceptibility thermometer since in this case, the experimental parameters are known to a higher degree of accuracy.

To illustrate the importance of the high sensitivity of this bridge, the following calculation is interesting. The mutual inductance between a single turn of a secondary coil and the primary coil is given by $M = (300 H_a A/cI_p)$ H where H_a is the primary field, A is the cross-sectional area of the secondary coil, c is the speed of light and I_p is the primary current. (The field is in units of gauss, area is in units of cm^2, the speed of light is in units of cm/sec and the current is in units of amperes.) If the primary is approximated as a solenoid of infinite length, then $H_a/I_p = (4\pi n_p/10)$ G/A and the mutual inductance becomes $M = 120\pi A n_p/c =$

1.94×10^{-6} H. Although the thermometer was designed to have zero mutual inductance between the secondary and the primary with the CMN absent (the secondary was in the form of an astatic pair) the experiments with the CMN absent found a temperature independent mutual inductance of $M \sim 3.2 \times 10^{-7}$ H. Therefore, the degree of mismatch between secondary coils was equivalent to only 1/6 that of the mutual inductance between a single secondary turn and the primary. This indicates that the secondary coils were well matched in the astatic configuration. Further, Eq. (10) indicates that the contribution of the CMN to the mutual inductance was $M \sim 4.3 \times 10^{-9}/T$. Thus, the mutual inductance changes associated with the temperature dependence of the CMN were but a small fraction of the mutual inductance due to the secondary coil mismatch. Theoretically, the CMN must cool from 4.2 K to 2.2 mK to generate a mutual inductance change equal to the secondary coil mismatch. Hence, the useful operation of this thermometer with such small quantities of CMN required a very high resolution bridge.

As mentioned earlier, high resolution was achieved by using a SQUID in the null detection circuit as well as using bandpass filters and an integrating digital voltmeter (at the higher temperatures at least). Good low-noise operation of the bridge required, in addition to the items already mentioned, the cable connecting the mutual inductance bridge to the cryostat to have individually shielded pairs of conductors for the primary and nulling signals so they did not interact. Further, the bridge cable and the SQUID control cable were strung in close proximity between the electronics rack and the experiment (the two cables were tightly lashed together with string). Failure to do

so created a large pickup loop in the bridge circuit as was demonstrated by hanging the bridge cable from the ceiling and running the SQUID cable on the laboratory floor. The resulting pickup was so severe that the SQUID feedback loop unlocked thus rendering the bridge inoperable.

As with the dc susceptibility thermometer, the effects of the interaction of the CMN magnetization with the superconducting materials in the ac susceptibility thermometer may be analyzed. The influence of the Nb shielding tube upon the measuring field of the CMN is similar to the dc susceptibility thermometer case except the induced currents in the tube are now time dependent. A calculation similar to that in Sec. II shows that the error in T associated with induced currents in the tube was $\sim 3.7 \times 10^{-6}$ K which is 6.6 times smaller than the calculated value for the dc susceptibility thermometer. This result is due to the much larger size of the Nb tube in this case along with the r^{-3} dependence of the CMN dipolar flux. In contrast to the flux transformer of the dc susceptibility thermometer, the presence of the superconducting secondary of the ac susceptibility thermometer does not have a parasitic influence on the CMN measuring field. When the bridge is at null, the ac flux in the secondary due to the CMN is canceled by the ac flux from the nulling mutual inductance thus allowing the flux conservation required by a superconducting secondary to be maintained at all times. Since there was a small dc field trapped in the Nb tube, the resulting temperature dependent moment induced in the CMN did create spontaneous dc currents in the secondary to maintain flux conservation. It was in this fashion that the thermometer was used in a fully

dc mode when the bridge was turned off. However, these ever-present dc currents had no effect upon the ac operation of the thermometer--in fact, during the experiments, the dc currents in the secondary were manifested as a dc voltage superimposed upon the ac output voltage of the SQUID null detector.

Several comments on the convenient aspects of this thermometer are in order. In addition to its high sensitivity, this thermometer had several other positive attributes: (a) Flux jumps (which occurred infrequently) were not a problem with this system since the SQUID was used only as a null detector and the exact operating point (or quantum state) of the SQUID was of no consequence. (b) The day-to-day reproducibility of the fit parameters of the CMN versus the germanium thermometers was excellent. (c) The run-to-run reproducibility of the Curie law constant, especially if the CMN had not been changed, was very good. (d) The run-to-run values for the bridge gain (voltage output per bridge unit) and the phase on the lock-in amplifier were quite consistent. Hence, it suffices to say that this ac susceptibility thermometer was extremely easy and convenient to use in practice.

IV. NUCLEAR ORIENTATION THERMOMETRY

For present purposes, nuclear orientation may be defined as the polarization of nuclear spins along an axis of quantization z such that the population of the lowest magnetic sublevel is significantly greater than that of the higher energy sublevels. The direction of emission of γ-radiation from an oriented nucleus is well known to have an anisotropic probability distribution with respect to the axis of quantization. Since this distribution is different for each of the nuclear magnetic sublevels and since an ensemble of nuclei is generally examined experimentally, the observed radiation pattern is a weighted average of the sublevel patterns. Because the relative populations of the sublevels are governed by Boltzmann statistics, the radiation intensity, measured at some well defined angle relative to the quantization axis, may be used to determine the temperature of the nuclear spin system <u>if</u> the details of the hyperfine interaction are known.

The angular distribution of the radiation from a particular γ-transition selected from a cascade of transitions may be written as[34]

$$F(\theta) = \sum_{k=0}^{\lambda} B_k U_k F_k P_k(\cos\theta) \qquad (11)$$

where λ is the smaller of 2L or 2I (2^L being the multipolarity of the radiation and I being the spin of the parent nucleus). Since γ-transitions conserve parity, k takes on only even values and for the experiments considered here, only k=2 and 4 are of interest. The B_k, which are the orientation parameters, contain all of the

temperature dependence and are thus a measure of the population distribution of the parent nuclei among the sublevels; the U_k are coefficients which depend upon the angular momenta of the states involved in all transitions preceding that observed; the F_k are the angular momentum coupling coefficients of the observed transition; the P_k are Legendre polynomials and θ is the angle between the orientation axis and the direction of emission. If the γ-cascade in question has been characterized, the U_k and F_k coefficients may be calculated exactly. The B_k are defined as

$$B_k(T) = \frac{(2k)!}{(k!)^2} I^k \left[\frac{(2I+1)(2k+1)(2I-k)!}{(2I+k+1)!}\right]^{1/2} f_k(I) \tag{12}$$

where the first two relevant spin distribution moments are given by

$$f_2(I) = (1/I^2)\left[\sum_{m=-I}^{I} m^2 p(m) - I(I+1)/3\right] \tag{13}$$

$$f_4(I) = (1/I^4)\left[\sum_{m=-I}^{I} m^4 p(m) - (6I^2+6I-5)\sum_{m=-I}^{I} m^2 p(m)/7 + 3I(I-1)(I+1)(I+2)/35\right] . \tag{14}$$

The p(m) in Eqs. (13) and (14) is the probability of finding the parent nucleus in the state with magnetic quantum number m--that is,

$$p(m) = \exp(-E_m/kT)\left[\sum_{m'=-I}^{I} \exp(-E_{m'}/kT)\right]^{-1} \tag{15}$$

where the E_m are the hyperfine interaction energy levels.

In an experiment, an average of $F(\theta)$ over the surface of a detector is measured since the detector subtends a finite solid angle at the

source. For the case of a cylindrical detector whose axis is parallel to that of the incident radiation, Rose[35] has shown that the form of the angular distribution function is unchanged but the coefficient of each term must be multiplied by a factor Q_k. These solid angle correction factors, which have been tabulated by Yates[36] for a variety of NaI(Tl) detectors, depend upon the size of the detector, its position with respect to the source and the energy of the γ-radiation under observation.

Although the absolute temperature may be determined from a knowledge of the angular distribution function, it is the count rate of the source at some angle θ that is measured during an experiment. Since $F(\theta)$ gives the γ-ray emission probability at an angle θ, it follows by definition that the measured count rate is $C = N_0 F(\theta)\Omega\eta$ where N_0 is the decay rate of the source, Ω is the solid angle subtended by the detector at the source and η is the efficiency of the detector. To determine the angular distribution function associated with partially oriented nuclei at some low temperature, measurements of the radiation intensity must be made at both the low temperature in question and at high temperatures (where kT is much greater than the hyperfine splitting--the nuclear sublevels are thus equally populated and the radiation pattern is spatially isotropic). The ratio of the low- and high-temperature count rates is then

$$\frac{C_{low}}{C_{high}} = \frac{(N_0 F(\theta)\Omega\eta)_{low}}{(N_0 F(\theta)\Omega\eta)_{high}} = \frac{F(\theta)_{low}}{F(\theta)_{high}} \quad . \tag{16}$$

Since $F(\theta)$ has the property of being equal to unity at high temperatures, the ratio of the count rates is just $F(\theta)$ evaluated at the low

temperature in question. This value may then be used along with a knowledge of the decay scheme and the hyperfine interaction to calculate the absolute temperature of the nuclear spin system.

The γ-ray source chosen for use in these experiments was a single crystal disk of ^{60}Co in hcp ^{59}Co. This thermometer has been employed to a significant extent by several research groups,[12,37] and a substantial amount of information about its performance is available. The attractive features of this thermometer are as follows: (1) The details of the decay scheme of ^{60}Co are well known and are illustrated in Fig. 5. The parent ^{60}Co nucleus decays to an excited state of ^{60}Ni via β decay whereupon two rapid ($\sim 10^{-12}$ seconds) γ-transitions take the nucleus to the ground state. Note that due to angular momentum considerations, both γ-transitions have the <u>same</u> angular distribution function thus allowing both the 1.17 and 1.33 MeV γ-rays to be used for thermometry in a straightforward fashion. In addition, for the decay scheme in Fig. 5, the coefficients U_2, F_2, U_4 and F_4 may be calculated exactly and are found to be[12,37] $U_2F_2 = -0.420560$ and $U_4F_4 = -0.242810$. (2) The hyperfine interaction of ^{60}Co in hcp ^{59}Co is also well known. The energy of the nuclear sublevels contains both a magnetic dipole and an electric quadrupole term and is[12]

$$E_m = \frac{\mu_n H_{hf}}{I} m + \frac{3e^2qQ}{4I(2I-1)} \left[m^2 - \frac{1}{3}I(I+1) \right] \qquad (17)$$

where $\mu_n H_{hf}/kI = -6.0668(34)$ mK and $3e^2qQ/4kI(2I-1) = -2.9(7)$ μK. (3) The spin-lattice relaxation time has been measured[38] by magnetic resonance techniques and is only ~75 seconds at 15 mK. This is an

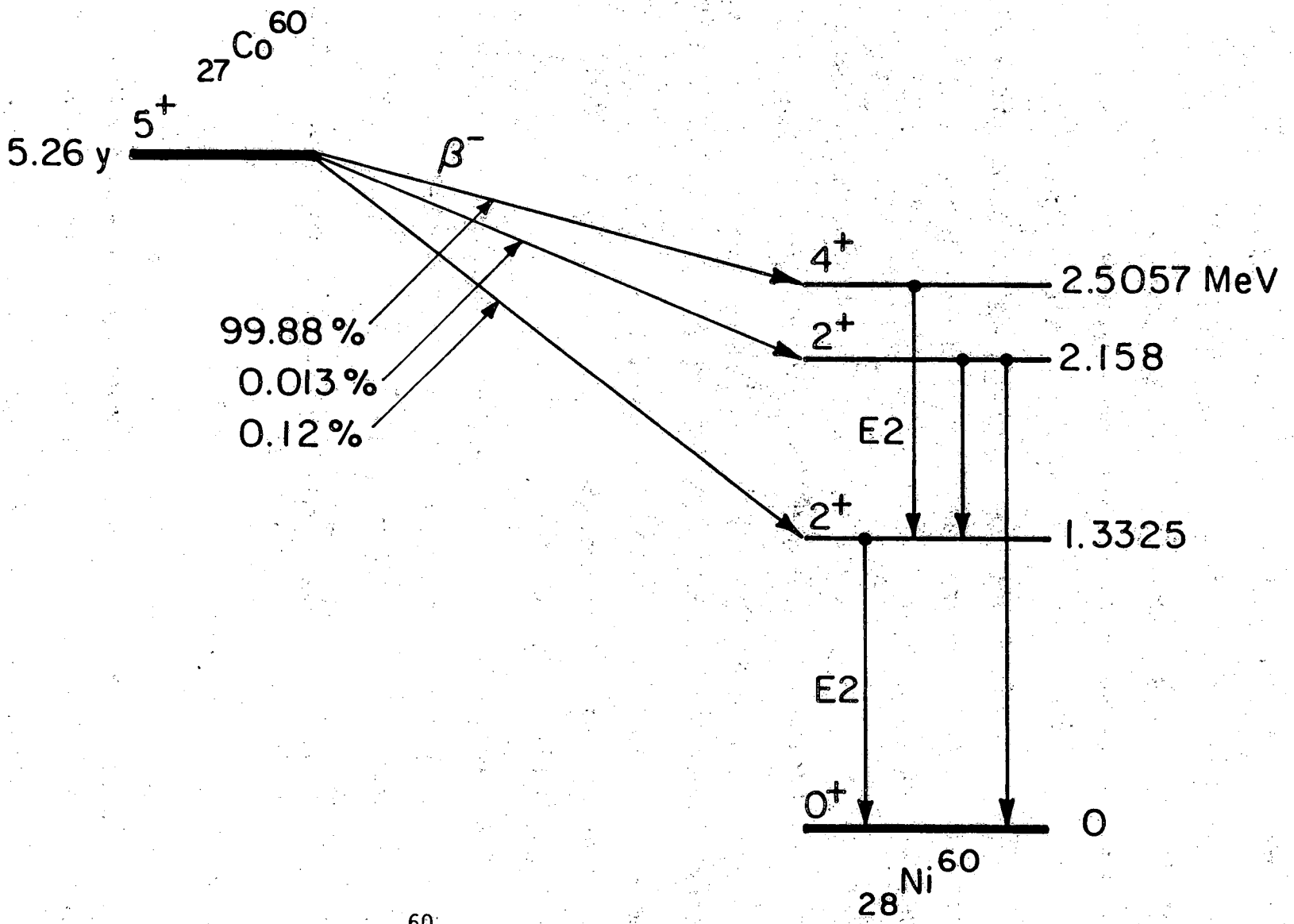

Fig. 5. The decay scheme of ^{60}Co. Indicated are the half-life, decay mode (E2 is electric quadrupole), spin, and parity assignments.

XBL 8210-6670

important consideration since the NOT measurement yields the nuclear spin temperature whereas it is the Co lattice temperature that is desired. (4) Since the Co single crystal is ferromagnetic, the domains in the disk are aligned in opposition to one another and parallel to the c-axis (easy axis) of the hcp crystal structure. Thus, the macroscopic quantization axis of the nuclear spin system is just the c-axis of the crystal and need not be produced by an external polarizing field.

A careful analysis of the thermometry errors associated with the use of a ^{60}Co in hcp ^{59}Co thermometer has been made by Marshak and Soulen[39] (also see Ref. 12 for a few recent comments). They have analyzed the uncertainties in each of the factors expressed in Eq. (11) and find that the ^{60}Co temperatures are expected to be accurate to better than one percent for $T \gtrsim 15$ mK. The largest uncertainty in the temperature determinations is associated with the possible existence of closure domains in the Co crystal. Since Co has a hexagonal structure and possesses a high magnetocrystalline anisotropy, domain formation in the bulk is based on the parallel wall structure. However, the domain structure on the c-axis plane is not well known. For example, Chikazumi[40] has interpreted experimental domain patterns both on the c-plane and on a surface parallel to the c-axis as indicating a free-pole structure with wedge-type reverse domains (which are effective in decreasing the magnetostatic energy associated with free poles without adding much wall energy). In this case, there are no closure domains and all of the nuclei in the crystal share a common quantization axis.

On the other hand, Craik and Tebble[41] have interpreted domain patterns on the c-plane of Co single crystals as indicating a closure domain structure which is only transformed to a free-pole structure by applied fields of several thousand gauss. If this is indeed the case, Eq. (11) does not apply to those nuclei in the closure domains since they do not have a quantization axis which parallels the c-axis of the crystal. Experimental tests with the NOT were conducted which were sensitive to the existence of any significant volume of closure domains in the Co single crystal used in these experiments (see Sec. VII).

A block diagram of the γ-ray spectrometer used in these experiments is given in Fig. 6. A γ-ray is detected by a standard 3" x 3" NaI(Tl) scintillation crystal whose light output is collected at the cathode of the photomultiplier tube (PMT). The photocathode is maintained at ~1000 volts by a high voltage (HV) power supply. The signal is subsequently amplified by the PMT, the preamplifier (PA) and the linear amplifier. An important auxiliary function of the linear amplifier module is to provide the necessary pulse shaping circuits for the spectrometer. Since a signal from the detector essentially appears as a pulse of current whose charge is proportional to the energy absorbed by the scintillator, pulse shaping circuits are needed to generate a voltage waveform whose maximum pulse height is proportional to the charge in the detector pulse. In these experiments, delay line (DL) pulse shaping (with a delay time of ~1μs) was used. Delay line shaping is commonly used with scintillation detectors[42] and has the desirable feature of returning the voltage pulse rapidly to zero volts thus

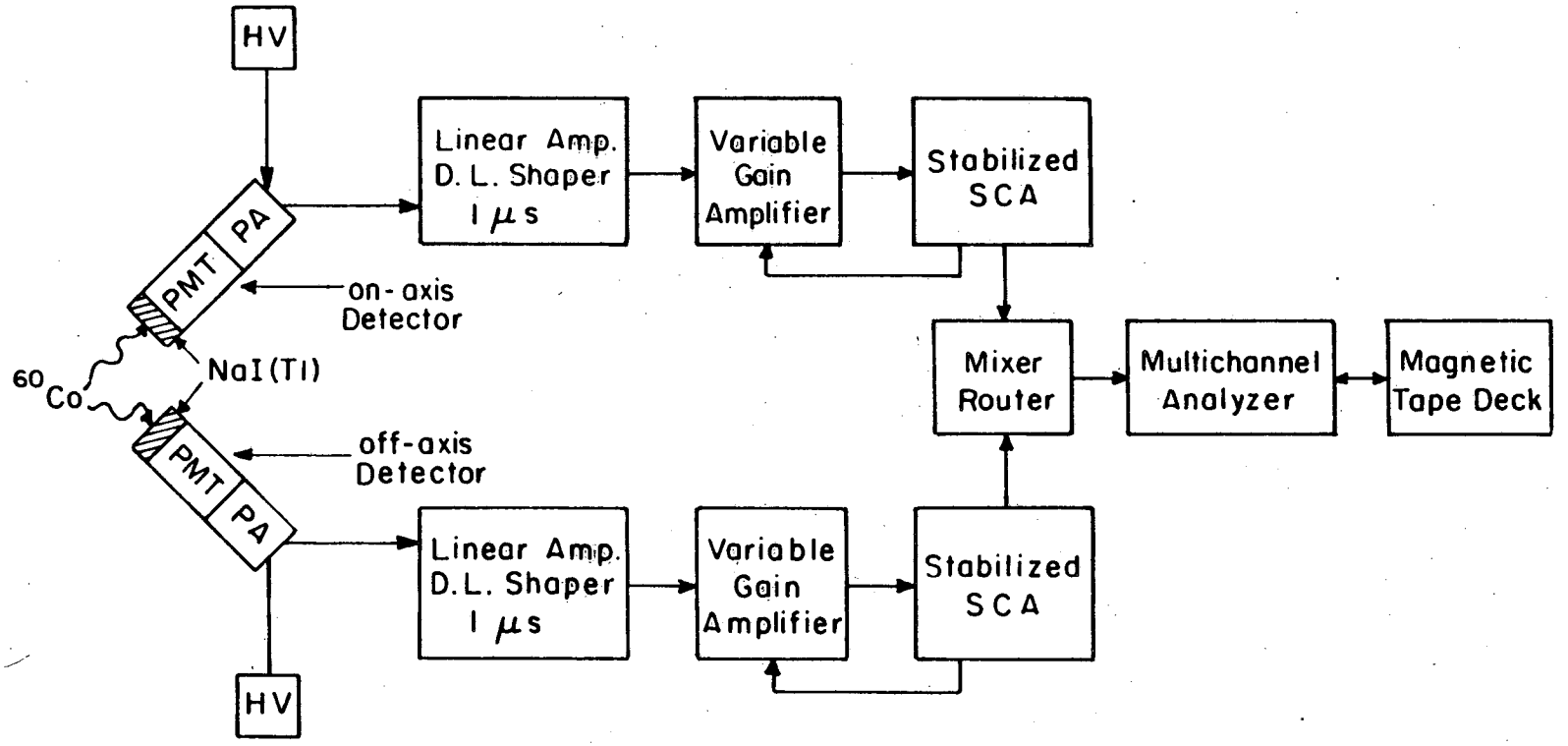

Fig. 6. Block diagram of the γ-ray spectrometer. The abbreviations are explained in the text.

minimizing the effects of pulse pile up. The output pulse of the linear amplifier module is then a positive-going unipolar pulse of ~1μs duration whose amplitude is proportional to the energy deposited in the detector.

Gain stabilizers were incorporated into the system since it is well known that it is difficult to maintain a constant gain in the spectrometer circuits.[43] Without the stabilizers, the system gain was invariably observed to decrease slowly in a monotonic fashion under stable environmental conditions and to increase or decrease in response to changes in the ambient temperature. To compensate for gain drifts, the stabilizers employ an electronic "window" or stabilized single channel analyzer (SCA) whose upper, lower, and midpoint energies may be fixed. The linear amplifier gain is adjusted to position a γ-ray peak in the spectrum under observation symmetrically in the window. It is then the difference in the number of γ-ray pulses counted in the two halves of the window that drives the variable gain amplifier which is used with the stabilized SCA in a negative feedback loop. Thus, for example, if the gain of the PMT decreases, the count rate in the lower half of the SCA will exceed that in the upper half and the variable gain amplifier will act to increase the gain in an attempt to recenter the peak in the window. The performance of the gain stabilizers is discussed in some detail in Sec. VII.

Since most of the measurements in these experiments employed two detectors, a mixer-router was used to identify a given pulse as being from one detector or the other before being passed on to the multichannel analyzer (MCA) for pulse height analysis. (More details on

the mixer-router are given in Sec. VII.) In this way, two spectra may be accumulated simultaneously, one in each half of the 2048 channel memory of the MCA. Since a ^{60}Co spectrum consists of a histogram of counts per channel versus channel number (or energy), any portion of a spectrum may be integrated by summing the contents of those channels in the MCA memory which correspond to the energy region of interest. Finally, the contents of the MCA memory may be dumped to a seven track magnetic tape for permanent storage. The data recorded include (a) a tagword to identify a group of spectra, (2) an automatically incrementing index which identifies each spectrum within a group when operating in a cycling mode, (3) the clock time each spectrum is recorded and (4) the spectrum data in the form of counts per channel for all 2048 channels. The data on the tape may be reentered into the MCA memory for analysis at a later date or used for input data in more sophisticated computer analyses as described in Sec. VII.

A γ-ray may interact with the NaI(Tl) scintillator via the photoelectric effect, Compton scattering or, if the γ-ray energy exceeds 1.02 MeV, via pair production. In Fig. 7, a comparison between an experimental pulse-height distribution and a theoretical electron energy distribution (which assumes single events) is given.[44] The theoretical distribution represents electron energies in the scintillator owing to interactions with the γ-rays and is characterized by the full energy absorption at E_o associated with the photoelectric effect and the continuous distribution due to Compton scattering which extends from zero energy up to the Compton edge (that energy which

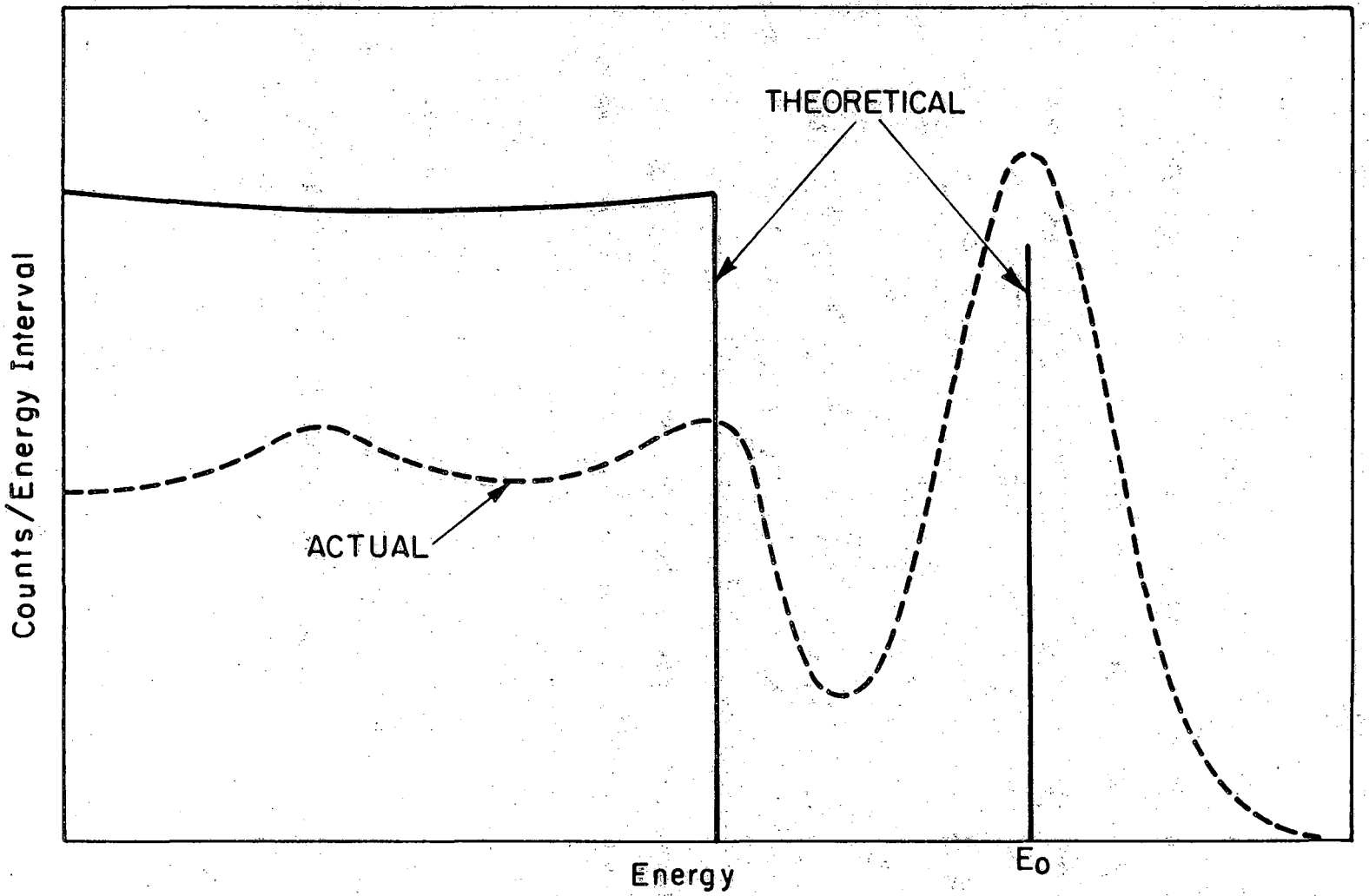

Fig. 7. Theoretical electron energy distribution (assuming single events) for Compton and photoelectric interactions in a NaI(Tl) detector compared with an experimental pulse height distribution obtained with a 3" x 3" NaI(Tl) detector. XBL 8210-6671

corresponds to the maximum energy loss in a 180° scattering event). The experimental spectrum is broadened relative to the theoretical distribution due to statistical fluctuations in (1) the number of photons emitted per γ-ray absorbed, (2) the number of photons collected at the photocathode, (3) the number of electrons emitted by the photocathode per incident photon, (4) the number of electrons collected by the first dynode of the PMT and (5) the secondary emission ratio at each dynode.

In Fig. 8, pulse height spectra of ^{60}Co, taken with the γ-ray spectrometer used in these experiments, are presented for (1) the Co crystal located immediately in front of a detector and (2) the Co crystal mounted in the cryostat. In the former case, the 1.17 and 1.33 MeV photopeaks clearly dominate the spectrum. Also illustrated are the calculated energies at which structure is expected in the spectrum based upon the known interaction mechanisms of the γ-rays with the scintillator. (The backscatter peak arises from the total absorption of the energy of γ-rays which have undergone 180° Compton scattering events in the Co crystal. The single and double escape peaks are due to the escape from the detector of one or both of the 0.511 MeV photons produced by positron annihilation following pair production.) In the latter case, the Compton scattering due to the imposition of the cryostat between the source and the detector dominates the spectrum. Although the 1.17 and 1.33 MeV photopeaks are still well resolved, the only feature of the Compton continuum which remains is the 1.17 MeV Compton edge. For each of the above environments, the FWHM resolution of the photopeaks may be calculated. With

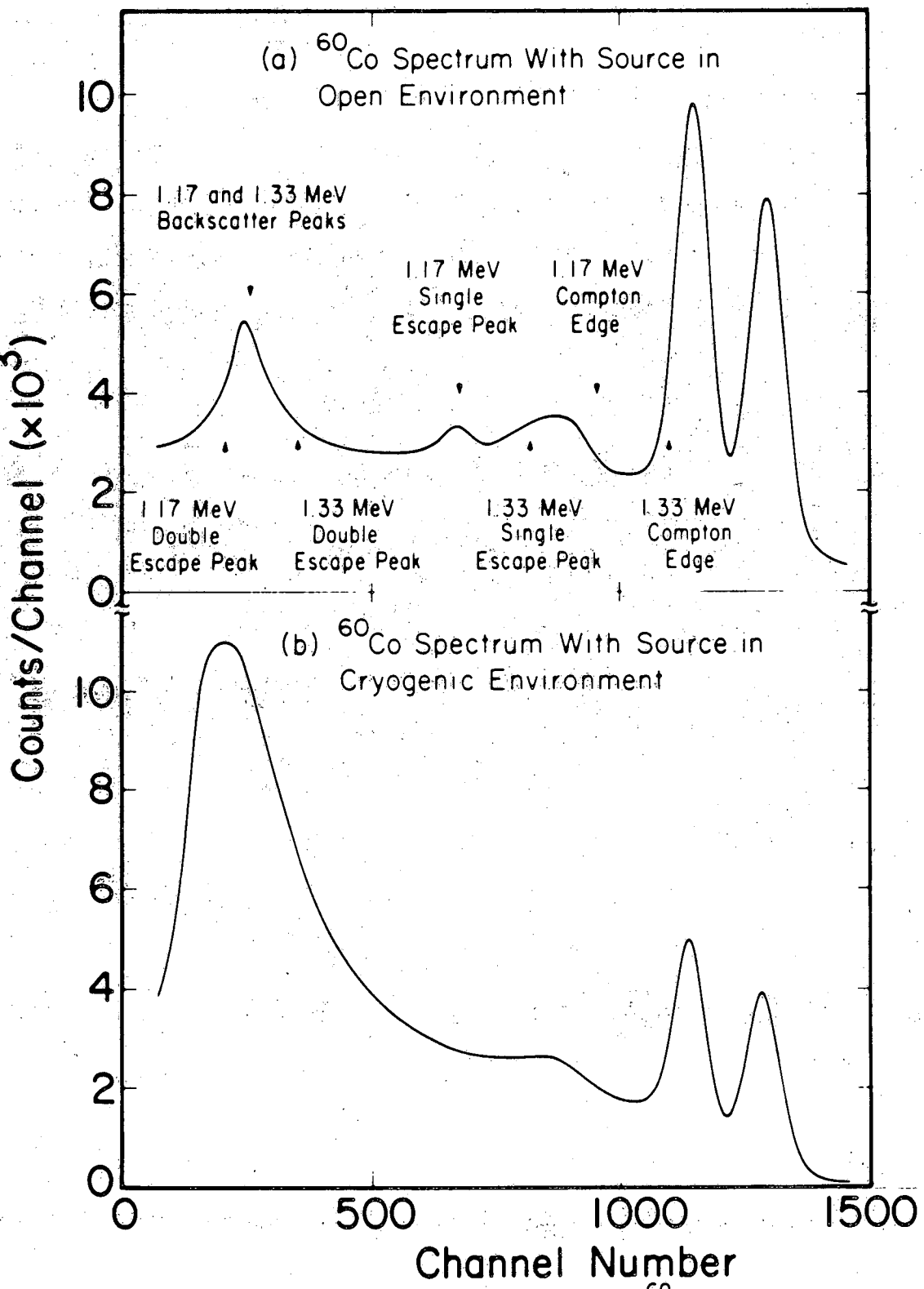

Fig. 8. Comparison of pulse height spectra with the ^{60}Co source in (a) an open environment and (b) in the cryostat. The effects of scattering in the cryostat are evident in (b). Various calculated γ-ray spectrum features are illustrated in (a). XBL 8210-2843

the source in an open environment, the 1.17 and 1.33 MeV resolutions are 8.4% and 7.4% while with the source in the cryostat, the resolutions are 8.7% and 7.6%, respectively. Thus, since the resolutions for the two configurations agree to within experimental error (~0.3%), the large low-energy peak associated with Compton scattering in the cryostat does not adversely affect the shapes of the ^{60}Co photopeaks. To minimize scattering effects, the 1.33 MeV photopeak was used with the gain stabilization system. This choice lessens any temperature dependence of the stabilization peak shape which may arise from the temperature dependent anisotropy of the ^{60}Co radiation pattern.

In these experiments, the scintillation detectors were placed at 0° and 90° with respect to the c-axis of the Co single crystal. (These two directions are generally referred to in this thesis as the on- and off-axis directions, respectively.) The on-axis direction is the natural choice for a ^{60}Co NOT since, for that direction, the thermometer sensitivity is the most favorable. The second detector was placed off-axis because an angular separation of ~90° between the two detectors was desired to test the Co crystal for closure domains or defects in the otherwise single crystal (see Sec. VII). For both the on- and off-axis directions, the symmetry properties of the Legendre polynomials require $dT/d\theta = 0$ -- a result which serves to minimize the error in temperature determinations due to uncertainties in the detector alignment. In Fig. 9, the fractional temperature sensitivities of the on- and off-axis directions are given. Note that the off-axis direction is considerably less sensitive than the on-axis direction.

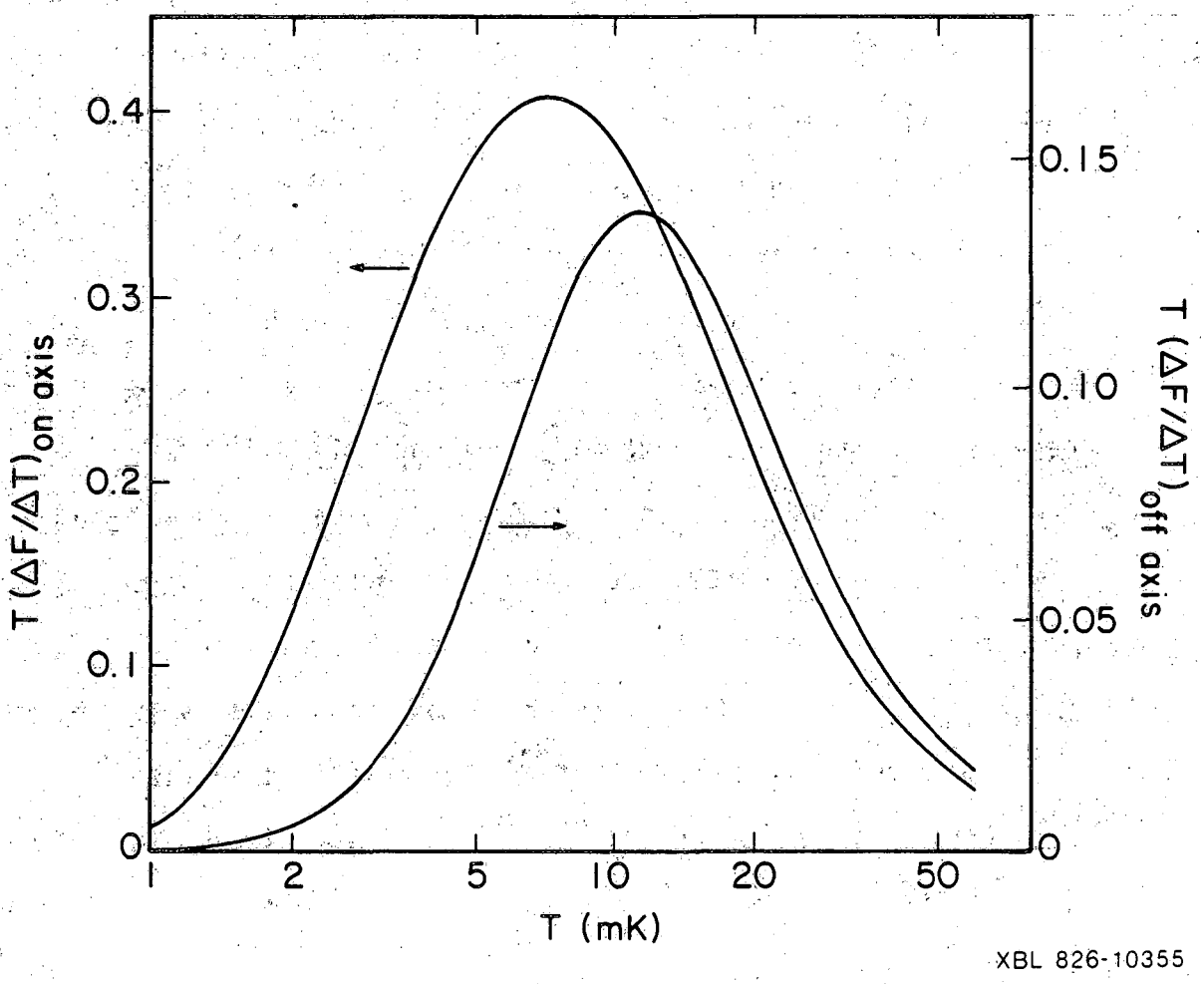

Fig. 9. The sensitivity function for both on- and off-axis directions versus temperature for the ^{60}Co in hcp ^{59}Co nuclear orientation thermometer.

In Figs. 10 and 11, the percentage temperature error due to the misalignment of the detectors with respect to the Co crystal c-axis is given as a function of temperature. To keep temperature errors below one percent at the minimum temperature employed in these experiments (~16 mK), alignment errors of ~6° and 4° can be tolerated on- and off-axis, respectively. These tolerances present no difficulty as the estimated uncertainty in the positioning of the detectors is less than 2° (see Sec. VI).

When using the NOT, it must be remembered that it is an inherently statistical device. The measured intensities referred to in Eq. (16), and the temperatures thus derived, are somewhat uncertain due to both the statistical nature of radioactive decay as well as the statistical fluctuations involved in the detection process. Because of these statistical considerations, repeated measurements of the intensity for a time t will be distributed according to a Poisson distribution which, in the case of a large number of γ-ray counts, goes over into a Gaussian distribution.[45] This well known distribution is characterized by a standard deviation $\sigma = N^{1/2}$ where N is the number of counts observed in the time interval t. If a single measurement of N is made, there are 68.2%, 95.4%, and 99.7% probabilities that N is within $\pm 1\sigma$, $\pm 2\sigma$, and $\pm 3\sigma$ of the mean value of N. To increase the accuracy of a γ-ray intensity determination, longer counting times may be used--that is, the fractional uncertainty $N^{1/2}/N$ may be reduced to an arbitrarily low value. Note, however, that this improvement accrues only at the rate of $t^{1/2}$.

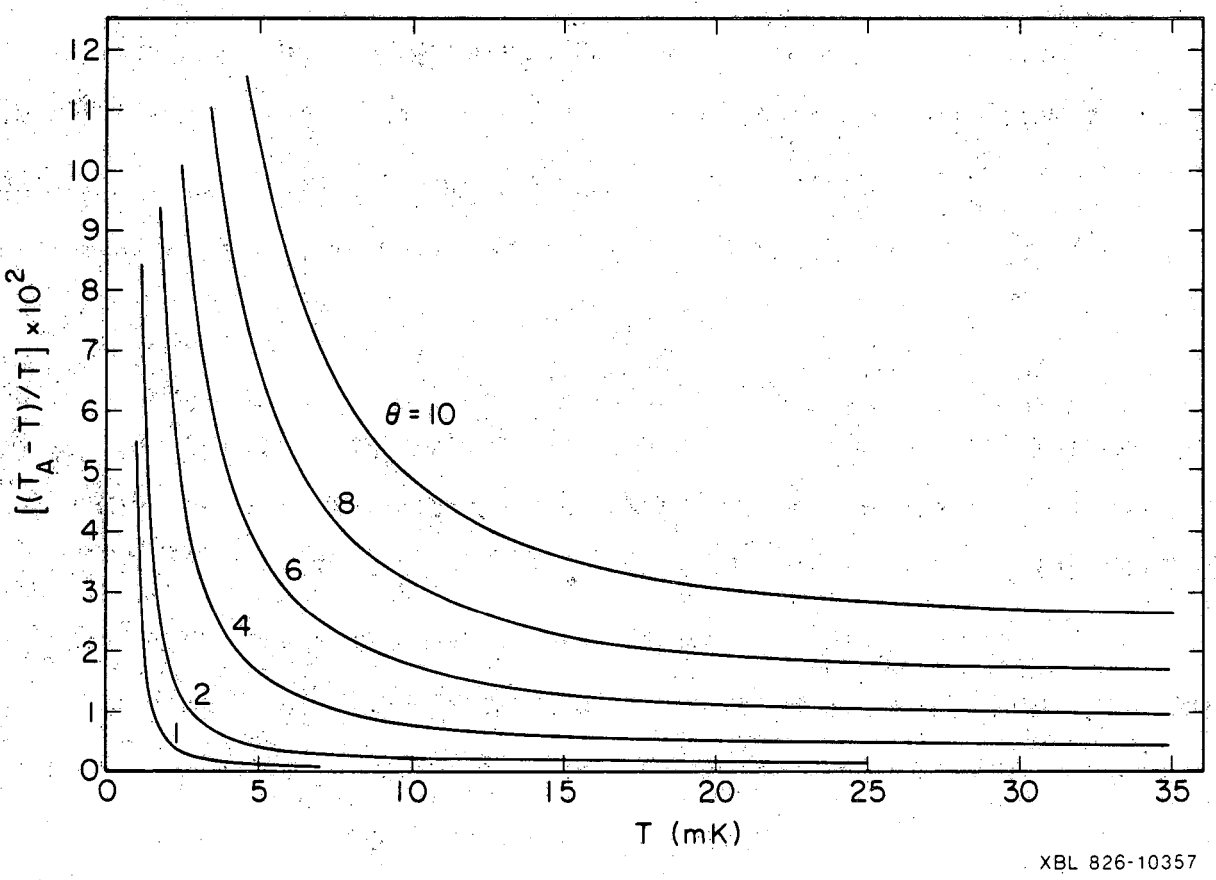

Fig. 10. The percentage temperature error due to the misalignment of the on-axis detector versus temperature. θ is the angular location (in degrees) of the detector with respect to the Co crystal c-axis, T_A is the apparent temperature (calculated assuming $\theta = 0°$) and T is the correct temperature.

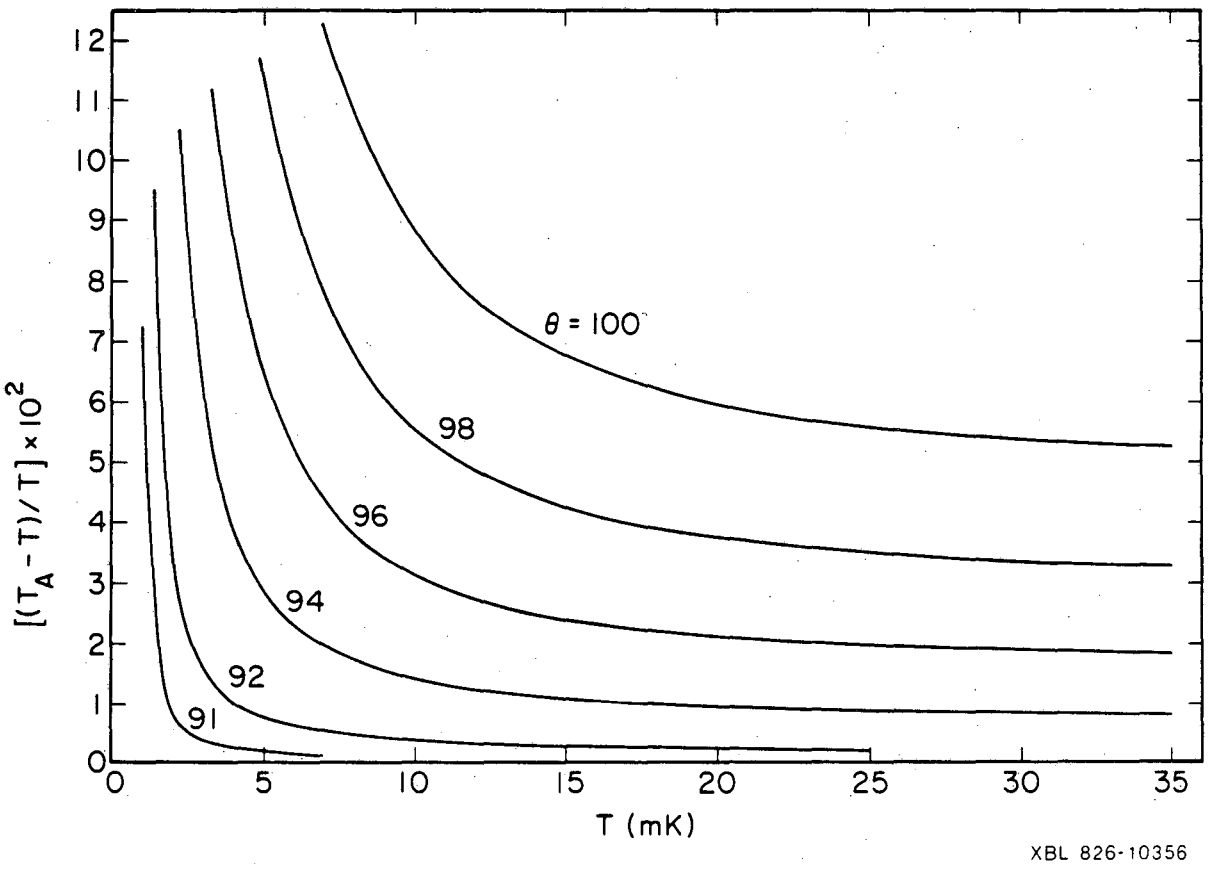

Fig. 11. The percentage temperature error due to the misalignment of the off-axis detector versus temperature. θ is the angular location (in degrees) of the detector with respect to the Co crystal c-axis, T_A is the apparent temperature (calculated assuming θ = 90°) and T is the correct temperature.

To illustrate the importance of statistical considerations on the NOT in these experiments, it is instructive to calculate the counting time required to achieve a one percent temperature uncertainty with various levels of statistical confidence. (The count rates used in this calculation are those for the 1.33 MeV ^{60}Co photopeak.) At 17 mK, the minimum temperature achieved in these experiments, counting times of 28, 111, and 249 minutes are required for 68.2%, 95.4%, and 99.7% confidence levels on axis while counting times of 5.3, 21.2, and 47.4 hours are required for a similar performance off axis. The much poorer performance off axis is due partly to a lower count rate but primarily to the intrinsically poorer thermometer sensitivity in that direction. At 50 mK, the highest temperature used in these experiments, counting times of 15.6, 62.4, and 140 hours are required for 68.2%, 95.4%, and 99.7% confidence levels on axis while off axis, the same performance requires 112, 448, and 1008 hours of counting time. Since reasonable temperature stability for these experiments was only available for periods up to ~20 hours (due to experimental constraints), it is clear that these statistical considerations are of extreme importance when evaluating the usefulness of the NOT at any given temperature. The above situation could be improved by using a ^{60}Co source with higher activity or by subtending larger solid angles with the detectors. However, the data for the above calculations were taken with the detectors as close to the source as possible and the source activity cannot be increased substantially due to thermometer self-heating difficulties (see Sec. VII). From this point of view, it

should be noted that the NOT is inherently inefficient as only ~0.4 percent of the γ-rays emitted by the source are counted under the photopeaks of the on-axis detector at a distance of 10 cm.

V. GERMANIUM RESISTANCE THERMOMETRY

As mentioned in the introduction, the most important goal of these experiments was the recalibration of two GRT, the GE1751 and the GE2345. These two low resistance thermometers (R ~5 Ω at 77 K and R ~ 40 Ω at 4.2 K), which are best suited as working thermometers for T < 1 K, had been calibrated previously using single crystal CMN and the conventional mutual inductance bridge in a blind extrapolation of the vapor pressure temperature scale to temperatures below 1 K. The recalibration utilized our current vapor pressure scale as represented on a medium resistance thermometer, the GE2776 (R = 5 Ω at 77 K and R = 240 Ω at 4.2 K), and its extrapolation to low temperatures via powdered CMN where it was independently checked with the NOT. All three of the GRT were obtained from Cryocal, Inc.[46] and are standard encapsulated four lead devices having either nitrogen or no exchange gas in the housing.

Since the subject of resistance thermometry has received a thorough treatment in the literature,[47] the arrangement used in these experiments, which has been employed in the laboratory for a number of years, will be discussed only briefly. The thermometer current supply is driven by a 10.8 volt mercury battery pack which, along with a resistance network, approximates a constant current supply. The thermometer current passes through one of several Leeds and Northrup[48] standard resistors (0.01 percent) such that an appropriate voltage measurement across the resistor determines the thermometer current precisely and accurately. The voltage across the

standard resistor and across the thermometer resistance element is measured with a six dial Rubicon double potentiometer. The power for the potentiometer is also derived from mercury batteries, thus avoiding ac derived power sources which may cause difficulties with ground loops and ripple. When measuring the voltage across the thermometer, it is frequently convenient to operate the potentiometer off null, particularly during heat capacity experiments when the temperature of the system is usually drifting slowly. The off-null voltage of the potentiometer is then amplified with a Keithley Model 147 nanovolt null detector,[49] typically by a factor of 10^5 or 10^6, and then displayed on a Speedomax recording potentiometer.[48] This output voltage may be calibrated in units of the Rubicon potentiometer dials so that the null voltage on the potentiometer may be determined at any desired time. Since this system operates at dc, measurements of and small corrections for the thermal voltages generated in the thermometer circuit must be made. The resistance value of a thermometer at any desired point may then be determined by dividing the corrected thermometer voltage by the thermometer current.

For low noise operation of this system, all pairs of conductors must be carefully shielded to avoid pickup in the cables connecting the electronics rack to the cryostat. To eliminate ground loops, the entire system is grounded to power line ground at a single point--that point being the low side of the Keithley 147 output. Finally, to minimize thermal voltages in the thermometer circuit, the lead system in the cryostat is constructed in a symmetric fashion.

In an earlier calibration in a different apparatus, the GE2776 was carefully calibrated against the GE897 which carries the laboratory temperature scale for 0.3 K < T < 30 K. For the present work, the 1-4 K region, for which the laboratory temperature scale is a representation of the $^3He/^4He$ (T_{62}/T_{58}) vapor pressure scale, was of primary concern. In this region, the calibration of the GE2776 thermometer utilizes 28 data points spaced at intervals of ~ T/20. Each data point consisted of determining the resistance of each thermometer at a common constant temperature. After converting the resistances of the GE897 to temperatures, the R_{2776} versus T_{897} data were fit by a power series of the form

$$T_{897}^{-1} = \sum_n A_n(\log_{10}R_{2776})^n \qquad (18)$$

to find the coefficients A_n. A difference table of $(T_{897}-T_{fit})/T_{fit}$ was generated to compensate for systematic deviations from the fit. The fit coefficients and the resulting difference table then completely define the helium vapor pressure temperature scale on the GE2776 thermometer.

VI. EXPERIMENTAL LAYOUT AND PROCEDURES

The dilution refrigerator used in these calibrations was homemade and produced temperatures of ~0.015 K on the outside of the mixing chamber. The graphite-copper structure shown in Fig. 12, which surrounded the dilution refrigerator, was designed to support a variety of experiments. Since the experimental arrangement was largely dictated by the requirements of proposed experiments on liquid ^{3}He, and only the thermometry experiments conducted with it are of concern here, several of the considerations leading to this complex design will not be dealt with.

The "^{4}He pot stage" was a cylindrical piece of oxygen-free high-conductivity (OFHC) copper which fit around and was attached to the ^{4}He refrigerator. It was designed to be refrigerated to ~1.25 K and to serve as a support for the lower portions of the apparatus. A lip machined around its outer edge held a radiation shield which surrounded the entire low-temperature stage. The next stage, referred to as the "mixing chamber stage," was also of cylindrical symmetry and made of OFHC copper. As shown in Fig. 12, this stage was positioned around the lower portion of the dilution refrigerator. It was suspended from the ^{4}He pot stage via six graphite rods (which provided thermal isolation) and made thermal contact to the mixing chamber through a copper braid-threaded mechanical copper joint assembly. These threaded copper joint assemblies are known to give excellent thermal contact.[50] The main thermometer bus, which was suspended from the mixing chamber stage by three graphite rods, was a relatively massive ring of OFHC copper to which all of the thermometers used in these experiments were attached.

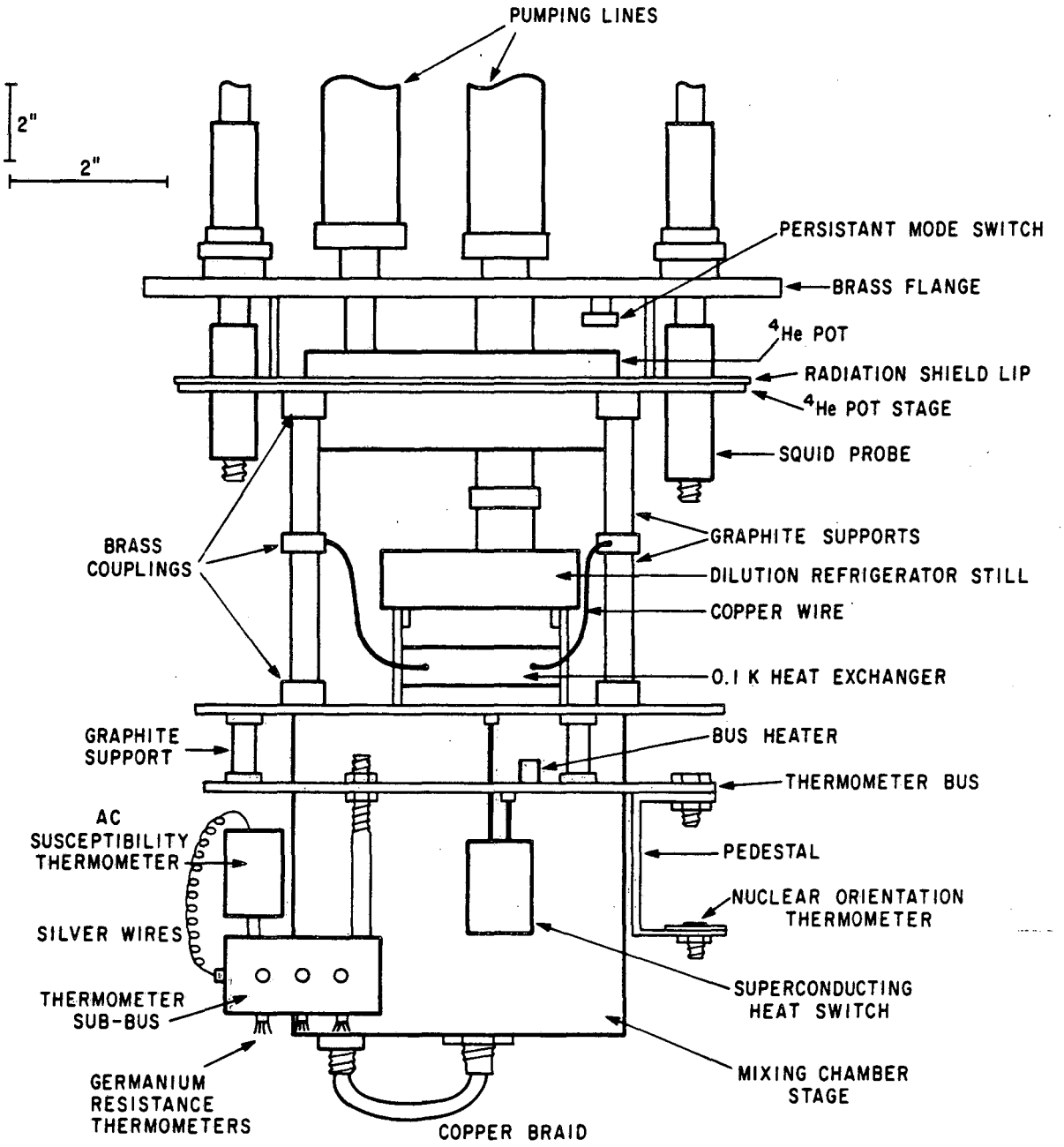

Fig. 12. The cryogenic layout of the thermometry experiment. The dc susceptibility thermometer (not shown) was mounted on the thermometer bus behind the mixing chamber stage.

The bus was thermally connected to the mixing chamber stage via a superconducting heat switch utilizing high purity 0.02 in. diameter Pb wire. The Pb wire was indium soldered to copper wires which were in turn connected to the two copper stages with threaded copper joints. The bus could then be thermally connected or isolated from the mixing chamber stage depending upon whether the field in the surrounding superconducting solenoid was on or off. The superconducting solenoid was wound with 0.006 in. diameter Nb wire on brass formers in two opposing sections and was attached to the wall of the mixing chamber with nylon screws using a thin piece of mylar and GE7031 varnish to achieve electrical isolation. The inner section of the solenoid had 591 turns/cm on a 1.02 cm diameter former while the outer section had 262 turns/cm on a 1.54 cm diameter former. This design generated the necessary critical field (~800 G) inside the solenoid with a current of ~2.5 A. It also resulted in the dipole moment of the solenoid being very nearly zero, substantially reducing the fringe field of the solenoid in the experimental volume. As will be described in some detail in Secs. VIII and IX B, this fringe field was still large enough to interfere with some of the dc susceptibility measurements on CMN. The heat switch solenoid was equipped with a persistent mode switch to allow the switch to remain closed without dissipating heat in the ^{4}He bath. This feature proved essential as the power generated in the solenoid leads greatly diminished the helium bath life of the experiment. The persistent mode switch was placed on the underneath side of the brass top of the vacuum can such that heat generated by its heater was released harmlessly to the bath.

Since a heater was employed on the bus to regulate temperatures at desired values, a crucial design consideration was to ensure that temperature gradients in the bus produced by the heater power were negligible insofar as equilibrium between the various thermometers was concerned. Reasonable estimates can be made of the heat flow through the graphite supports and the heat switch as well as the resulting temperature gradients in the bus using the data in Table I. It will become apparent as the experimental procedures are discussed that it is convenient to divide the full temperature range into three intervals:

(1) $T \lesssim 0.1$ K. In this region, the heat switch must be closed to attain the desired temperatures. This is because the background sources of heating such as radiation and vibration combine with the high thermal resistance of the open heat switch and the graphite supports to maintain a steady-state temperature on the bus of ~0.1 K even though the mixing chamber stage is at 0.015 K. With the heat switch closed, the data in Table I indicate that almost all the input heater power required to regulate the bus will pass through the switch. For this reason, the bus heater was located on the bus at the point of contact of the heat switch lead. In this way the vast majority of the heat will not pass through a significant length of the bus to create thermal gradients. The actual bus gradients may be estimated by calculating the heat leak through the three graphite supports and assuming that this heat passes through an effective length of the copper bus equal to one-half its circumference. Using the data in Table I, the heat flow through the graphite rods when the bus is at 0.1 K (worst case) is

Table I. Pertinent data for calculating the heat flux from and temperature gradients in the thermometer bus. A is the cross sectional area, l is the length and κ is the thermal conductivity of the appropriate material.

	Graphite	Normal Pb	Superconducting Pb	OFHC Cu
A/l (cm)	0.520	2.03×10^{-3}	2.03×10^{-3}	6.45×10^{-2}
κ(W/cm-K)	$5.0\times10^{-6}T^{1.86}$ [a]	$2.9\ T^{0.98}$ [b]	$2.1\times10^{-2}T^{3.3}$ [c]	$1.5T^{0.93}$ [d]
κA/l (W/K)	$2.6\times10^{-6}T^{1.86}$	$5.9\times10^{-3}T^{0.98}$	$4.2\times10^{-5}T^{3.3}$	$9.7\times10^{-2}T^{0.93}$

[a] Ref. 51
[b] Ref. 52
[c] Ref. 53
[d] Ref. 54

$$\dot{Q}_{gr} = \int_{0.016}^{0.10} 2.6 \times 10^{-6}\ T^{1.86}\ dT = 1.2 \times 10^{-9}\ W\ . \qquad (19)$$

This heat flux flowing through the bus at 0.1 K produces a temperature difference

$$\Delta T_{bus} = \frac{1.2 \times 10^{-9}}{(9.7 \times 10^{-2})\ (.1)^{.93}} = 1.1 \times 10^{-7}\ K \qquad (20)$$

in the bus which is orders of magnitude too small to be of concern. As an aside, note that the calculated heat flux through the open heat switch at 0.1 K is $\sim 4.9 \times 10^{-10}$ W. This indicates that the total heat flow necessary to maintain the bus at 0.1 K while the mixing chamber stage is at 0.015 K is only 1.7×10^{-9} W.

(2) 0.1 K < T < 1.0 K. Above 0.1 K, the regulation power input may be reduced substantially by opening the heat switch. However, even in this configuration, the heat switch dominates the heat flux between the bus and the mixing chamber stage. The bus gradients in this range may be estimated with a calculation similar to that in Eqs. (19) and (20). The heat flux through the graphite with the bus at 1 K is $\dot{Q}_{gr} = 9.1 \times 10^{-7}$ W and the resulting temperature difference in the bus is $\Delta T_{bus} = 9.4 \times 10^{-6}$ K. The expected gradient is again found to be negligible.

(3) 0.75 K < T < 3.75 K. In this region, the heat switch remained open. However, this interval is described separately since the regulation power became so large (the heat switch became a relatively poor thermal resistance as the T_c of Pb was approached), that normal dilution refrigerator operation was disrupted. Instabilities developed in the refrigerator and temperature regulation became exceedingly diffi-

cult. This problem was eliminated by circulating only a small portion of the $^3He/^4He$ mixture in the refrigerator which resulted in cooling the mixing chamber to ~0.75 K. Subsequent regulation of the bus to 3.75 K was then achieved without any temperature instability problems. Estimating the heat flux and the resulting thermal gradient in the bus results in $\dot{Q}_{gr} = 3.9\times10^{-5}$ W and $\Delta T_{bus} = 1.2\times10^{-4}$ K which is only a 0.003 percent uncertainty in the bus temperature at 3.75 K.

The above calculations, which guided the design of the apparatus, indicate that even if the estimated thermal conductances (which are average values taken from the literature) are in error by an order of magnitude, significant thermal equilibrium problems on the bus are not expected in any of the three operating ranges.

The validity of the above design estimates may be checked by using subsequent experimental data on the power required to regulate the bus at different temperatures. Several examples follow: (1) T = 0.112 K. Here, the heat switch was closed and the observed regulation power was 6.6×10^{-6} W. For this power input, the refrigeration curve of the dilution refrigerator indicates that the mixing chamber temperature was ~0.050 K. The calculated heat fluxes are

$$\dot{Q}_{gr} = \int_{0.05}^{0.112} 2.6\times10^{-6}T^{1.86}dT = 1.5\times10^{-8}\ W \qquad (21)$$

and

$$\dot{Q}_{hs} = \int_{0.05}^{0.112} 5.9\times10^{-3}T^{0.98}dT = 3.1\times10^{-5}W \qquad (22)$$

where $\dot{Q}_{hs}$ is the heat flux through the heat switch. Hence, the observed heat flux is ~5 times smaller than predicted. (2) T = 0.505 K. The heat switch was open at this temperature and the observed regulation power was 8.2×10^{-7} W. The heat fluxes are predicted to be $\dot{Q}_{gr} = 1.3\times10^{-7}$ W and $\dot{Q}_{hs} = 5.2\times10^{-7}$ W for a total heat flow of 6.5×10^{-7} W which is only 25 percent less than that observed. (3) T = 0.867 K. The heat switch was again open and the observed regulation power was 4.9×10^{-6} W. Here the predicted heat fluxes are $\dot{Q}_{gr} = 6.0\times10^{-7}$ W and $\dot{Q}_{hs} = 5.3\times10^{-6}$ W for a total of 5.9×10^{-6} W which is only 15 percent more than observed. (4) T = 3.024 K. At this point, the mixing chamber stage was found to be at 0.78 K and the regulation power was 7.2×10^{-4} W. The predicted heat fluxes are $\dot{Q}_{gr} = 2.1\times10^{-5}$ W and $\dot{Q}_{hs} = 1.14\times10^{-3}$ W for a total of 1.2×10^{-3} W which is ~40 percent greater than observed. Thus, the predictions are in reasonable agreement with subsequent experimental observations (especially considering that the thermal conductivities of Pb and graphite may vary by as much as an order of magnitude from sample to sample depending upon purity, sample preparation details, etc.). This level of agreement gives confidence that the design estimates were reasonable and all thermometers on the bus were in adequate thermal equilibrium under all experimental conditions.

In the planning stage of these experiments, the experimental data to justify the above calculations were, of course, not available so an even more conservative approach to the design was taken. The ac susceptibility thermometer and the three GRT were placed on a separate bus (referred to as the sub-bus in Fig. 12) which was attached to the

main bus by a 0.25 in. diameter OFHC copper rod utilizing threaded joints for thermal contact. Since the sub-bus was an appendage to the main bus, the only heat currents flowing through it were those due to radiation, vibration and the inevitable joule heating of the GRT, all of which were negligible. Hence, all sub-bus thermometers were expected to be in excellent thermal equilibrium. The NOT was not placed on the sub-bus since it was only employed in the lower temperature range where the regulation power was either small or nonexistent. In the later calibration experiments, the dc susceptibility thermometer was added owing to a suspicion that the ac susceptibility thermometer was in error for $T < 0.1$ K. Although it should logically have been placed on the sub-bus, space limitations prohibited doing so. It was simply screwed into the main thermometer bus approximately equidistant between the sub-bus and the NOT (not visible in Fig. 12) since at that time the experimental data verifying the heat leak projections were in hand.

The sub-bus was a plate of OFHC copper with dimensions 2 in. x 2 in. x 0.25 in. Three holes were drilled into one edge to accomodate the GRT, Apiezon N grease being used for thermal contact. Three short copper rods, which had been welded to the sub-bus, served as thermal anchor posts for the leads to the GRT thus ensuring no direct heat leaks into the resistance elements. The ac susceptibility thermometer screwed into the sub-bus and the silver wires, which penetrated the CMN slurry, were soldered into a short threaded copper rod which was in turn screwed into the sub-bus to make thermal contact.

The NOT employed ^{60}Co in hcp ^{59}Co with an activity level of ~2 μCi. The crystal was cut in the form of a disk ~1 cm in diameter and ~1/2 mm thick. Thermal contact to the crystal was made by soft soldering it onto the flat head of an OFHC copper screw. This crystal-screw assembly was subsequently mounted in an x-ray diffractometer to determine the location of the c-axis of the hcp structure. The c-axis was found to lie within one degree of the plane of the disk and its orientation on the surface of the disk was recorded by a parallel scribe mark. The assembly was then screwed and soldered into a rectangular copper slab (2.5 cm x 0.9 cm x 0.15 cm) such that the long dimension of the slab was parallel to the scribe mark on the Co crystal (the screw projected through the slab by ~1/2 in.). The copper slab was used only as part of the alignment mechanism and played no role in establishing thermal contact. As shown in Fig. 12, a support pedestal for the NOT was attached to the main thermometer bus. The pedestal was fabricated from brass and copper (the brass providing strong mechanical support and the copper providing a high thermal conductivity path) and had a lower platform whose dimensions matched those of the copper slab. The NOT assembly was screwed into the platform of the pedestal, stopping at a point when the sides of the copper slab and platform were parallel. The assembly was then locked into place with a copper nut. Thus, the c-axis of the crystal should have been parallel to the sides of the platform and thermal contact to the bus was maintained via a continuous path of OFHC copper. To align the c-axis of the crystal with the scintillation counters, the orientation

of the platform upon which the NOT crystal was mounted had to be determined. This was done as follows: A "pointer" was machined from brass and designed to have one end mate snugly with the bare copper-brass platform. The c-axis of the crystal was then coincident with a line bisecting the pointer. Two grooves were cut into the brass, groove 1 being located exactly 6.00 in. from the center of the NOT mounting location. Two plumb bobs were hung from a rigid aluminum arm attached to the carefully leveled top flange of the apparatus. The plumb bobs were located on the aluminum arm such that their support wires passed exactly through the grooves cut in the brass pointer. Both the position of the NOT crystal and the direction of its c-axis were then known relative to the positions of the two plumb bobs. It was a simple matter, after mounting the crystal and placing the apparatus in the cryostat, to align the scintillation counters relative to the plumb bob locations. An uncertainty in the location of the c-axis of less than two degrees and an uncertainty in the location of the crystal center of ~1.5 mm are estimated. At 0.015 K, a two degree error in the c-axis determination results in on-axis and off-axis temperature errors of only 0.14 percent and 0.26 percent, respectively.

A systematic error in the NOT temperature will occur if the Co crystal runs "hot"--that is, if the combination of the heat generated by beta decay and the thermal resistance of the crystal to the bus is such as to generate a significant temperature difference between the bus and the crystal. This possibility may be examined in the following way: After taking data with the NOT at some very low temperature,

an amount of heat equal to or greater than the estimated beta heating can be put into the top of the Co crystal by means of an external heater. This heat must, of course, flow through the crystal-bus interface along with the everpresent beta decay heat and the resulting temperature difference across the interface will increase. By monitoring the NOT (which gives the temperature of the crystal) and the CMN thermometers (which give the bus temperature) and by using increasing power levels in the NOT heater, it will become apparent if the inherent beta heating results in a significant self-heating of the Co crystal. With this in mind, a small heater assembly was constructed by wrapping 575Ω of 0.001 in. diameter Pt-W heater wire around a copper foil cylinder, thermal contact being made with GE7031 varnish. The foil supporting the heater was attached to the top of the Co disk with varnish, being careful not to short the foil directly to the copper portion of the crystal platform. Since the cobalt crystal had ~2 μCi of ^{60}Co, the beta heating was estimated[37] to be $\sim 1.3 \times 10^{-9}$ W. The heater dissipated this power when using a current of 1.5 μA.

Before concluding this section, several comments concerning the key steps in the development of the low-temperature stage of the apparatus are in order. As stated above, the free-standing dilution refrigerator attained a minimum temperature of ~0.015 K (without a radiation shield). In the first experiment, after adding the copper-graphite structure, the ^{4}He pot stage cooled to only 1.8 K (instead of 1.25 K) and the thermometer bus to only 0.080 K. Several experiments were required to elucidate the difficulties leading to this unsatis-

factory performance. Briefly, three main changes were required to return the system to normal operating conditions: (1) The ^{4}He pot stage was not thermally anchored to the pot adequately. This was important as the temperature of this stage determined the heat leak down the graphite rods to the mixing chamber stage. Since the thermal conductivity of graphite is proportional to T^2, the heat leak is proportional to T^3 and was three times larger than anticipated. Additional thermal links to the pot resulted in refrigerating the ^{4}He pot stage to 1.25 K, thus eliminating this problem. (2) To reduce the heat leak from the 1.25 K stage to the mixing chamber stage even further, copper clamps, which were thermally connected to the 0.1 K exchanger of the dilution refrigerator, were varnished to the surface of the graphite rods near their midpoint. This technique proved to be only marginally effective and superior performance was achieved only after replacing the existing graphite rods with ones which had brass couplings (refrigerated to 0.1 K) at their midpoints. This would seem to suggest that the copper clamps were unable to achieve adequate thermal contact to the graphite. (3) A significant reduction in the minimum temperature resulted from the use of the radiation shield in the experiments. This shield, which was supported from the ^{4}He pot stage and thus refrigerated to 1.25 K, was constructed of copper and enclosed the whole of the experimental volume below the 1.25 K stage.

VII. NUCLEAR ORIENTATION THERMOMETER DEVELOPMENT AND SELF-CONSISTENCY TESTS

At first glance, using an NOT to measure low temperatures appears to be a straightforward task--the intensity of the radiation from the crystal in a known direction is measured at both high and low temperatures and the low temperature is calculated from the ratio of the intensities using the theory expressed in Eq. (11). However, this simple picture assumes that only those γ-rays which are emitted into the solid angle subtended by the detector are counted. In practice, this is certainly not the case since, as shown in Fig. 8, the experimental environment unavoidably gives rise to a substantial amount of γ-ray scattering. As a result, a large number of the γ-rays counted by the detector are not emitted by the source directly into the solid angle subtended by the detector. Since γ-rays lose energy in Compton scattering events, this difficulty may be minimized by counting only those events which occur in the energy range of the photopeaks, i.e., those γ-rays for which the energy loss is minimal. However, it is not clear over what energy range a temperature determination is sufficiently immune to scattering complications and, in the case of ^{60}Co, it is tempting to analyze the 1.17 MeV peak along with the 1.33 MeV line even though the former lies in the Compton background of the latter. (This temptation arises from a desire to acquire good statistics as rapidly as possible during an experiment.) In the past, most experimentalists have simply counted the two photopeaks of ^{60}Co in the 1.0-1.5 MeV range with a single channel analyzer and have not

systematically examined the influence of the energy region of the analysis on the deduced temperatures. In the experiments reported here, since the data were recorded with a multichannel analyzer, independent temperature determinations from the same spectra could be carried out using, for example, the four energy regions illustrated in Fig. 13 as A, B, C, and D. (Before summing over the indicated regions of interest, a "background" spectrum, which was acquired by running the γ-ray spectrometer without the ^{60}Co source present, was subtracted from the experimental spectra. The background spectrum served to correct the experimental spectra for environmental radiations--particularly ^{40}K which has a γ-ray line at 1.460 MeV and occurs in the concrete of the laboratory. After correcting the spectra for background radiations, the ^{60}Co data were summed over the four regions of interest and independent temperatures were calculated.) Some results from the on-axis detector, which are typical of all the NOT spectra, are 17.13, 17.09, 16.92, and 17.09 mK for regions A, B, C, and D, respectively. (The spread in the off-axis temperatures is somewhat greater owing to the poorer thermometer sensitivity in that direction.) These results appear to preclude any substantial systematic influence (>1 percent in temperature) of γ-ray scattering upon deduced temperatures in the 1.0-1.5 MeV range and thus allow the use of any convenient energy interval in this range for experimental analysis. This result is indirectly consistent with those of Soulen and Marshak[12] who found that ^{60}Co temperatures, which were calculated using the 1.0-1.5 MeV range, were in agreement with independent

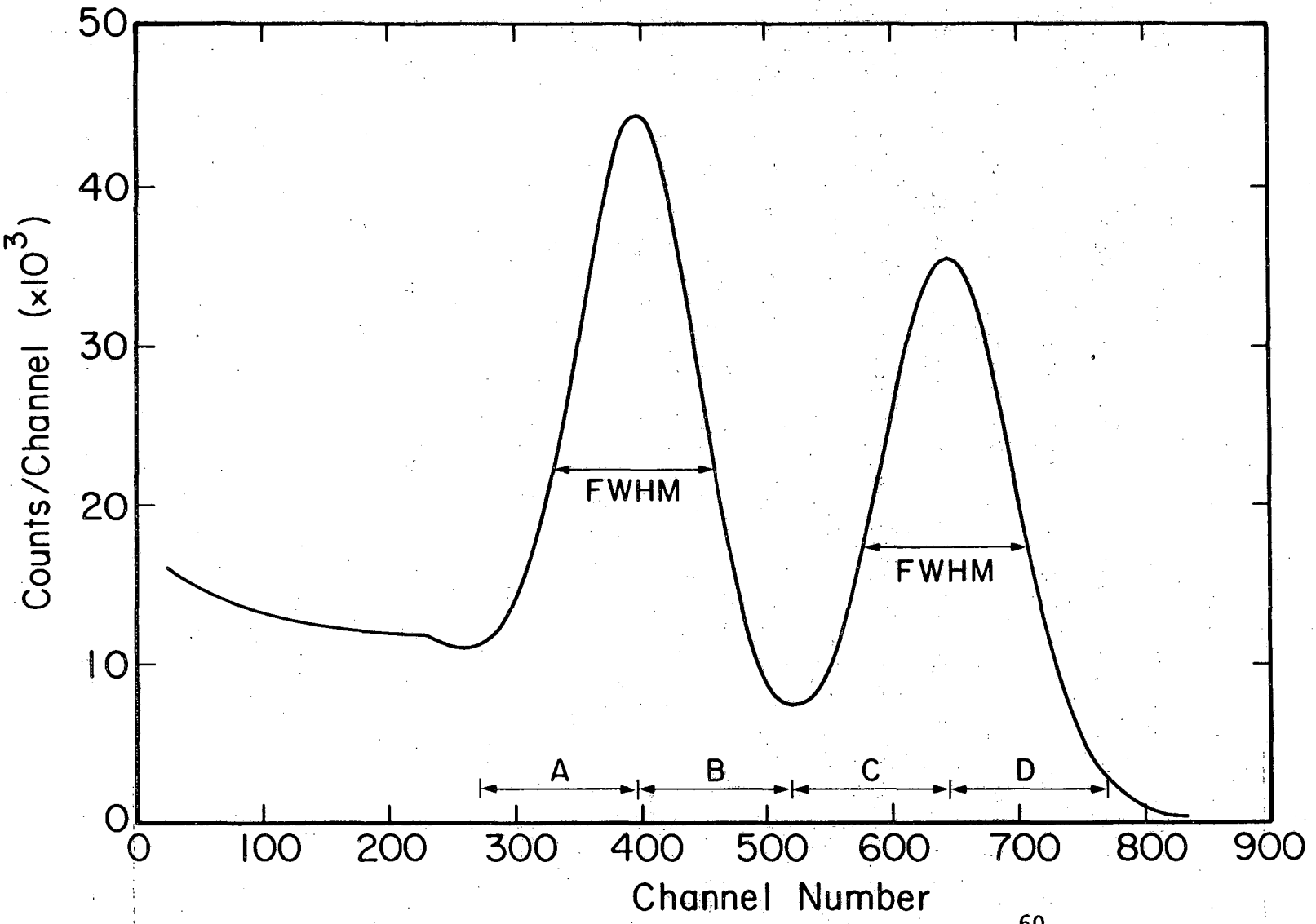

Fig. 13. Spectrometer data illustrating the 1.17 and 1.33 MeV photopeaks of ^{60}Co in XBL 8210-2842 counts/channel versus analyzer channel number. Temperatures have been determined using regions A,B, C, and D to examine the influence of the energy interval on the calculated temperatures. Also illustrated are the FWHM regions which were frequently employed in temperature determinations.

absolute temperatures from a Johnson noise thermometer to ~1/2 percent. If the Compton scattering background of the 1.33 MeV peak under the 1.17 MeV peak had a substantial influence on deduced temperatures, such agreement would not be expected. A more extensive analysis of the temperatures deduced from the 1.17 MeV and 1.33 MeV peaks will be presented later.

In the earliest experiments with the NOT, there were clearly difficulties in maintaining a constant gain in the NOT electronics. This could be seen by a visual examination of the ^{60}Co spectra on the cathode ray tube display. Since it was not unusual for the γ-ray peaks to shift by 5-10 channels (0.65 keV/channel) on a day-to-day basis, it was decided to introduce gain stabilizers into the system at that time (see Sec. IV). When operated properly, the stabilizers were able to regulate the gain such that the visual drift in the spectra was no longer apparent. Thus, to see if the system was performing to within statistics, another test of stability had to be developed.

In the discussion on statistics in Sec. IV, it was concluded that repetitive measurements of the number (N) of γ-rays counted in a specified energy range for a time t will define a Gaussian distribution which has a standard deviation $\sigma = \bar{N}^{1/2}$ where $\bar{N}$ is the true mean value of N. In the context of that discussion, the time interval t was very long (10-20 hours) so as to minimize the fractional uncertainty $N^{1/2}/N$ and a given measurement of N was made only once. It was then assumed that $N^{1/2}$ represented the usual statistical variation about the true mean. This approach is fine if the NOT system is rigorously

stable. However, to determine if this is in fact the case, the above statistical arguments may be used in the following way: The total counting time of 10-20 hours is divided into a number of subintervals, the number of γ-rays detected over a specified energy range (spectrum integrals) being determined for <u>each</u> short interval. Since the short spectrum integrals should also define a distribution about a true mean value, an examination of the deviations of the spectrum integrals from the experimental mean ($\bar{N}_{exp}$) should yield $\sigma \sim (\bar{N}_{exp})^{1/2}$. If over the total counting time the NOT system has been unstable, the distribution of N about the mean will be wider than expected and $\sigma > (\bar{N}_{exp})^{1/2}$. It is important that the number of such short intervals be rather large--otherwise it is difficult to determine if deviations of σ from $(\bar{N}_{exp})^{1/2}$ are due to electronic instabilities or due to the statistics associated with a small sample of events. Thus, while 10-20 subintervals, whose computations may be done easily by hand, yield marginal results, the best results were only obtained with 100-200 subintervals of 200-500 seconds of counting time each. Efficient handling of this amount of data required the writing of a computer program to read the data on the seven track tape and do the appropriate statistical analyses. An analysis which is typical of all such long counting intervals reported in this thesis is given in Table II. The energy intervals used in this analysis utilize full-width at half-maximum (FWHM) integrals for each peak from each detector--hence the four independent analyses. The FWHM interval was chosen because of symmetry considerations since, to first order, the

Table II. Statistical analysis of the on- and off-axis ^{60}Co photopeaks to check the γ-ray spectrometer stability. N1, N2, N3, and N4 are the FWHM integrals while $\overline{N1}$, $\overline{N2}$, $\overline{N3}$, and $\overline{N4}$ are the respective mean values of the integrals. σ is the calculated standard deviation of each distribution and N_{TOT} is the sum of all integrals for each photopeak. A total of 164 spectra, each being 300 seconds in length, have been analyzed.

	ON AXIS				OFF AXIS			
Index	N1	$\overline{N1}$-N1	N2	$\overline{N2}$-N2	N3	$\overline{N3}$-N3	N4	$\overline{N4}$-N4
1	30810	91	25046	0	17144	11	13701	90
2	31019	-118	25159	-113	17241	-86	13797	-6
3	30823	78	25074	-28	17057	98	13866	-75
4	31287	-386	24982	64	17178	-23	13886	-95
5	31006	-105	25085	-39	16904	251	13877	-86
6	30573	328	24943	103	17096	59	13691	100
7	30852	49	24803	243	17212	-57	13921	-130
8	30554	347	25169	-123	17151	4	13714	77
9	30878	23	25061	-15	17067	88	13803	-12
10	30620	281	25060	-14	17221	-66	13920	-129
11	30537	364	25268	-222	16993	162	13848	-57
12	30829	72	25028	18	17137	18	14000	-209
13	30548	353	24935	111	17535	-380	13695	96
14	31328	-427	24962	84	16991	164	13836	-45
15	30691	210	25298	-252	17166	-11	13874	-83
16	30973	-72	25146	-100	17042	113	13847	-56
17	30807	94	25081	-35	17116	39	13928	-137
18	30823	78	25004	42	17151	4	13666	125
19	30971	-70	24772	274	17078	77	13678	113
20	31192	-291	24974	72	17185	-30	13936	-145
21	30884	17	25116	-70	17137	18	13740	51
22	30992	-92	25341	-295	17381	-226	13520	271
23	30865	36	25376	-330	17118	37	13695	96
24	30929	-28	25282	-236	17191	-36	13815	-24
25	30912	-11	25110	-64	17086	69	13868	-77
26	30860	41	24974	72	17314	-159	13635	156
27	30512	389	25261	-215	17044	111	13696	95
28	30783	118	24917	129	17339	-184	13848	-57
29	31156	-255	25051	-5	17194	-39	13829	-38
30	30997	-96	25090	-44	17075	80	13846	-55
31	30914	-13	24954	92	16873	282	13871	-80
32	30982	-81	24872	174	17442	-287	13563	228
33	30652	249	24741	305	17328	-173	13709	82
34	31191	-290	24874	172	17126	29	13771	20
35	30765	136	24690	356	17288	-133	13796	-5
36	30815	86	24729	317	17350	-195	13910	-119
37	30811	90	24959	87	17200	-45	13805	-14
38	31068	-167	24987	59	17098	57	13977	-186
39	30718	183	24868	178	17072	83	13796	-5
40	30975	-74	25044	2	17208	-53	13855	-64
41	30728	173	25176	-130	17155	0	13754	37
42	30863	38	24705	341	17123	32	13613	178
43	31054	-163	25117	-71	17210	-55	13938	-147
44	30602	299	25267	-221	17340	-185	14023	-232
45	30946	-45	25245	-199	17417	-262	13845	-54
46	30671	230	25105	-59	17121	34	13733	58
47	30816	85	25438	-392	17050	105	13614	177
48	30925	-24	24864	182	17285	-130	13669	122
49	30807	94	25076	-30	17162	-7	13914	-123
50	30639	262	25074	-28	17187	-32	13672	119
51	30994	-93	24928	118	17345	-190	13968	-177
52	31011	-110	25370	-324	16878	277	13673	118

Table II. (Continued)

	ON AXIS				OFF AXIS			
Index	N1	$\overline{N1}$-N1	N2	$\overline{N2}$-N2	$\overline{N3}$	$\overline{N3}$-N3	N4	$\overline{N4}$-N4
53	30848	53	25061	-15	17153	2	13736	55
54	30868	33	25103	-57	16875	280	13661	130
55	31088	-187	24946	100	16690	465	13404	387
56	31201	-300	25053	-7	17254	-99	13891	-100
57	31019	-118	25153	-107	17135	20	13823	-32
58	31214	-313	24998	48	17125	30	13656	135
59	30934	-33	24723	323	17107	48	13722	69
60	30744	157	24837	209	17241	-86	13604	187
61	30680	221	25181	-135	17187	-32	13726	65
62	30814	87	25175	-129	16973	182	13760	31
63	31132	-231	25012	34	17117	38	13949	-158
64	31142	-241	24940	106	17210	-55	13960	-169
65	30661	240	24948	98	17143	12	13683	108
66	30957	-56	25081	-35	17154	1	13954	-163
67	30825	76	25046	0	17360	-205	13681	110
68	30649	252	24640	406	17318	-163	13857	-66
69	31048	-147	24726	320	16888	267	13728	63
70	31155	-254	24945	101	17368	-213	13769	22
71	30928	-27	25207	-161	17331	-176	13679	112
72	30957	-56	25124	-78	17199	-44	13656	135
73	31087	-186	25068	-22	17072	83	13633	158
74	31299	-398	24903	143	17111	44	13730	61
75	30896	5	24956	90	17454	-299	13798	-7
76	31206	-305	25174	-128	17407	-252	13699	92
77	30890	11	25241	-195	17139	16	13734	57
78	31063	-162	25015	31	17358	-203	13771	20
79	31282	-381	24899	147	16971	184	13756	35
80	31201	-300	25369	-323	17176	-21	13643	148
81	30856	43	24852	194	17130	25	13954	-163
82	30812	89	25191	-145	17054	101	13899	-108
83	30935	-34	24963	83	17318	-163	13772	19
84	30805	96	25257	-211	17381	-226	14034	-243
85	30837	64	24949	97	17028	127	13986	-195
86	30857	44	25022	24	17052	103	13952	-161
87	30544	357	25003	43	17198	-43	13819	-28
88	30853	48	25078	-32	17180	-25	13795	-4
89	30874	27	25194	-148	17234	-79	13752	39
90	30824	77	25245	-199	17246	-91	13850	-59
91	31178	-277	25141	-95	17113	42	13744	47
92	30877	24	24823	223	17017	138	13632	159
93	30936	-35	25057	-11	17150	5	13767	24
94	30785	116	25106	-60	17350	-195	13798	-7
95	30925	-24	25029	17	16922	233	13869	-78
96	30875	26	25534	-488	17235	-80	13787	4
97	30967	-66	25009	37	17085	70	13845	-54
98	30940	-39	24943	103	16959	196	13875	-84
99	31125	-224	24890	156	17130	25	13787	4
100	31096	-195	25171	-125	17104	51	13794	-3
101	30828	73	25148	-102	16981	174	13620	171
102	30866	35	25117	-71	17302	-147	13822	-31
103	30808	93	24928	118	17007	148	13775	16
104	30846	55	24875	171	17067	88	14044	-253
105	30754	147	24827	219	17064	91	13733	58
106	30879	22	25048	-2	17129	26	13581	210
107	30958	-57	25136	-90	17034	121	13945	-154
108	31125	-228	25335	-289	17242	-87	13644	147
109	30934	-33	25076	-30	16974	181	13897	-106
110	31022	-121	25028	18	17099	66	13572	219
111	30967	-66	25138	-92	17078	77	13722	69
112	30620	281	24991	55	17067	88	13701	90
113	30570	331	25235	-189	17040	115	13724	67
114	30850	51	25041	5	17448	-293	14021	-230

Table II. (Continued)

	ON AXIS				OFF AXIS			
Index	N1	$\bar{N}1-N1$	N2	$\bar{N}2-N2$	N3	$\bar{N}3-N3$	N4	$\bar{N}4-N4$
115	30759	142	25073	-27	17214	-59	13960	-169
116	31324	-423	25026	20	17092	63	13870	-79
117	30717	184	24993	53	16979	176	13529	262
118	31133	-232	25088	-42	17170	-15	14016	-225
119	30749	152	25201	-155	17170	-15	13868	-77
120	30719	182	24823	223	17243	-88	13721	70
121	30511	390	25133	-87	17250	-95	13843	-52
122	31031	-130	25107	-61	17112	43	13904	-113
123	31309	-408	25108	-62	17165	-10	13748	43
124	30721	180	24841	205	17368	-213	13859	-68
125	30858	43	25059	-13	17199	-44	13750	41
126	30863	38	25073	-27	17148	7	13841	-50
127	30869	32	25111	-65	17248	-93	13733	58
128	31105	-204	25128	-82	17181	-26	14052	-261
129	30882	19	25170	-124	17465	-310	13797	-6
130	31261	-360	25093	-47	17147	8	13871	-80
131	30640	261	24983	63	17106	49	13846	-55
132	30928	-27	24950	96	17171	-16	13888	-97
133	30978	-77	24999	47	17333	-178	13859	-68
134	31046	-145	25092	-46	17062	93	13524	267
135	30748	153	25099	-53	17152	3	13858	-67
136	30694	207	24776	270	17376	-221	13944	-153
137	30895	16	25016	30	17100	55	13801	-10
138	31120	-219	25062	-16	16876	279	13742	49
139	30960	-59	24933	113	17183	-28	13479	312
140	30910	-9	25032	14	17105	50	13805	-14
141	31016	-115	24956	90	16976	179	13736	55
142	30702	199	24977	69	17127	28	13835	-44
143	30667	234	24930	116	17121	34	13812	-21
144	31146	-245	24863	183	17162	-7	13616	175
145	30769	132	25046	0	17179	-24	13803	-12
146	31052	-151	25161	-115	17174	-19	13729	62
147	30876	25	24839	207	17204	-49	13963	-172
148	30696	205	24974	72	17051	104	13973	-182
149	30880	21	25008	38	17347	-192	13744	47
150	30771	130	24945	101	17182	-27	13909	-118
151	31295	-394	25160	-114	17067	88	13865	-74
152	30914	-13	25077	-31	17093	62	13783	8
153	31021	-120	25193	-147	17049	106	13699	92
154	30851	50	25183	-137	17071	84	13788	3
155	30805	96	24956	90	17009	146	13592	199
156	30898	3	25189	-143	17096	59	13745	46
157	30913	-12	25262	-216	17166	-11	13623	168
158	30933	-32	25141	-95	17239	-84	13823	-32
159	30755	146	24932	114	17216	-61	13890	-99
160	30885	12	25053	-7	17230	-75	13836	-45
161	30887	14	24984	62	17042	113	13850	-59
162	30991	-90	25054	-8	17111	44	13870	-79
163	30933	-32	25245	-199	17222	-67	13696	95
164	30816	85	25123	-77	17061	94	13926	-135

	INTEGRAL 1	INTEGRAL 2	INTEGRAL 3	INTEGRAL 4
$\bar{N}$	30901	25046	17155	13791
$(\bar{N})^{\frac{1}{2}}$	175	158	130	117
σ	181	152	133	121
N_{TOT}	5067887	4107575	2813536	2261834
$(N_{TOT})^{\frac{1}{2}}$	2251	2026	1677	1503

integrals are insensitive to small shifts in the spectrometer gain. The analysis of each subinterval, which was 300 seconds long, proceeds by summing the channels in each FWHM region to get the four integrals for the γ-ray peaks. Background integrals, which are obtained by summing the same channels of the background spectrum, are then subtracted from the four integrals and the final results are tabulated as N1, N2, N3, and N4. When all the spectra have been analyzed, the program calculates the mean value of the integrals for each peak, the deviation of each integral from its mean value and the standard deviation of each of the four distributions. To determine if the data are within statistics, three related points are examined: (1) The results should indicate that $\sigma \sim (\overline{N}_{exp})^{1/2}$. (2) An examination of the deviations of the integrals from a mean value should find random signs and magnitudes as a function of time, i.e., no evidence of any systematic variations or oscillations should be apparent. (3) Gaussian statistics predict 68.3%, 95.4% and 99.7% of the integrals should be within 1σ, 2σ and 3σ of the mean, respectively. (The results of such tabulations of the data in Table II are shown in Table III.) The data in Table II satisfy all three tests and are thus considered to represent stable data. Finally, the program computes a "master" spectrum by summing the individual spectra channel by channel and subtracting the background spectrum channel by channel. In the case of the data in Table II, this corresponds to a single spectrum 13.7 hours in length. The results reported in Table II are typical of many such tests conducted during the course of the experiments and were

Table III. Comparison of the distribution of the photopeak integrals about their mean values with theory. The number of integrals within 1σ, 2σ, and 3σ of the mean are tabulated for each photopeak and expressed as a percentage of the total number of integrals (=164).

Range	Theory	Integral 1		Integral 2		Integral 3		Integral 4	
1σ	68.3 %	109	66.5 %	111	67.7 %	115	70.1 %	108	65.9 %
2σ	95.4 %	152	92.7 %	153	93.3 %	152	92.7 %	156	95.1 %
3σ	99.7 %	164	100 %	163	99.4 %	163	99.4 %	163	99.4 %

taken as evidence of successful gain stabilization over periods of 10-20 hours.

When the stability of the spectrometer is examined on a longer time scale, a somewhat different picture emerges. The most convenient way to analyze long term stability is to examine the high-temperature normalization data throughout an experiment. After correcting for the ^{60}Co half-life of 5.27 years, the count rate (and hence the spectrum integrals) should be constant to within statistics. In Table IV, the results of such an analysis which span 31 days are presented. Once again, the four ^{60}Co photopeaks have been integrated using FWHM regions of interest. In general, the total counting times of the spectra (9.7-27.8 hours) are not the same so the total number of counts (N_{TOT}) in each photopeak of each spectrum were normalized to a 55,000 second period and are tabulated in the table. After calculating mean values, the deviation of each of the four spectrum integrals from their respective mean was determined. To obtain proper statistical weighting for a given spectrum, the mean was scaled to the actual time of that spectrum and $N_{TOT} - N_{MEAN}$ determined in units of $(N_{MEAN})^{1/2}$. These deviations (δ) are tabulated in Table IV. As 68 percent of the observations are expected to be within 1σ of the mean, the data clearly are not in accord with statistics. The most conspicuous deficiency, which is observed in all four sets of integrals, is an apparently increasing count rate as a function of time. This result is not surprising, however, since expectations of absolute stability of the spectrometer over a period of a month are unrealistic[55] (and unnecessary for

Table IV. Long term stability test of the NOT spectrometer using high-temperature normalization data from Run 5. The data, which were taken over a 31 day period, have been corrected for the intrinsic decay of the ^{60}Co source. Individual master spectra, which vary in length from 9.7–27.8 hours, are labeled by their magnetic tape tagword (e.g., SE0023). The photopeak integrals N1, N2, N3, and N4 have been evaluated using FWHM regions of interest between fixed analyzer channels. The calculation of the mean values and the deviations from the mean, δ, (expressed in standard deviation units) are discussed in the text.

		ON AXIS				OFF AXIS			
Label	Day	N1	δ_{N1}	N2	δ_{N2}	N3	δ_{N3}	N4	δ_{N4}
SE0023	0	5,082,174	-3.2	4,006,682	-2.2	2,815,064	-1.2	2,297,542	-2.1
SE0030	4	5,084,145	-1.7	4,008,845	-0.7	2,813,939	-1.6	2,296,097	-2.6
SE0039	9	5,085,710	-1.0	4,009,438	-0.4	2,817,597	+0.6	2,297,891	-1.4
SE0041	11	5,084,074	-1.4	4,011,187	+0.4	2,814,654	-1.0	2,300,051	0.0
SE0052	15	5,091,417	+2.1	4,008,279	-1.3	2,815,181	-1.2	2,299,650	-0.6
SE0056	17	5,089,862	+0.9	4,008,865	-0.7	2,811,229	-3.2	2,299,426	-0.4
SE0058	26	5,088,026	0.0	4,012,925	+1.1	2,820,186	+1.7	2,302,998	+1.5
SE0059	28	5,092,523	+2.4	4,013,341	+1.8	2,823,037	+4.4	2,303,559	+2.7
SE0061	31	5,093,264	+3.1	4,012,052	+1.1	2,819,168	+2.2	2,303,587	+3.0
Mean		5,087,911		4,010,179		2,816,673		2,300,089	

γ-ray thermometry). More importantly, disturbing variations in the integrals on a day-to-day basis occur periodically. One source of this difficulty is believed to be the poor temperature stability in the laboratory--variations of 5°F are not uncommon and in extreme situations, 15-20°F variations over a 24 hour period have been observed. The light output of the NaI(Tl) crystals and the gain of the photomultiplier tubes are well known to be temperature dependent although the gain stabilizers should act to compensate for these effects. Indeed, the feedback voltages generated by the stabilizers clearly respond to changes in the room temperature. Significantly, there is also evidence that temperature variations adversely affect the performance of the stabilizers themselves. Although data similar to that in Table II indicate stable performance of the spectrometer over 10-20 hour intervals, the data in Table IV reveal that non-statistical behavior does occur occasionally over intervals of several days. It thus appears that such behavior is gradual enough to escape detection by the statistical criterion used in Table II but may be observed using the methods employed in Table IV. In any case, non-statistical temperature variations were observed periodically. From the results of Tables II and IV, two important conclusions may be drawn: First, it is imperative that the high- and low-temperature data required to calculate NOT temperatures be taken as close together as possible to minimize the effects of spectrometer drift. In the experiments reported here, the general procedure was to warm to 0.5 K after completing a low-temperature count and to begin acquiring

high-temperature normalization data immediately. For very important NOT determinations, high-temperature data were taken both before and after the low-temperature data. Second, since the occurrence of non-statistical behavior is unpredictable, significant NOT determinations should be repeated several times in order to ensure accurate results.

It is important to note that nonstatistical spectrometer performance does not necessarily yield unacceptable results. For example, a 15 hour spectrum at 17 mK, which utilizes FWHM integrals, has an on-axis 1σ uncertainty of 0.17 percent in temperature. Thus, two successive observations that differ by 2σ (which has only a 5 percent chance of occurring and may well be due to malfunctioning of the spectrometer) result in a temperature uncertainty of only 0.34 percent--a figure which is well within the goal of 1 percent absolute temperatures. On the other hand, the same 2σ variation yields a 1.16 percent temperature uncertainty off-axis at 17 mK due to the poorer thermometer sensitivity and count rate in that direction. The NOT becomes more sensitive below 17 mK where the on- and off-axis directions reach their peak sensitivities at 7 and 11 mK, respectively. Clearly a given level of NOT temperature resolution may be achieved in a shorter time in the 7-11 mK region thus decreasing the demands on the spectrometer stability. Conversely, since the thermometer sensitivities decrease at high temperatures (the on- and off-axis sensitivities are both a factor of ~2 lower at 30 mK than at 17 mK--see Fig. 9), for a fixed counting time, correspondingly larger temperature uncertainties result and the need for proper statistical operation of

the spectrometer increases. Due to the need for increased counting time at higher temperatures and the attendant spectrometer stability problems, the vast majority of the NOT work in these experiments was done in the lowest accessible temperature range, i.e., 16-20 mK.

It is clear that integrating NOT data between fixed channels of the multichannel analyzer (FWHM or otherwise) will lead to somewhat erroneous temperature determinations if the spectra have a tendency to drift due to gain stabilization difficulties. This is simply because the integrated energy regions of the high- and low-temperature spectra are not then exactly the same. If it is known to what degree and in which direction the various photopeaks drifted, a first order correction can be made by integrating between different analyzer channels for the high- and low-temperature spectra in an attempt to analyze identical energy regions. (Such a procedure is not exact, of course, as the shape of each spectrum depends on the details of the spectrometer drift throughout the 10-20 hour data accumulation interval.) Unfortunately, a visual examination of the spectra is not sensitive enough to determine the proper changes in the channels of integration of the analyzer. In an attempt to be more sophisticated in analyzing the NOT data, a computer program was written which would fit a photopeak to a modified Gaussian function via a nonlinear least squares routine. The form of the function used was[56,57]

$$y(x) = y_0 \, e^{-\left(\frac{x-x_0}{w}\right)^2} \left[1 + \alpha_1 (x-x_0)^4 + \alpha_2 (x-x_0)^{12}\right] \qquad (23)$$

where y_o, x_o and w are typical Gaussian parameters characterizing the amplitude (in counts), location, and width (both in analyzer channel numbers) of the peak. The parameters α_1 and α_2 are necessary to compensate for the well known deviation of a photopeak from a Gaussian lineshape. (The deviation is believed to be due to the light collection properties of the scintillation crystal.[56]) Since the objective of these fits was to determine the center of a peak as accurately as possible, it was important to determine the uncertainty in the fit parameters as well. If the weighting factor (w_i) associated with the count in the i^{th} channel (y_i) is chosen such that $(w_i)^{-1/2}$ is a good estimate of the standard deviation of y_i, estimates of the standard deviations of the calculated parameters (y_o, x_o, w, α_1 and α_2) may be made.[57] Since the y_i represent the counting of random events for a fixed time, they are expected to have a Poisson probability distribution in which case $\sigma_i = (y_i)^{1/2}$ which implies the proper weighting per channel of data is $w_i = (y_i)^{-1}$. It may be shown that the standard deviation of the fit parameters is of the form[58] $\sigma_j = [R^2 A_{jj}/(n-m)]^{1/2}$ where j is an index identifying a fit parameter, A_{jj} is a diagonal matrix element of the matrix $A = A1^{-1}$ (the matrix A1 is set up in a standard fashion to solve simultaneous equations), R^2 is the minimum value of the sum of the squares of the deviations of the data from the fit, n is the number of data points in the fit and m (=5) is the number of parameters. The input data for such analyses were the master spectra referred to in conjunction with Table II--that is, the sum of all short spectra taken

for a given high- or low-temperature data accumulation. The 1.17 MeV peak was not used in this analysis since it is heavily contaminated with Compton scattered 1.33 MeV γ-rays and, as a result, shows substantial deviations from a Gaussian lineshape. Most of the low-energy side of the 1.33 MeV peak was also deleted from the fit interval for the same reason. The fit intervals typically included ~15 channels of data (0.65 keV/channel) on the low-energy side of the 1.33 MeV peak (to provide enough information to locate the peak channel) and extended to the half-maximum point and beyond on the high-energy side of the peak. As shown in Table V, seven intervals of each peak were fit to test the sensitivity of the fit parameters to the fit interval. The results indicate that the peak amplitude, width, and position, when compared with their respective uncertainties, are all independent of the fit interval. Thus, this modified Gaussian represents the ^{60}Co 1.33 MeV photopeak extremely well and, in particular, is capable of accurately determining the photopeak center.

There are two ways in which the photopeak centers may be used. First, instead of integrating a photopeak between fixed analyzer channel numbers (which ignores the possibility of spectrum drift), an NOT temperature determination may be keyed to the actual peaks in the data--that is, the 1.33 MeV photopeaks of the high- and low-temperature data may be integrated over the same energy interval relative to the peak positions as determined by the fits. Second, the photopeak positions may be used to probe successive spectra in a given run (a run being defined as a series of measurements without an intermediate

Table V. Typical results of modified Gaussian fits to the on- and off-axis 1.33 MeV photopeaks. These data are high-temperature normalization counts from Run 2, spectrum SE0376 which represents 17.8 hours of data accumulation. FWHM corresponds to ~120 channels. y_0 and σ_y are in units of counts while x_0, σ_x, w and σ_w are in units of analyzer channel numbers. The definitions of the fit parameters and their uncertainties are given in the text.

ON AXIS

Channels	y_0	σ_y	x_0	σ_x	w	σ_w	α_1	σ_{α_1}	α_2	σ_{α_2}
620-700	48,845	64	636.49	0.28	73.41	1.11	1.46×10^{-9}	1.79×10^{-9}	-2.0×10^{-24}	4.0×10^{-24}
620-710	48,831	60	636.45	0.28	73.83	0.90	5.26×10^{-10}	1.03×10^{-9}	4.6×10^{-25}	7.0×10^{-25}
620-720	48,849	57	636.52	0.26	73.32	0.73	1.30×10^{-9}	6.68×10^{-10}	-5.5×10^{-26}	1.6×10^{-25}
620-730	48,852	56	636.54	0.25	73.25	0.61	1.32×10^{-9}	4.60×10^{-10}	6.9×10^{-27}	4.5×10^{-26}
620-740	48,858	53	636.58	0.24	73.10	0.52	1.48×10^{-9}	3.34×10^{-10}	-1.2×10^{-26}	1.5×10^{-26}
620-750	48,846	53	636.50	0.24	73.41	0.47	1.20×10^{-9}	2.50×10^{-10}	5.6×10^{-27}	5.2×10^{-27}
620-760	48,854	53	636.56	0.23	73.22	0.43	1.34×10^{-9}	2.06×10^{-10}	3.2×10^{-27}	2.2×10^{-27}

OFF AXIS

Channels	y_0	σ_y	x_0	σ_x	w	σ_w	α_1	σ_{α_1}	α_2	σ_{α_2}
1675-1755	27,293	46	1693.10	0.31	72.32	1.32	6.00×10^{-11}	2.42×10^{-9}	1.2×10^{-24}	6.8×10^{-24}
1675-1765	27,277	42	1693.04	0.30	73.03	1.05	-1.32×10^{-9}	1.30×10^{-9}	2.0×10^{-24}	1.1×10^{-24}
1675-1775	27,305	40	1693.17	0.29	71.79	0.82	9.18×10^{-10}	8.60×10^{-10}	-3.0×10^{-25}	2.7×10^{-25}
1675-1785	27,290	38	1693.07	0.28	72.42	0.71	5.90×10^{-11}	5.53×10^{-10}	-1.3×10^{-26}	6.9×10^{-26}
1675-1795	27,281	38	1693.01	0.28	72.76	0.63	-2.98×10^{-10}	3.80×10^{-10}	4.4×10^{-26}	2.1×10^{-26}
1675-1805	27,288	36	1693.07	0.26	72.51	0.53	-8.75×10^{-11}	2.77×10^{-10}	2.9×10^{-26}	7.2×10^{-27}
1675-1815	27,304	36	1693.23	0.26	71.91	0.48	3.65×10^{-10}	2.31×10^{-10}	1.4×10^{-26}	3.0×10^{-27}

warmup to room temperature) to search for signs of spectrometer drift. In Table VI, the results of a peak position analysis of data from Runs 2 and 4 are presented. Several conclusions may be drawn from the results: (1) The stability of x_o for Run 2 is much better than that for Run 4--the x_o values in Run 4 shift by $1\frac{1}{2}$ - 2 channels on a spectrum to spectrum basis whereas the variations observed in Run 2 are on the order of the statistical uncertainty of 0.3 channel (except for a shift between the 3rd and 4th entries off-axis). It is interesting to note that the room temperature stability was much poorer for Run 4 than for Run 2. (2) The shifts in x_o for the two directions in Run 4 correlate well both in sign and magnitude suggesting the cause of the difficulty was the same in both cases. (3) The photopeak positions do not vary systematically with high- versus low-temperature data. This result is very important as it indicates that the gain stabilizers <u>are not</u> adversely affected by using γ-ray lines whose amplitudes change during the experiment. Had a value of x_o shifted back and forth correlating with high- and low-temperature data, the conclusion might be drawn that the shape (as well as the amplitude) of the peaks may vary with the bus temperature due to the changing interaction between the anisotropic radiation distribution and the scattering environment. Since the stabilizers are sensitive to the shapes of the peaks, it would then have been necessary to lock the stabilizers onto an added γ-ray line in the spectrum whose lineshape was time independent.

A substantial effort was made in these experiments to determine error-free absolute temperatures with the NOT. The potential sources

Table VI. Results of a peak position analysis and associated uncertainties for 1.33 MeV photopeaks from the data in Runs 2 and 4. The spectrum label, the day of the run each spectrum was taken, the length of each spectrum (in hours) and the thermometer bus temperature (in K) are tabulated for each entry. x_o and σ_x (in units of analyzer channel numbers) are defined and discussed in the text.

RUN 2

				ON AXIS		OFF AXIS	
Spectrum	Day	Length	T	x_o	σ_x	x_o	σ_x
SE0370	3	13.9	0.5	636.32	0.32	1694.13	0.31
SE0373	4	8.9	0.017	636.44	0.44	1694.31	0.34
SE0374	5	6.1	0.5	636.86	0.34	1694.02	0.39
SE0375	6	10.0	0.017	636.60	0.35	1692.66	0.36
SE0376	7	17.8	0.5	636.49	0.28	1693.10	0.31
SE0378	8	22.2	0.5	637.07	0.25	1693.15	0.27
SE0381	9	21.1	0.5	636.94	0.29	1693.33	0.29

RUN 4

				ON AXIS		OFF AXIS	
Spectrum	Day	Length	T	x_o	σ_x	x_o	σ_x
SE0001	1	20.0	0.5	643.36	0.40	1716.98	0.49
SE0003	5	9.4	0.018	644.92	0.39	1717.77	0.50
SE0005	8	15.3	0.018	642.99	0.46	1716.14	0.54
SE0006	9	13.7	0.5	644.32	0.35	1717.44	0.53
SE0007	10	9.9	0.017	644.64	0.47	1718.24	0.51

of error are conveniently divided into two classes. The first or "fundamental" class concerns uncertainties in (1) the hyperfine structure of ^{60}Co in hcp ^{59}Co, (2) the E2/M3 radiation admixture for the 1.17 MeV γ-ray and (3) the reorientation tendency of the ^{60}Ni nucleus after the β decay of ^{60}Co. The second or "practical" class concerns uncertainties in (1) the existence of non-single-crystal portions of the Co thermometer, (2) the existence of a substantial volume of closure domains, (3) the location of the c-axis in the Co crystal, (4) the alignment of the c-axis with respect to the scintillation counters, and (5) the degree of superheating of the Co crystal (due to β-ray absorption) above the bus temperature. Note that the concerns of the first group are intrinsic to <u>any</u> ^{60}Co in hcp ^{59}Co thermometer whereas those of the second group may vary from one thermometer to another. Since Soulen and Marshak[12] have demonstrated that a single-crystal ^{60}Co in hcp ^{59}Co thermometer yields temperatures in the 0.01-0.05 K range which agree to $\pm$0.5 percent with a Johnson noise thermometer, it may be concluded that the concerns of the first group have been dealt with adequately. Thus, in these experiments, the practical problems of implementing a <u>particular</u> Co thermometer were addressed. Of special concern here is the work of Chandra and Radhakrishnan[59] who investigated the temperature dependence of the on- and off-axis intensities for each of two Co single crystals. The first crystal had a needle-like shape while the second was in the shape of a flat disk (which, in order to minimize the thermal resistance between the Co crystal and the Cu bus, was the

geometry used in our experiments). Their results yielded an on- versus off-axis relationship which was in accord with theory for the needle but which was anomalous for the disk. They concluded this disparity was due to the presence of a large volume of closure domains in the disk and estimated that fully 18 percent of all ^{60}Co atoms must have been in such an environment. Since all the practical concerns stated above (except that of superheating) will yield inconsistent temperature determinations when measured in independent directions, the on- versus off-axis self consistency tests were crucial to the successful implementation of the NOT. Clearly, the single-axis counting utilized by most research groups offers no protection against the systematic errors mentioned above. The final practical concern, associated with the superheating of the Co crystal, was examined by measuring the thermal resistance between the Co crystal and the bus. The on- versus off-axis comparisons and the superheating tests are described below.

On- and off-axis temperatures were compared a number of times in each of several runs. In Table VII, the results of those comparisons which utilized significant counting times in Runs 2, 4, and 5 are reported. For each master spectrum, both the 1.17 and the 1.33 MeV photopeaks were integrated using FWHM regions of interest between fixed analyzer channel numbers. The results reported for each direction are an average of the two photopeak temperatures, i.e., $\bar{T} = (T_{1.17} + T_{1.33})/2$. The combined statistical uncertainty in temperature is represented by $\sigma_{TOT} = [(\Delta T_{ON})^2 + (\Delta T_{OFF})^2]^{1/2}\ 100/T_{ON}$ where ΔT_{ON} and ΔT_{OFF} are the 1σ uncertainties in the on- and off-axis temperatures. The factor

Table VII. Results of the on- and off-axis temperature comparisons using the data from Runs 2, 4, and 5. The magnetic tape label and the length of counting time (in hours) is given for each spectrum. The reported temperature (in mK) for each direction is an average of the 1.17 and 1.33 MeV photopeak temperatures as determined by FWHM integrals. δ is the percentage difference between the on- and off-axis temperatures and σ_{TOT}, which is expressed as a percentage to facilitate comparison with δ, is the square root of the sum of the squares of the 1σ temperature uncertainties of the on- and off-axis temperature determinations. Calculated temperatures with and without the coincidence correction (discussed in the text) are given.

			No Correction			Coincidence Correction			
Run	Spectrum	Time	$\overline{T}_{ON}$	$\overline{T}_{OFF}$	δ	$\overline{T}_{ON}$	$\overline{T}_{OFF}$	δ	σ_{TOT}
2	SE0366	9.4	17.10	16.45	+3.95	17.14	16.98	+0.94	0.73
2	SE0368	11.7	17.12	16.37	+4.58	17.16	16.89	+1.60	0.65
2	SE0373	8.9	16.95	16.53	+2.54	16.99	17.07	-0.47	0.73
2	SE0375	10.0	16.82	16.39	+2.62	16.86	16.92	-0.35	0.63
				Average =	+3.42		Average =	+0.43	
4	SE0003	9.4	18.18	17.60	+3.30	18.22	18.20	+0.11	0.69
4	SE0005	15.3	17.70	17.02	+4.00	17.73	17.58	+0.85	0.53
4	SE0007	9.9	17.42	16.77	+3.88	17.45	17.32	+0.75	0.66
				Average =	+3.73		Average =	+0.57	
5	SE0028	15.3	18.48	18.08	+2.21	18.52	18.71	-1.02	0.60
5	SE0034	11.1	18.03	17.40	+3.47	18.07	17.99	+0.44	0.68
5	SE0035	5.6	18.01	17.54	+2.68	18.05	18.14	-0.50	0.97
5	SE0037	4.2	17.86	17.21	+3.78	17.90	17.79	+0.62	1.10
5	SE0038	8.3	17.68	17.28	+2.31	17.72	17.85	-0.73	0.77
5	SE0040	8.3	17.62	17.08	+3.16	17.66	17.72	-0.34	0.76
5	SE0045	12.5	17.58	16.96	+3.66	17.61	17.52	+0.51	0.61
5	SE0051	13.9	17.41	17.02	+2.29	17.45	17.58	-0.74	0.62
				Average =	+2.94		Average =	-0.22	
			Total Average =		+3.23	Total Average =		+0.11	

of $100/T_{ON}$ puts σ_{TOT} on a percentage temperature basis to facilitate a comparison with the observed percentage difference (δ) between $\overline{T}_{ON}$ and $\overline{T}_{OFF}$. Although the experiment was warmed to room temperature between runs and the Co crystal-scintillation counter alignment was independently adjusted before each run, no significant run-to-run variations in the comparisons were ever observed. The status of the comparisons at the conclusion of these experiments is given in columns 4, 5, and 6 (under the heading "No Correction") and is seen to yield a rather consistent 3 percent temperature disagreement between the two directions. It is significant to note that the sense of the discrepancy, that is $T_{ON} > T_{OFF}$, is inconsistent with the above mentioned concerns of closure domains, misalignment of the crystal c-axis, etc. In later work with the spectrometer, it was noticed that the value of the spectrum integrals for both the on- and off-axis channels differed depending upon whether the channels were counted together or separately through the mixer-router (MR). Simultaneous acquisition of data from both channels yielded smaller integrals than separate counting thus indicating some form of nonideal operation of the spectrometer. This erroneous behavior was found to be inherent in the design of the MR. When a suitable γ-ray pulse enters an input channel of the MR, a lower level discriminator (LLD) fires and remains on for the duration of the pulse (~1 μs). One of the functions of a LLD pulse is to inform a logic network as to which input a given γ-ray pulse entered. This information is in turn sent to the multichannel analyzer (MCA) where it controls the two most

significant bits of memory address for the γ-ray pulse being analyzed. Thus, depending upon which input a given pulse enters, the resulting pulse height information (from the A/D conversion in the MCA) is routed to a different portion of the MCA memory. (This is just the routing function of the MR. Although these experiments utilized only two inputs, the MR has four inputs, four LLD's and can route information into the four quadrants of the MCA memory). A problem arises, however, when pulses from the two detectors arrive at two inputs of the MR at essentially the same time (within 1.2 μs). Such coincidence events are sensed by another logic network which continuously monitors the output state of all LLD's and is activated when any two of them are on simultaneously. Unique routing information for the two pulses is thus not available and, in any case, the summing or mixing of the two pulses in the mixer circuit destroys the individual pulse shapes of both γ-ray pulses. Although the distorted combination of the two mixed pulses is sent to the MCA for A/D conversion, the MR logic sends a reject pulse to the MCA which prevents storage of the A/D result in the MCA memory. This operation has been verified experimentally by acquiring data with the spectrometer and a room-temperature Co source. Using an external counter, the number of reject pulses generated by the MR was shown to be consistent with the observed decrease in the full spectrum integrals of the two channels when counting together as opposed to counting separately. Thus, the net effect of this process is to act as though the coincident pulses never existed. Even though taking the ratio of low- to high-

temperature integrals compensates for the error to first order (both count rates are abnormally low), the number of coincidence events depends upon the count rates in both directions and each of these has a different temperature dependence. This arbitrary deletion of experimental data adversely affects the NOT results.

Since the mechanism which caused the low count rates was known, the initial idea for correcting the NOT data took the following form: If the approximate count rate in each channel was known and if the coincidence time of the circuit was measured, the coincidence count rate could then be calculated and an appropriate correction applied to the existing NOT data. The count rate in each channel is easily obtained from the data by integrating the whole spectrum (all counts processed) and dividing by the acquisition time. The circuit coincidence time was determined with an oscilloscope by measuring the length of time a LLD stays on when processing a γ-ray pulse. If, for each of two independent channels, the γ-ray pulses are distributed over time in accordance with the Poisson law, it can be shown that the number of coincidences expected in a period of time t is[60]

$$N_{CH} = \frac{N_1 N_2 t}{N_1 - N_2} \left[e^{-N_2(\tau_1+\tau_2)} - e^{-N_1(\tau_1+\tau_2)} \right] \qquad (24)$$

where N_1, N_2 and τ_1, τ_2 are the count rates and pulse durations, respectively, for the two input channels. Since $\tau_1 = \tau_2 = \tau = 1.2\ \mu s$ and since the count rates in these experiments were quite low, $N\tau << 1$ and the above expression reduces to the intuitive form $N_{CH} = 2N_1N_2\tau t$.

However, a test of this relation with the spectrometer revealed that the observed number of coincidence counts (as measured by the number of reject pulses generated by the MR) was an order of magnitude greater than that predicted. Only at this point was it realized that some of the pulses in the two channels were in fact correlated in time and that the source of this correlation was the simultaneous detection of two γ-rays from the same ^{60}Co nucleus. Thus, in an effort to double check the NOT results by conducting simultaneous measurements in two directions, these experiments inadvertently incorporated a 90° angular correlation measurement of the two γ-ray transitions in the ^{60}Ni cascade. Both the "chance" coincidences as described by the Poisson law formalism above and the "real" coincidences associated with angular correlations contribute to the total number of coincidence counts lost in the NOT experiments and must be accounted for accordingly.

As an example of applying a correction for chance coincidences, the 18 mK spectrum SE0003 of Run 4 has been selected. For 34,000 seconds of data acquisition, the full spectrum integrals for on- and off-axis are 4.209×10^7 counts and 2.752×10^7 counts, respectively. The number of chance coincidences for that spectrum is then $N_{CH} = 8.176 \times 10^4$ counts and, to compensate for the coincidences, the on- and off-axis integrals should be increased by $(8.176 \times 10^4 / 4.209 \times 10^7)\ 10^2 = 0.1942$ percent and $(8.176 \times 10^4 / 2.752 \times 10^7)\ 10^2 = 0.2971$ percent, respectively. A similar calculation for SE0001, the 72,000 second high-temperature normalization spectrum used

with SE0003, results in 0.1805 percent and 0.3511 percent higher on- and off-axis integrals. Hence, the correction factors for the angular distribution functions F(0) and F(90) are 1.000137 and 0.999462 which in turn result in on- and off-axis temperature increases of 0.051 percent and 0.515 percent. Similar corrections have been calculated for all the NOT data.

Unfortunately, determining the correction factors associated with real coincidences is rather complex. Due to this complexity and the importance of the correction, it will be described in some detail. The theory of the angular correlation between γ-rays emitted from oriented nuclei is discussed rigorously, although quite formally, in Ref. 61. More accessible discussions which specifically concern the ^{60}Ni cascade, but do not consider oriented nuclei, may be found in Refs. 62, 63. The angular correlation function (ACF), $W(\theta)$, is defined such that $W(\theta)d\Omega_1 d\Omega_2$ is the probability that if the first γ-ray is emitted into the solid angle $d\Omega_1$, then the second γ-ray will be emitted into the solid angle $d\Omega_2$ where θ is the angular separation between $d\Omega_1$ and $d\Omega_2$. Given this definition, it follows that the real coincidence count rate actually measured in an experiment is[64]

$$N_{RC} = 2N_0\Omega_1\eta_1\Omega_2\eta_2 W(\theta) \qquad (25)$$

where N_0 is the disintegration rate of the source, Ω_1 and Ω_2 are the solid angles subtended by the detectors at the source, and η_1 and η_2 are the efficiencies of the detectors. Further, theory

predicts[61,63] that the ACF may be expressed as a finite series of even Legendre polynomials

$$W(\theta) = \sum_{k}^{k_{max}} A_{2k} P_{2k}(\cos\theta)$$

where $k_{max} = 2$ for the ^{60}Ni cascade. Since the information about the spins and parities of excited nuclear states obtained from angular correlation measurements is contained in the relative coefficients of the Legendre polynomials, it is conventional to omit all angle independent factors when calculating the coefficients A_{2k}.[63] In addition, theoretical treatments "normalize" the ACF by dividing each coefficient A_{2k} by A_o such that $W(\theta) = 1 + A_2P_2(\cos\theta) + A_4P_4(\cos\theta)$. For the ^{60}Ni cascade at high temperatures, where the parent ^{60}Co nuclei are equally distributed between the magnetic substates, theory predicts[63]

$$W(\theta) = 1 + 0.1020\ P_2(\cos\theta) + 0.0092\ P_4(\cos\theta) \quad . \qquad (26)$$

This prediction has been carefully substantiated by angular correlation measurements[65] and verifies the ^{60}Ni cascade as being 4(E2)2(E2)0. However, due to the various manipulations of the A_{2k} coefficients mentioned above, the form of Eq. (26) is not normalized in the sense required by Eq. (25). In addition, insofar as Eq. (25) is concerned, the normalization of $W(\theta)$ also depends upon the solid angle convention being used--that is, Ω may be thought of as a fraction of the surface area of a sphere or as a fraction of 4π steradians.[66] Consistency in the Ω and $W(\theta)$ conventions is required since N_{RC} is a

measured quantity and is therefore independent of the convention used. In this work, Ω is taken to be the fraction of the surface area of a sphere occupied by a detector. To properly normalize Eq. (26), let $W(\theta) = K[1+0.1020\ P_2(\cos\theta) + 0.0092\ P_4(\cos\theta)]$ and determine K in the following way: Choose a coordinate system such that the first γ-ray is emitted from the ^{60}Ni nucleus along the z-axis. $W(\theta)$ then gives the probability of observing the second γ-ray at an angle θ. Thus, if $W(\theta)$ is integrated over the surface of a unit sphere, the resulting probability must be unity--that is,

$$1 = (4\pi)^{-1} \int_0^{2\pi} d\phi \int_0^{\pi} W(\theta) \sin\theta\, d\theta \quad .$$

(The $[4\pi]^{-1}$ factor is required due to the solid angle convention adopted.) In performing such an integration, the Legendre polynomials integrate to zero thus yielding K = 1. This value of the normalization constant has been verified experimentally by using coincidence test data from the spectrometer along with the combination of Eqs. (25) and (26) which yields

$$N_{RC} = 2N_0\Omega_1\eta_1\Omega_2\eta_2\{K[1+0.1020\ P_2(\cos\theta) + 0.0092\ P_4(\cos\theta)]\}. \quad (27)$$

This analysis used the data from the test mentioned earlier in which the on- and off-axis channels were counted simultaneously and the number of coincidences was determined by counting the number of reject pulses generated by the MR. Correcting the total number of coincidences for the number of chance coincidences and substituting the

known detector solid angles and efficiencies into Eq. (27) yields $K = 0.91 \pm 0.1$. This result agrees with the theoretical value to within experimental error. It has thus been demonstrated that Eq. (27), with $K = 1$, accurately describes the real coincidence counting rate for unoriented nuclei.

To correct the high-temperature NOT data for the loss of real coincidence counts, the on- and off-axis spectrum integrals must be increased by factors of $1+(N_{RC}/N_{ON})$ and $1+(N_{RC}/N_{OFF})$, respectively. For these experiments,[67] $\Omega_1\eta_1 = 0.0165$ and $\Omega_2\eta_2 = 0.0095$ and, since $\theta = 90°$, $W(\theta) = 0.952$. Since the single-axis count rates are $N_{ON} = 2N_0\Omega_1\eta_1$ and $N_{OFF} = 2N_0\Omega_2\eta_2$, the correction factors are, for on-axis,

$$1 + \frac{2N_0(0.0165)(0.0095)(0.952)}{2N_0(0.0165)} = 1.00902 \qquad (28)$$

and for off-axis,

$$1 + \frac{2N_0(0.0165)(0.0095)(0.952)}{2N_0(0.0095)} = 1.01568 \quad . \qquad (29)$$

Note that these factors are <u>independent</u> of the source disintegration rate and depend only upon the experimental geometry and the ACF of the ^{60}Ni cascade. Thus, as opposed to the chance coincidence corrections, no experimental data are required to establish these factors.

It remains to determine the proper real coincidence corrections for the low-temperature NOT data. These differ from the above since the unequal populations of ^{60}Co nuclei in the magnetic substates

(oriented nuclei) influence the ACF. This more complicated situation has been treated by Cox and Tolhoek[68] who, fortunately, evaluated their very formal results for the 4(E2)2(E2)0 transitions so as to facilitate comparison with experiments on the popular ^{60}Ni cascade. Once again, care must be taken with normalizing the ACF as Cox and Tolhoek use yet another convention. By taking the high-temperature limit of their expression for $W(\theta)$, the angular dependence of Eq. (26) emerges and the proper normalization constant of their expression may be determined by requiring consistency with the previous high-temperature results. This consistency is achieved if Cox and Tolhoek's ACF is multiplied by 1/4. To correct any low-temperature NOT point, the ACF must be evaluated at that temperature. This involves the evaluation of rather tedious but straightforward sums over magnetic substates. To correct the data in Table VII, the ACF is evaluated at 17 mK and yields $W(90) = 0.835$. The correction factors by which to increase the 17 mK spectrum integrals are again $1+(N_{RC}/N_{ON})$ and $1+(N_{RC}/N_{OFF})$ and are found to be, for on-axis,

$$1 + \frac{2N_0(0.0165)(0.0095)(0.835)}{2N_0(0.0165)(0.832)} = 1.00953 \qquad (30)$$

and for off-axis,

$$1 + \frac{2N_0(0.0165)(0.0095)(0.835)}{2N_0(0.0095)(1.081)} = 1.01274 \quad . \qquad (31)$$

Note the factors of 0.832 and 1.081 reflect the anisotropic γ-ray distribution at low temperatures and are necessary to yield the proper single-axis count rates (N_{ON} and N_{OFF}) at 17 mK. Combining Eqs. (28-31), the correction factors for the angular distribution functions F(0) and F(90) are 1.00050 and 0.99710. These factors yield temperature increases of 0.12 percent and 2.72 percent for the on- and off-axis directions, respectively. Thus, when adding the effects of real and chance coincidences, the on- and off-axis temperatures increase by 0.17 percent and 3.24 percent for a net difference of 3.07 percent. The coincidence corrections have been applied to all of the data in Table VII and the results are tabulated in columns 7-9. The average discrepancy between the on- and off-axis temperatures is now zero to within experimental error. Further, since 9 of the 15 comparisons have temperature differences which do not exceed the combined 1σ uncertainty level, the statistical integrity of the data is excellent (68 percent or 10 of the comparisons should be within the 1σ confidence level).

These NOT results obviously contradict those of Chandra and Radhakrishnan[59] and thus indicate that a large fraction of the volume of the Co disk used in the experiments reported here cannot be present in the form of closure domains. This is not surprising since hcp Co is a uniaxial material possessing a high magnetocrystalline anisotropy--a circumstance which does not favor the formation of closure domains (see Sec. IV). The results of Chandra and Radhakrishnan are more likely to be due to imperfections in their Co

crystal disk--a problem which can yield data similar to those of the closure domain hypothesis.

In Table VIII, the separate 1.17 and 1.33 MeV photopeak temperature determinations for the specta in Table VII are reported. All of the data have been corrected for γ-ray coincidences. The results of the three runs are similar and indicate that the 1.17 MeV photopeak temperature is consistently ~1/2 percent higher than that of the 1.33 MeV photopeak in the on-axis direction. However, no such consistency is observed for the off-axis direction where the overall temperature difference is nearly zero. (The on-axis differences have better precision than those off-axis due to the angular dependence of the thermometer sensitivity.) The null off-axis difference eliminates the concern of the admixture of M3 radiation in the otherwise E2 1.17 MeV transition since such an intrinsic occurrence would affect the 1.17 versus 1.33 MeV temperature comparison in both directions. As shown in columns 9 and 10 of Table VIII, the disagreement between the on- and off-axis 1.17 MeV temperatures is ~2.3 times greater than that for the 1.33 MeV photopeaks. Thus, at the several tenths of a percent level, the details of the Compton scattering as a function of angle may indeed play a role in determining absolute temperatures since the 1.33 MeV photopeak is largely free of Compton events compared to the 1.17 MeV photopeak. Clearly the most conservative spectrum analysis utilizes only the 1.33 MeV photopeak (although the rate at which statistics are accumulated is then substantially reduced due to the lower count rate). Based on these results, it is clear

Table VIII. Results of separate 1.17 and 1.33 MeV photopeak temperature determinations. All spectra have been analyzed using FWHM integrals with fixed channels of integration. The run number and magnetic tape label of each spectrum is given. δ_{ON} and δ_{OFF} are the percentage differences between the 1.17 and the 1.33 MeV photopeak temperatures for on- and off-axis, respectively. $\delta_{1.17}$ is the percentage difference between the two 1.17 MeV temperatures and likewise, $\delta_{1.33}$ is the percentage difference between the two 1.33 MeV temperatures. All temperatures are in mK.

		ON AXIS			OFF AXIS				
Run	Spectrum	$T_{1.17}$	$T_{1.33}$	δ_{ON}	$T_{1.17}$	$T_{1.33}$	δ_{OFF}	$\delta_{1.17}$	$\delta_{1.33}$
2	SE0366	17.14	17.15	-0.06	17.04	16.92	+0.71	+0.59	+1.36
2	SE0368	17.19	17.12	+0.41	16.94	16.84	+0.59	+1.48	+1.66
2	SE0373	17.05	16.93	+0.71	17.03	17.11	-0.47	+0.12	-1.05
2	SE0375	16.91	16.80	+0.65	16.92	16.92	0.00	-0.06	-0.71
4	SE0003	18.26	18.18	+0.44	18.10	18.31	-1.15	+0.88	-0.71
4	SE0005	17.80	17.66	+0.79	17.57	17.60	-0.17	+1.31	+0.34
4	SE0007	17.51	17.39	+0.69	17.37	17.27	+0.58	+0.81	+0.69
5	SE0028	18.61	18.44	+0.92	18.88	18.55	+1.78	-1.43	-0.59
5	SE0034	18.12	18.02	+0.55	18.07	17.92	+0.84	+0.28	+0.56
5	SE0035	18.12	17.99	+0.72	18.23	18.05	+1.00	-0.60	-0.33
5	SE0037	17.94	17.85	+0.50	17.76	17.82	-0.34	+1.01	+0.17
5	SE0038	17.79	17.66	+0.74	17.88	17.82	+0.34	-0.50	-0.90
5	SE0040	17.69	17.63	+0.34	17.58	17.86	-1.57	+0.63	-1.29
5	SE0045	17.71	17.51	+1.14	17.40	17.65	-1.42	+1.78	-0.79
5	SE0051	17.49	17.41	+0.46	17.62	17.54	+0.46	-0.74	-0.74
	Average			+0.60			+0.08	+0.37	-0.16

that the NOT absolute temperatures are uncertain to at least several tenths of a percent.

Although the NOT sensitivities degrade rapidly with increasing temperature, six on- versus off-axis comparisons were made in Run 5 at higher temperatures to check the temperature dependence of the comparison. The results, which are corrected for γ-ray coincidences, are given in Table IX. Since five of the six comparisons have differences which fall within the combined 1σ uncertainty range, it is apparent that the on- and off-axis temperatures are in agreement to within statistics in the 28-53 mK region. These results, together with the 17-20 mK results in Table VII, cover the useable range of the NOT available in these experiments.

The final test conducted with the NOT was designed to measure the thermal resistance between the Co crystal and the copper bus. In this test, energy was dissipated in a heater mounted on top of the Co crystal (see Sec. VI) and the resulting heat current generated a temperature difference (ΔT) across the soft-soldered crystal-bus interface. The NOT was used to monitor the Co crystal temperature while the dc susceptibility thermometer monitored the bus temperature. With the bus temperature at a steady 18 mK, 1.5 μA of heater current was applied to the 576Ω heater thus dissipating 1.3 nW of power. This is estimated to be equivalent to the self-heating of 2 μCi of ^{60}Co that arises from the absorption of β radiation in the crystal.[37] The bus was observed to warm 0.1 mK (since the energy input raises the mixing chamber temperature) and several hours of NOT data failed to detect any temperature difference across the interface to within experimental

Table IX. Results of on- versus off-axis temperature comparisons using data from Run 5. The magnetic tape label and the counting time (in hours) are given for each spectrum. The reported temperature for each direction (in mK) is an average of the 1.17 and the 1.33 MeV photopeak temperatures as determined by FWHM integrals. δ is the percentage difference between the temperatures and σ_{TOT}, which is expressed as a percentage to facilitate comparison with δ, is the square root of the sum of the squares of the 1σ temperature uncertainties of the on- and off-axis temperature determinations.

Spectrum	Time	$\bar{T}_{ON}$	$\bar{T}_{OFF}$	δ	σ_{TOT}
SE0056	16.7	28.23	27.99	+0.86	1.03
SE0055	4.2	28.63	29.01	-1.31	2.37
SE0054	4.2	41.00	37.91	+8.15	3.50
SE0057	9.7	40.90	40.34	+1.39	2.31
SE0053	11.1	53.64	55.13	-2.70	4.42
SE0060	16.7	53.44	53.64	-0.37	3.17

error. The power level was then increased twentyfold to 26.6 nW. The CMN thermometer reached a new steady-state temperature in ~1/2 hour and indicated that the bus had warmed by 1.26 mK to 19.12 mK. Four hours of NOT data were then taken which resulted in T_{ON} = 20.13 mK. Thus, the 26.6 nW generated a 1.01 mK temperature difference across the interface and, since $\Delta T << T$, $R = \Delta T/\dot{Q} = 3.80 \times 10^4$ K/W. Finally, the power level was doubled to 53.2 nW. The CMN warmed an additional 1.16 mK to 20.28 mK and the NOT yielded T_{ON} = 22.21 mK. This indicated a 1.93 mK difference between the crystal and the bus and $R = 3.63 \times 10^4$ K/W which is in excellent agreement with the 26.6 nW result. Thus, since the thermal resistance was found to be ohmic, an estimate of the temperature difference at the crystal-bus interface under the action of only the β-ray heating may be made. The result is $\Delta T = R\dot{Q} = 0.049$ mK. At 18 mK, this corresponds to 0.27 percent--an amount which is somewhat below the NOT resolution for modest counting times. Several interesting points follow from this result: (1) Using a Co crystal in the shape of a needle substantially reduces the crystal-bus surface area and may exacerbate the thermal contact problem to a significant extent. (2) Attempts to shorten data accumulation times by greatly increasing the activity level will result in the NOT running unacceptably hot.

In summary, the tests carried out on the NOT eliminate any significant problems associated with closure domains, misalignment of the crystal c-axis with respect to the detectors or superheating of the Co crystal. Although the results indicate that uncertainties of

only a few tenths of a percent exist in the NOT temperatures depending upon the interpretation of the spectra, on the basis of the results of Soulen and Marshak[12] the absolute accuracy of the temperatures may be uncertain to ~1/2 percent. The NOT may thus be reliably used in conjunction with the $^3He/^4He$ vapor pressure scale to establish an accurate CMN temperature scale in the 0.016-4.0 K region.

VIII. SUSCEPTIBILITY OF THE CMN SAMPLE HOLDERS

Before a resistance thermometer may be calibrated using the measured susceptibility of a CMN thermometer, the susceptibility of the empty CMN thermometer (without CMN) must be measured. This yields an accurate determination of the CMN susceptibility (χ_{CMN}) after subtracting that of the holder (χ_{MT}) in a CMN calibration experiment. The assumption is generally made, of course, that χ_{MT} is reproducible from experiment to experiment.

The susceptibility of both the epoxy and the copper CMN holders was carefully measured in the 1.3-3.5 K region versus the GE2776, in the 0.05-1.5 K region versus the GE1751 and the GE2345 and in the 0.016-0.05 K region versus the NOT. To check for any nonreproducibility associated with thermal cycling, the susceptibility of the CMN holders was measured in two successive runs. Within each run, numerous checks of day-to-day reproducibility were made. The only substantial difficulty encountered was associated with the rewinding of the flux transformer coils on the copper holder between the two experiments--a change which appears to have altered χ_{MT} significantly for $T > 0.75$ K.

The epoxy holder was measured using both 16 Hz and 160 Hz, the lowest and highest frequencies available with the bridge, to allow an examination of the frequency dependence of the CMN susceptibility. The 16 Hz data are displayed in Figs. 14-17 and the 160 Hz data in Figs. 18-21, as the in-phase ratio transformer setting (on a <u>greatly</u> expanded scale) versus T^{-1}. To keep the scatter and reproducibility

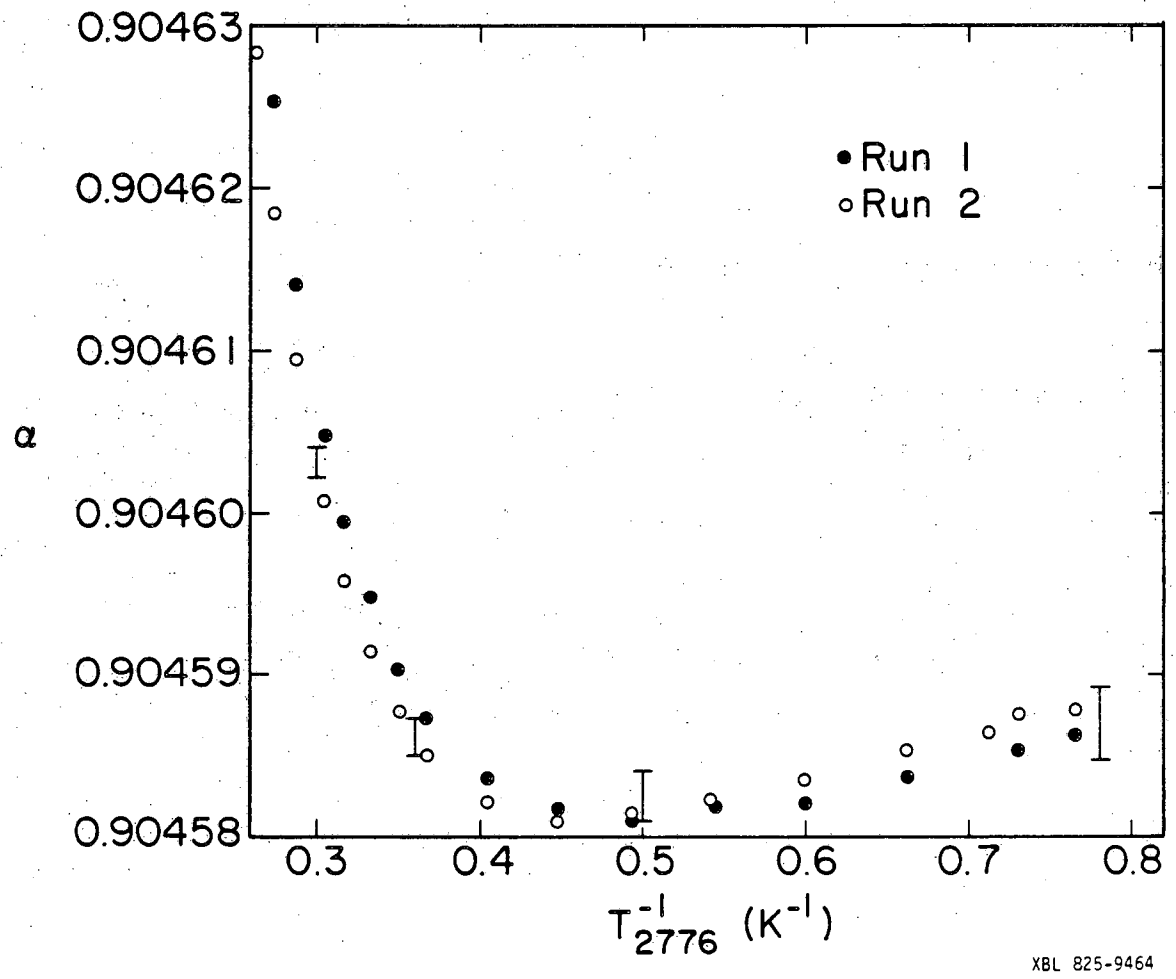

Fig. 14. The 16 Hz susceptibility of the epoxy CMN holder, expressed in units of the null in-phase ratio transformer setting (α) versus inverse temperature in the 1.3-3.8K region. Results from both Runs 1 and 2 are reported. The bars correspond to 0.05 percent in CMN temperature as explained in the text.

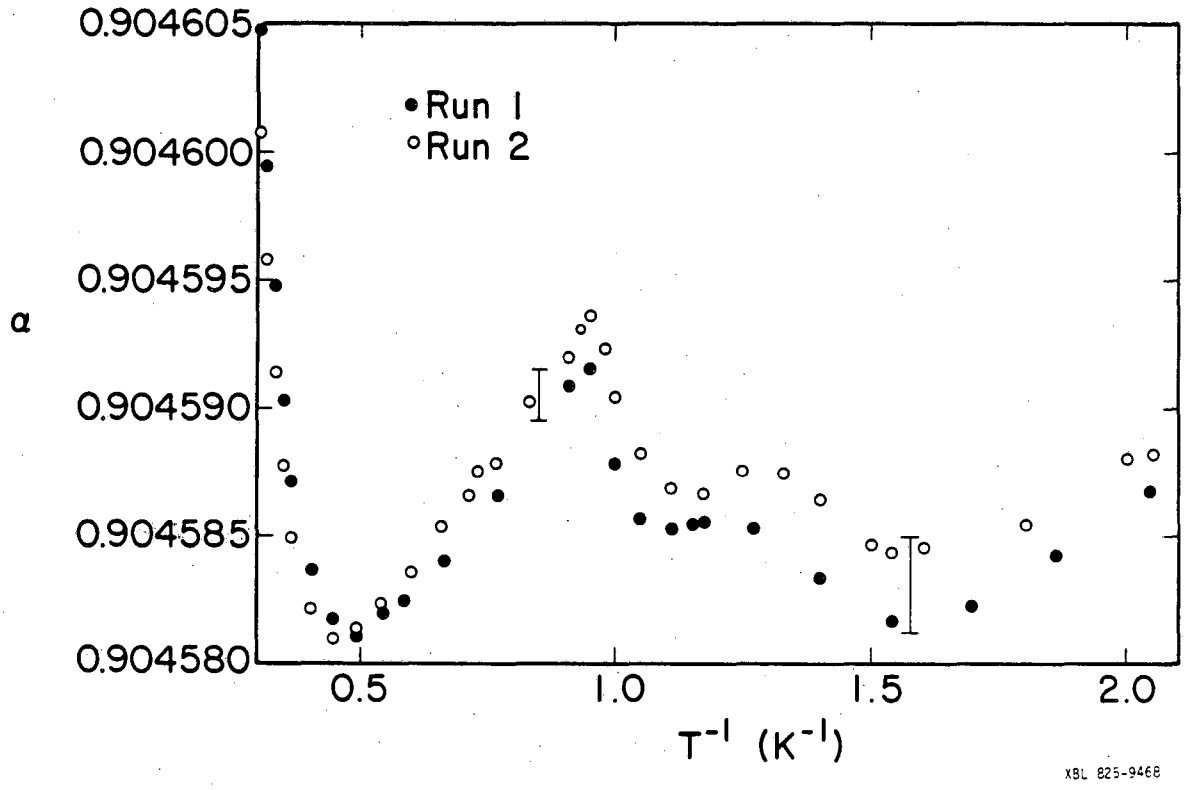

Fig. 15. The 16 Hz susceptibility of the epoxy CMN holder, expressed in units of the null in-phase ratio transformer setting (α) versus inverse temperature in the 0.5-3.3K region. Results from both Runs 1 and 2 are reported. The bars correspond to 0.02 percent in CMN temperature as explained in the text.

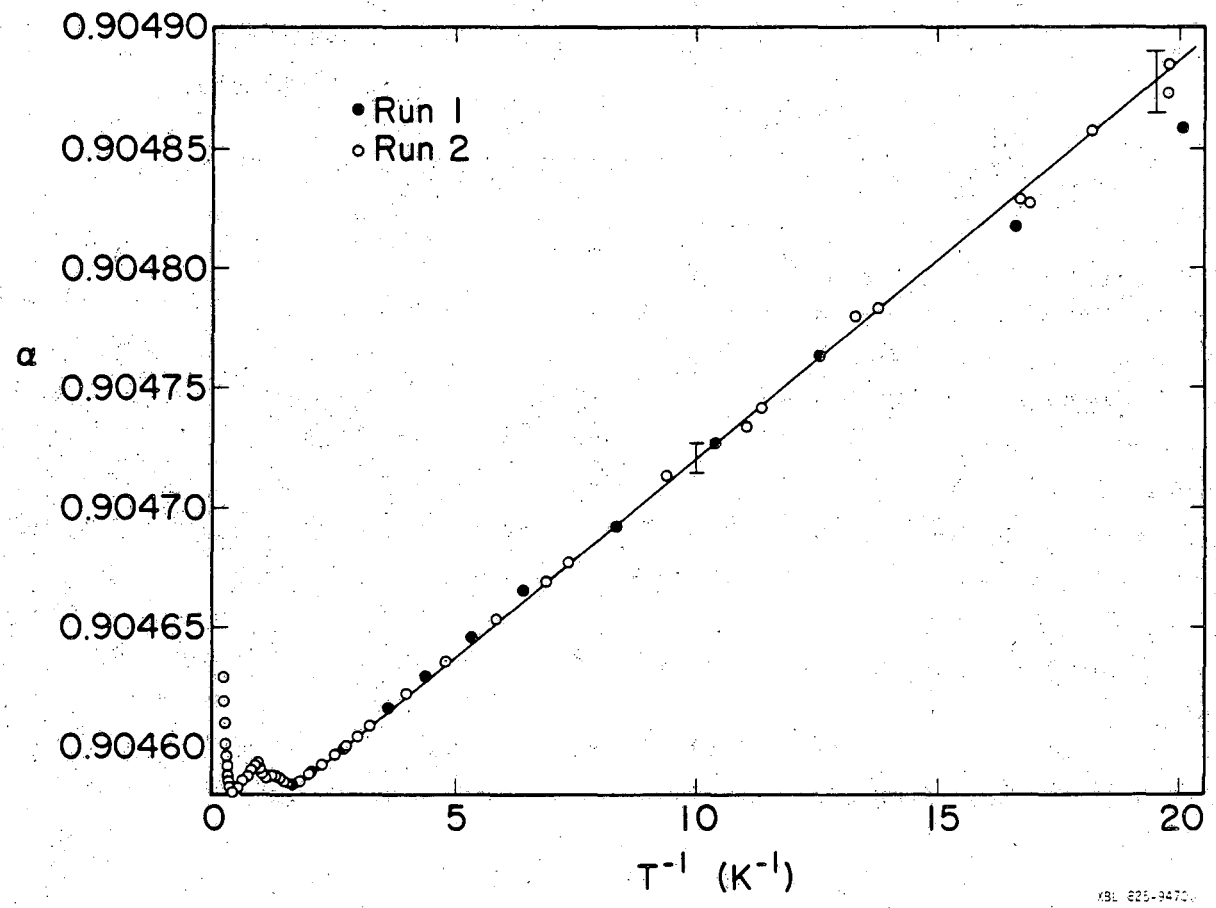

Fig. 16. The 16 Hz susceptibility of the epoxy CMN holder, expressed in units of the null in-phase ratio transformer setting (α) versus inverse temperature in the 0.05-3.8K region. Results from both Runs 1 and 2 are reported. The solid line represents a paramagnetic temperature dependence while the bars correspond to 0.01 percent in CMN temperature as explained in the text.

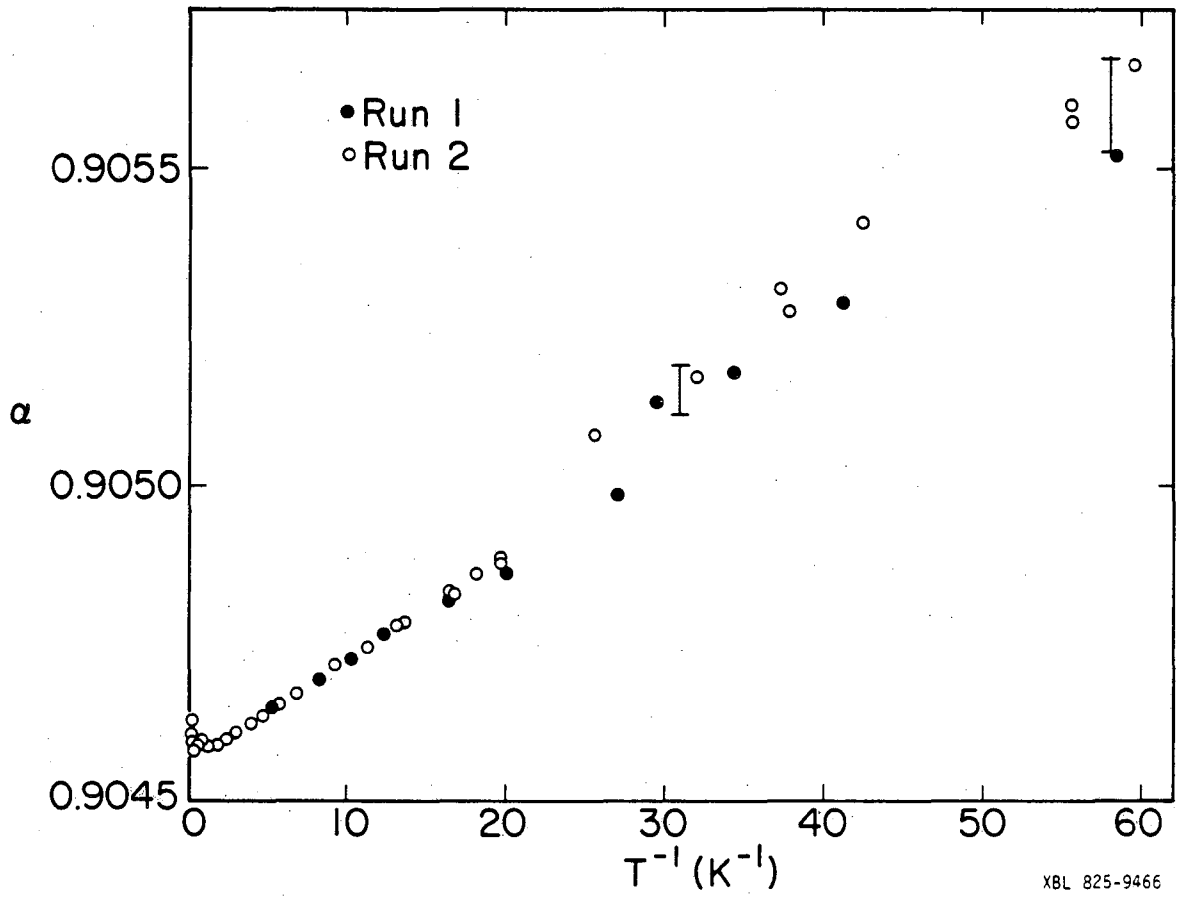

Fig. 17. The 16 Hz susceptibility of the epoxy CMN holder, expressed in units of the null in-phase ratio transformer setting (α) versus inverse temperature in the 0.017-3.8K region. Results from both Runs 1 and 2 are reported. The bars correspond to 0.02 percent in CMN temperature as explained in the text.

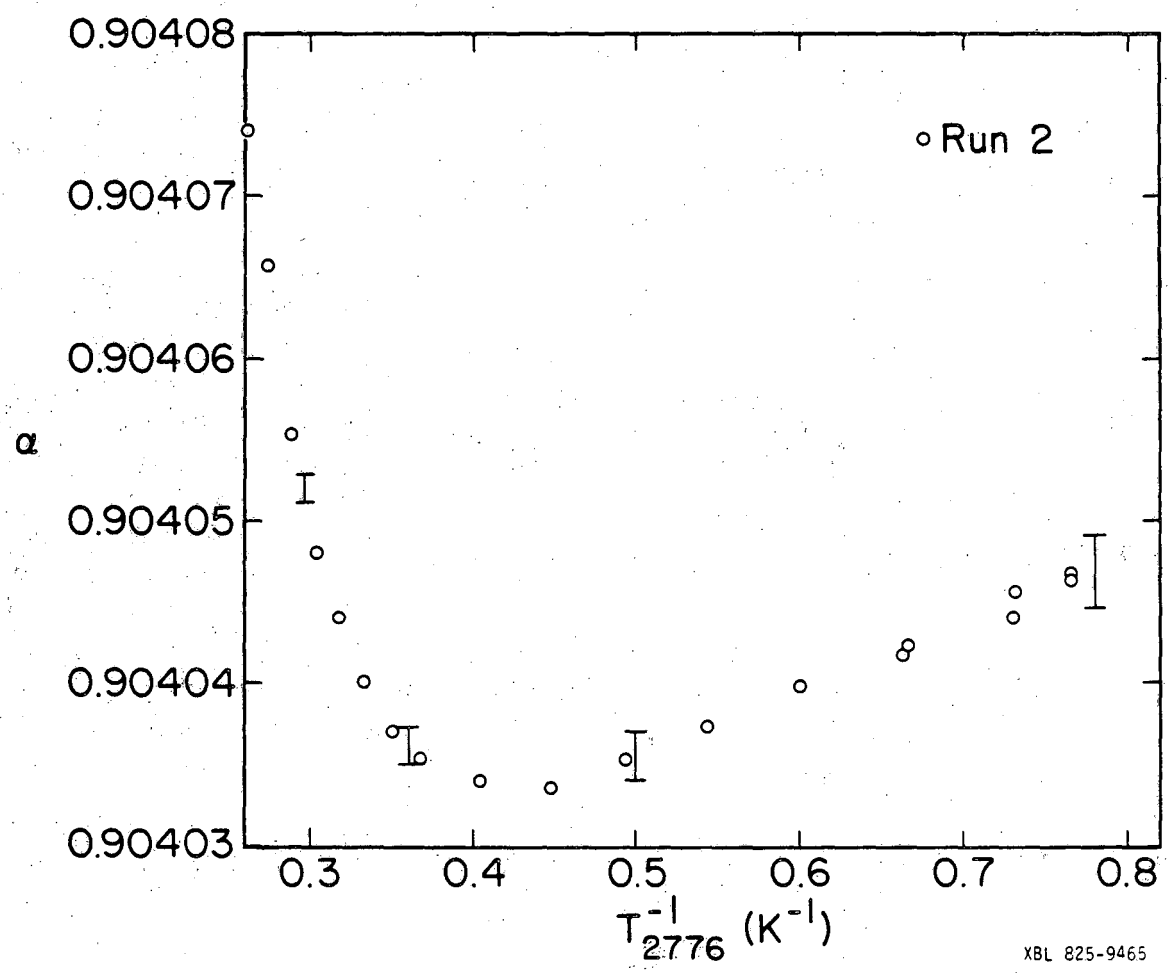

Fig. 18. The 160 Hz susceptibility of the epoxy CMN holder, expressed in units of the null in-phase ratio transformer setting (α) versus inverse temperature in the 1.3-3.8K region. The bars correspond to 0.05 percent in CMN temperature as explained in the text.

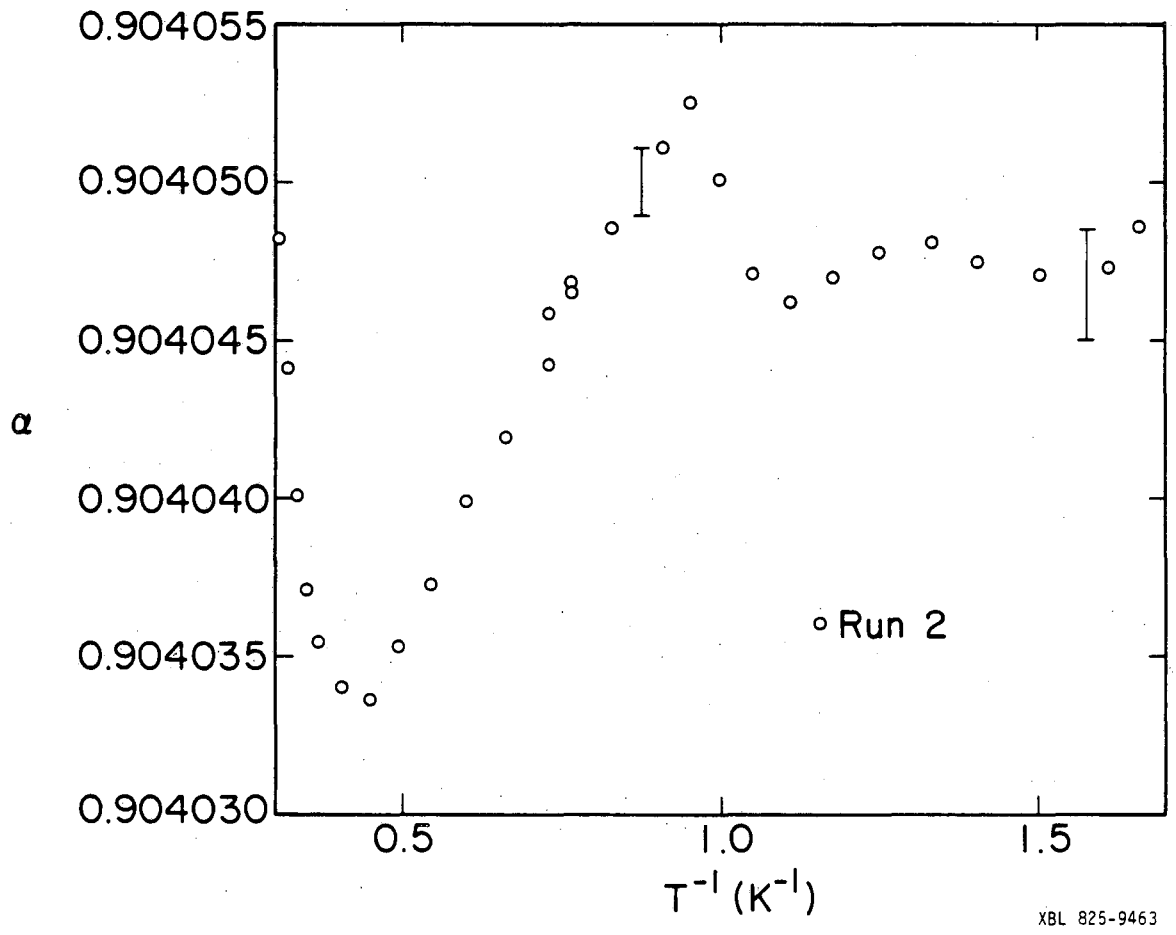

Fig. 19. The 160 Hz susceptibility of the epoxy CMN holder, expressed in units of the null in-phase ratio transformer setting (α) versus inverse temperature in the 0.6-3.3K region. The bars correspond to 0.02 percent in CMN temperature as explained in the text.

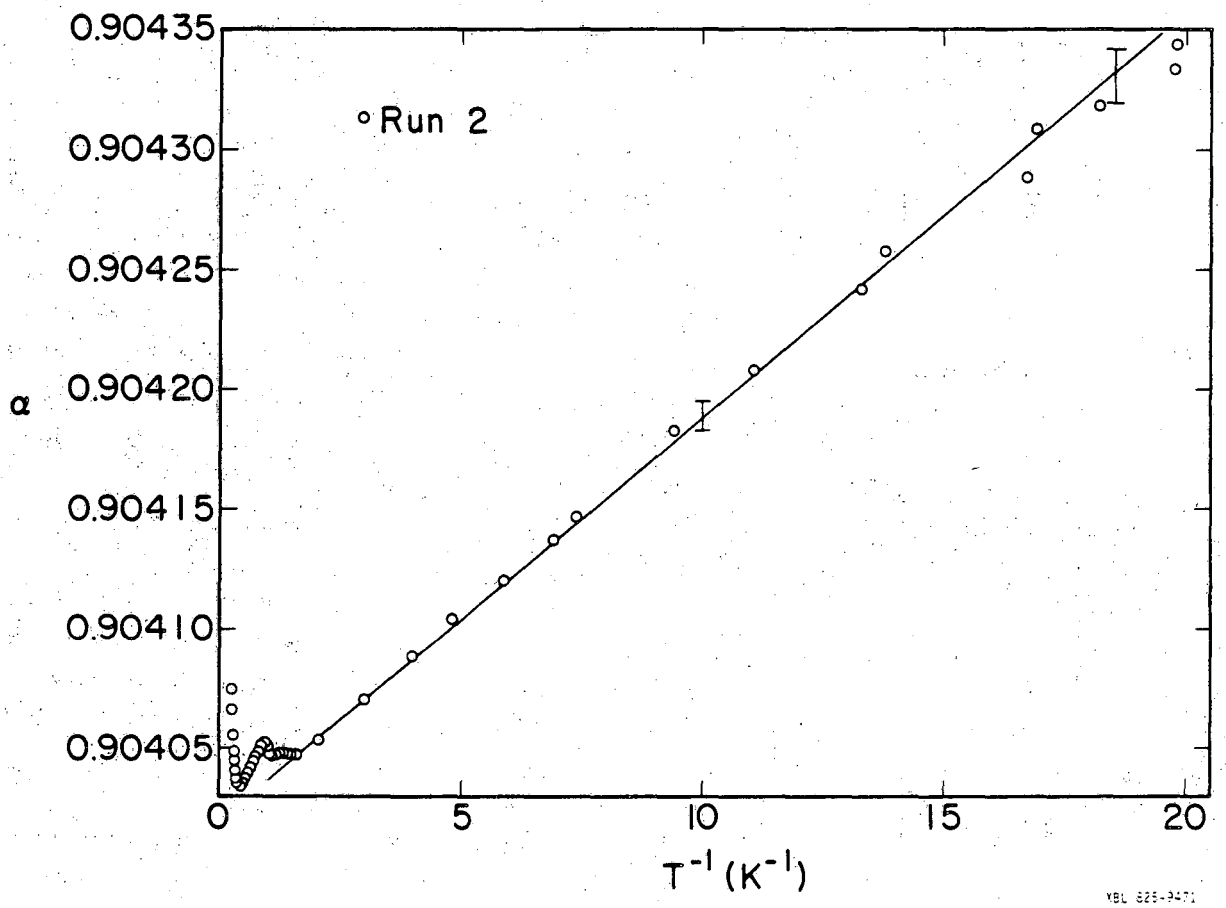

Fig. 20. The 160 Hz susceptibility of the epoxy CMN holder, expressed in units of the null in-phase ratio transformer setting (α) versus inverse temperature in the 0.05-3.8K region. The solid line represents a paramagnetic temperature dependence while the bars correspond to 0.01 percent in CMN temperature as explained in the text.

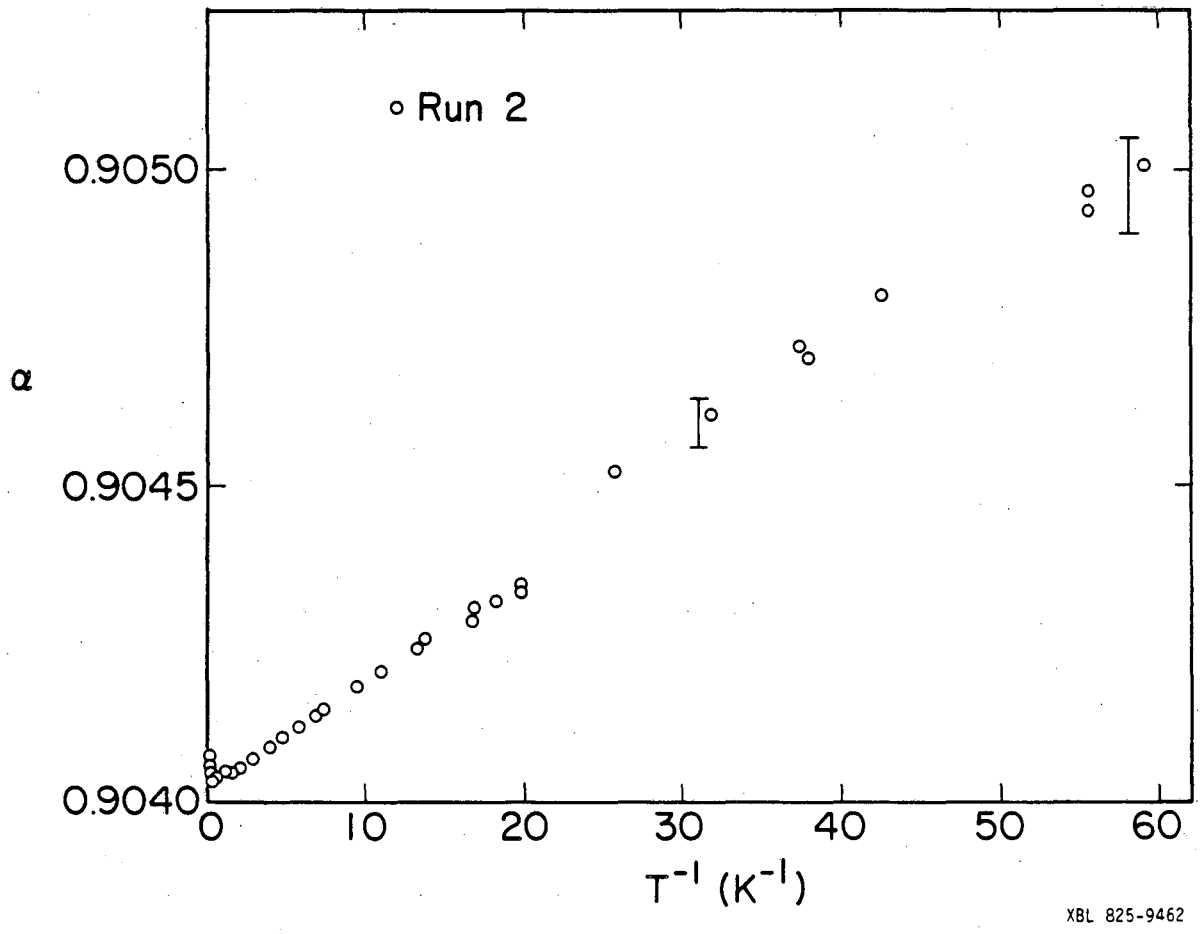

Fig. 21. The 160 Hz susceptibility of the epoxy CMN holder, expressed in units of the null in-phase ratio transformer setting (α) versus inverse temperature in the 0.017-3.8K region. The bars correspond to 0.02 percent in CMN temperature as explained in the text.

of the data in perspective, each plot has bars whose magnitudes of susceptibility translate into a percentage CMN temperature uncertainty which is given in each figure caption. The value of the CMN sensitivity used in these calculations was obtained from the final CMN experiments. The temperature uncertainties generally fall in the 0.005–0.10 percent range and show that, particularly for $T < 1$ K, the temperature dependence of χ_{MT} may be characterized in a straightforward fashion.

For 16 Hz, the data from the two separate runs have a similar temperature dependence but are displaced from one another by a constant fraction of a bridge unit. The variation in the bridge constant from run to run is believed to be due to small changes in the relative positions of the primary and secondary coils upon thermal cycling. This variation presents no problem, however, as only the temperature dependence of χ_{MT} is of importance, not its absolute magnitude. After normalizing the data from the two runs at 2 K (a constant fraction of a bridge unit was added to each data point of Run 1), excellent reproducibility of the temperature dependence of χ_{MT} is obtained. In addition, during each experiment, numerous data sets were taken which duplicated or overlapped each other to check the day-to-day reproducibility of the χ_{MT} temperature dependence. Small shifts of $\Delta\alpha \sim 1 \times 10^{-6}$ were sometimes found on a day-to-day basis--this factor corresponding to only 1/10 of one fine division on the ratio transformer rheostat and to ~5 times the noise level of the measurement. These shifts were well within the bridge specifications (see Sec. III) and were only observable when using substantial signal to noise averaging. (It is most likely that these shifts were associated with the temperature co-

efficients of the bridge components.) The standard procedure is to normalize individual data sets to the earliest work in a given run, generally using a single high temperature reference point. The resulting day-to-day agreement of the χ_{MT} temperature dependence is found to be essentially limited by the experimental noise level. For 160 Hz, due to problems with the bridge oscillator in the first experiment, only data for χ_{MT} from the second experiment are available. The temperature dependence and the day-to-day reproducibility of these data are similar to the 16 Hz data. In particular, between 0.05 K and 0.7 K, which was the bulk of the desired calibration range for the low-resistance GRT, χ_{MT} has a simple T^{-1} dependence with the slopes at the two frequencies being the same to within experimental error (~5 percent).

A conspicuous feature of both the 16 Hz and 160 Hz data is a relatively sharp anomaly in χ_{MT} at T ~ 1 K. Although the anomaly in this version of the epoxy CMN holder is not particularly large, an anomaly 20 times this size was found in the first epoxy holder. At that time, not only was the origin of the effect unknown, but it was feared that the anomaly might not be reproducible from run to run. Several experiments were conducted replacing parts of the holder one by one in an attempt to find the source of the anomaly. Only the final step, in which the former was replaced and new primary and secondary coils were wound, resulted in a marked reduction in the size of the anomaly. This may have been due to the magnetic properties of the Epibond 100A (although the replacement of the second insert, which was also fabricated from Epibond 100A, had no effect on the size of

the anomaly) or due to a more precise matching of the two halves of the secondary which were designed to minimize external perturbations. In any case, the final version of the holder was then used to conduct the run-to-run reproducibility check described above. Exhaustive tests for any hysteresis in the anomaly of the final epoxy holder were conducted by rapidly cycling above and below the anomaly between two reference temperatures, recording the bridge null point at each reference temperature. No evidence of any hysteresis was ever found.

The results of the two calibration experiments on the gold-plated copper holder are shown in Figs. 22-24. In both of these experiments, an attempt was made to trap 5 G in the Nb tube. (Other experimenters[7] report run-to-run variations in the final trapped field of 20 percent while our own experience, using observed sensitivities in CMN experiments, reveals variations of up to ~4 percent.) Unknown variations in the measuring field between an empty sample holder experiment and a CMN experiment result in a somewhat inappropriate characterization of χ_{MT} relative to the CMN experiment. (The ac susceptibility thermometer does not suffer from this difficulty since its measuring field is determined by the combination of the externally controlled primary current and the geometries of the primary coil and the Nb shielding tube.) An additional complication results from the fact that the flux transformer coils were rewound between the two experiments. However, the data from the two runs are in good agreement for $T < 0.1$ K where the copper holder has a simple paramagnetic temperature dependence. This would seem to indicate that the measuring field was reproducible for these two runs. In the 0.1-0.5 K region,

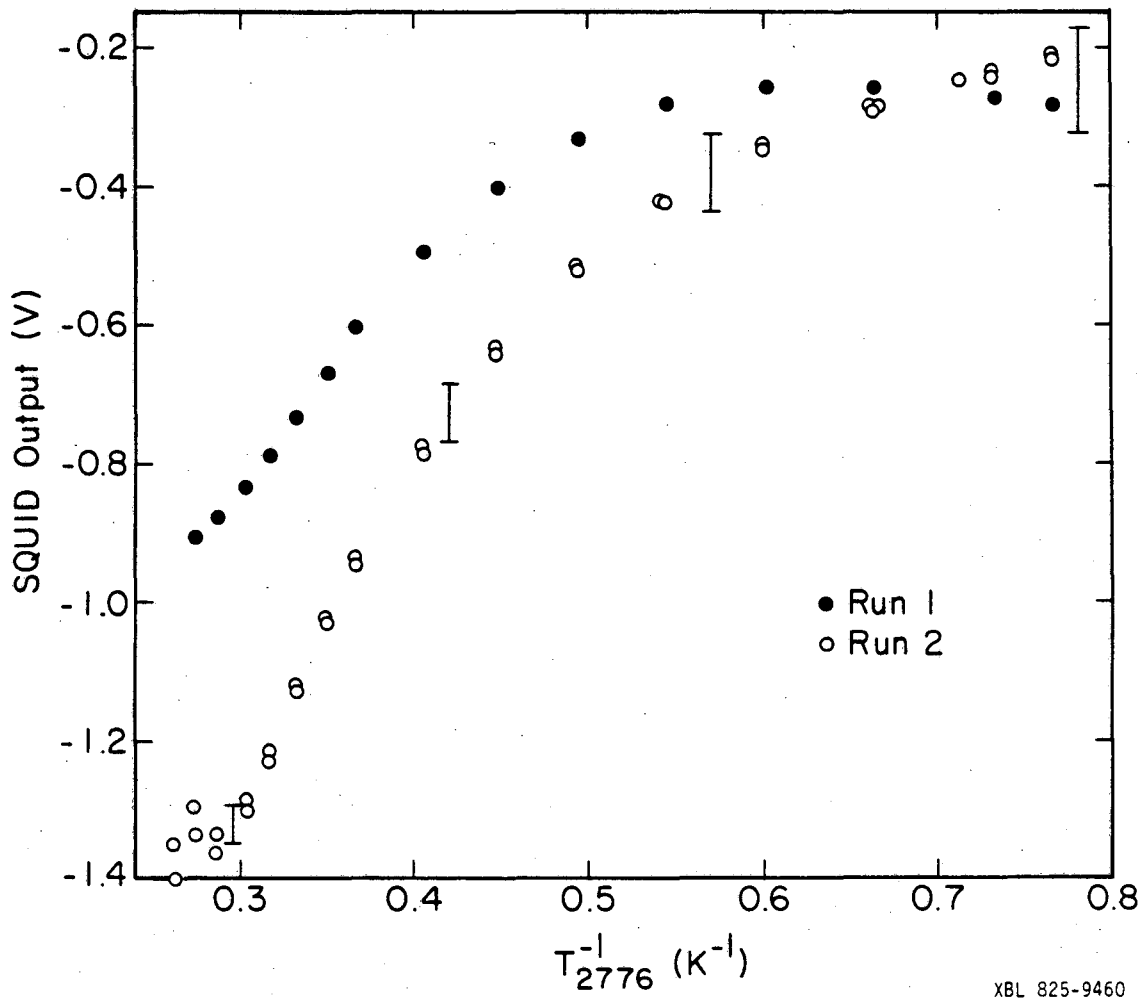

Fig. 22. The dc susceptibility of the copper CMN holder, expressed in units of the SQUID output voltage versus inverse temperature in the 1.25-3.6K region. Results from both Runs 1 and 2 are reported. The bars correspond to 0.5 percent in CMN temperature as explained in the text.

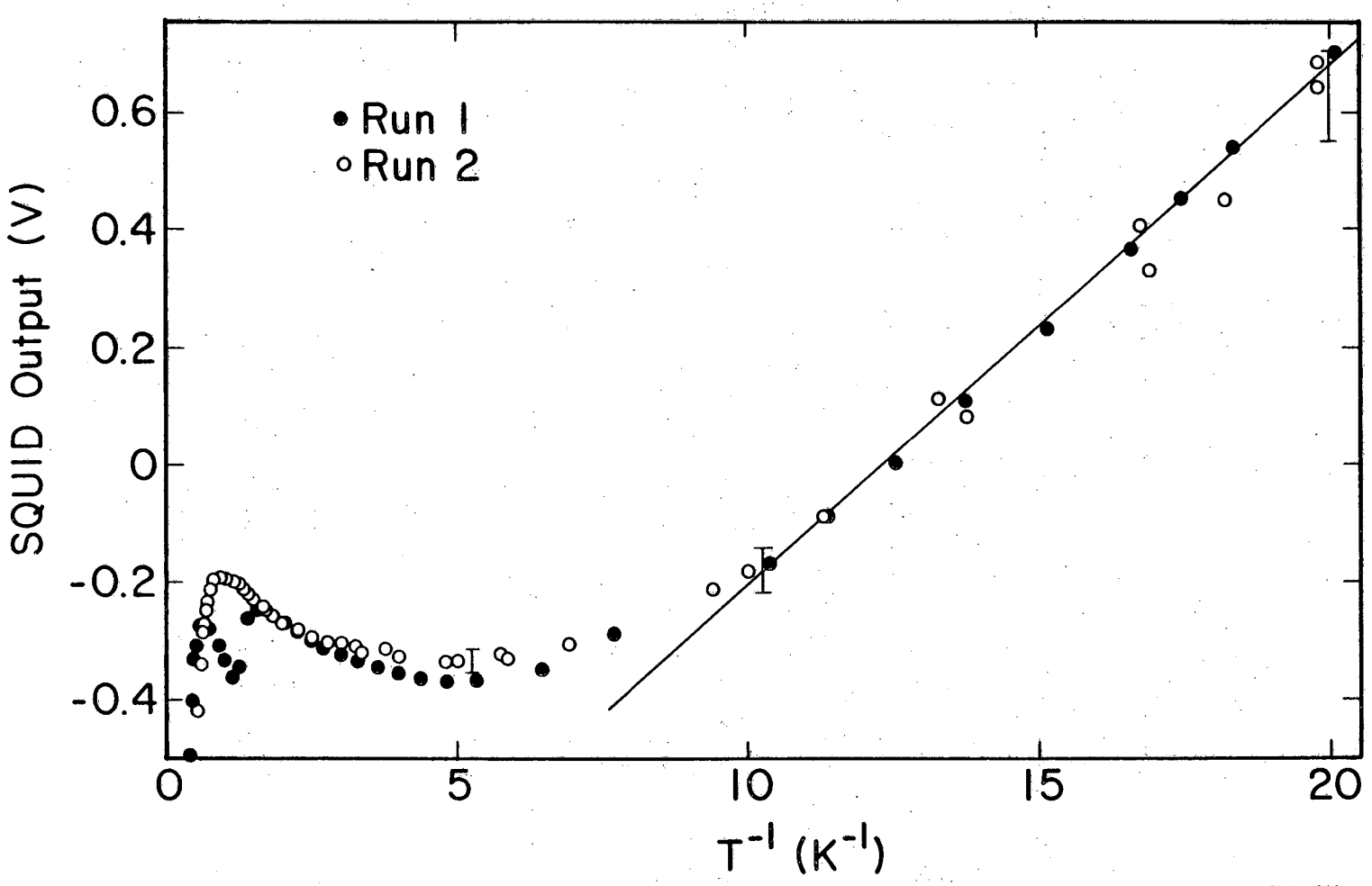

XBL 825-9469

Fig. 23. The dc susceptibility of the copper CMN holder, expressed in units of the SQUID output voltage versus inverse temperature in the 0.05-3.6K region. Results from boths Runs 1 and 2 are reported. The solid line represents a paramagnetic temperature dependence (the same as that in Fig. 24) while the bars correspond to 0.02 percent in CMN temperature as explained in the text.

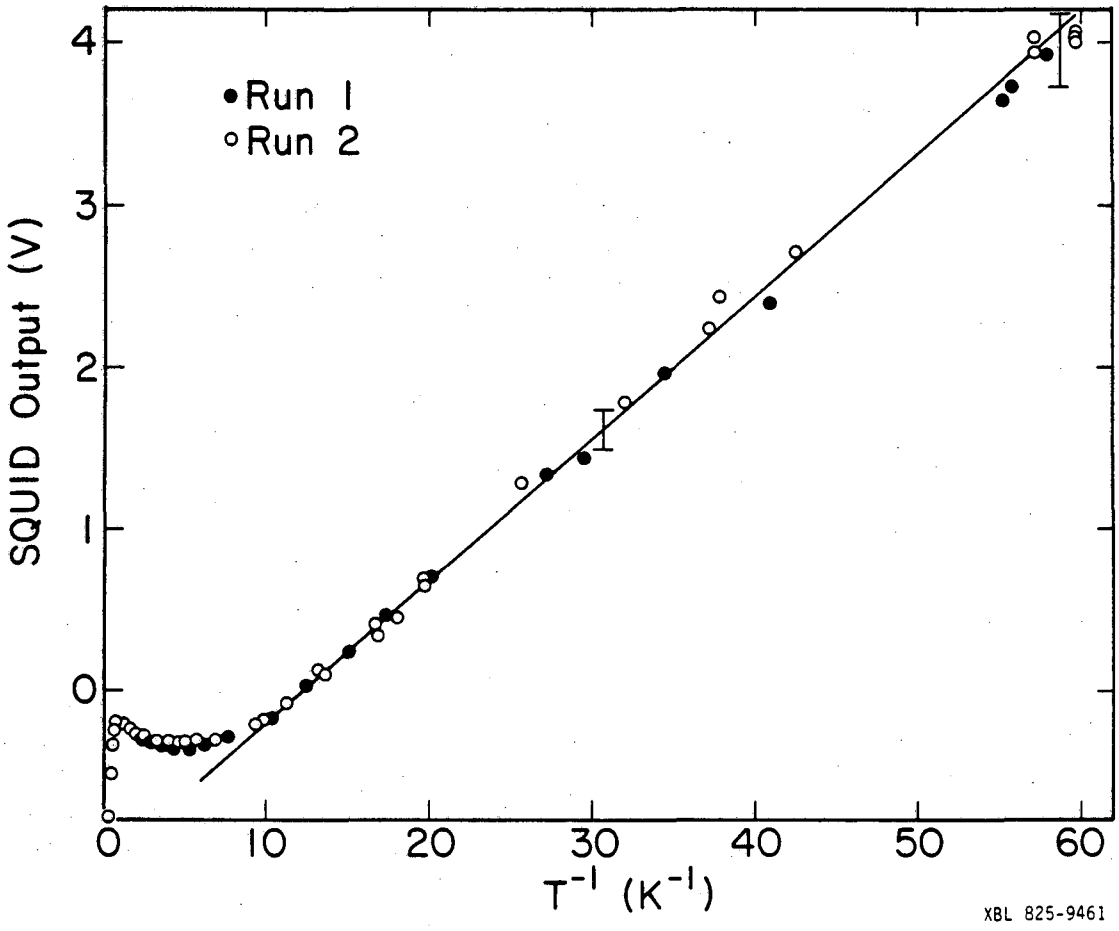

Fig. 24. The dc susceptibility of the copper CMN holder, expressed in units of the SQUID output voltage versus inverse temperature in the 0.017-3.6K region. Results from both Runs 1 and 2 are reported. The solid line represents a paramagnetic temperature dependence while the bars correspond to 0.02 percent in CMN temperature as explained in the text.

the two runs exhibit a similar temperature dependence where χ_{MT} goes through a shallow minimum. It is only for T > 0.75 K that the data from the two runs substantially fail to reproduce--a result which is attributed to rewinding the flux transformer. The day-to-day reproducibility of χ_{MT} for the copper holder was checked in a fashion similar to that for the epoxy holder. After normalizing each data set at some convenient high temperature (to allow for small day-to-day variations in the SQUID output as well as flux jumps), excellent reproducibility in the temperature dependence of χ_{MT} is observed.

A common feature in the χ_{MT} data for both the copper and epoxy holders is the rather strong temperature dependence observed for T > 1 K. Indeed, this feature has been present to some extent in every CMN holder used in these experiments. Such an effect is an unfortunate occurrence in this temperature interval since the CMN sensitivity decreases with increasing temperature. It thus becomes more likely that the uncertainties in χ_{MT} may limit significantly the accuracy of the final χ_{CMN} data. A possible explanation for the source of this feature is the temperature dependence of the penetration depth (λ) of the superconducting materials in the thermometers (Nb and NbTi). That is, as a thermometer is cooled below T_c (which is 9.2 K for both Nb and NbTi), flux is continuously expelled from the surface region of the superconductors as λ approaches a minimum or limiting value. To examine the temperature region over which this effect is observable, the susceptibility of a mass of the Nb wire used in the original version of the epoxy CMN holder was measured. As expected, a sharp diamagnetic signal associated with a bulk superconducting trans-

ition was observed at T_c. In addition, for temperatures below T_c, a diamagnetic tail to the transition was observed which extended well into the 1-4 K region. For the CMN holders, however, an attempt to fit χ_{MT} for $T > 1$ K to the expected temperature dependence of λ was not successful (perhaps due to a significant paramagnetic contribution of the sample holder materials to the total susceptibility).

The complication of the temperature dependence of χ_{MT} for $T > 1$ K is most likely to have an adverse effect on the results from the dc susceptibility thermometer if, indeed, the complication is associated with the penetration depth of the superconducting materials. Then, for the dc susceptibility thermometer, the magnitude of the effect will depend upon the value of the field trapped in the Nb tube since it is the ambient field which must be expelled from the superconductor. Thus, the temperature dependence of χ_{MT} may vary from run to run since this field may vary by 0-20 percent. For the ac susceptibility thermometer, both the primary field distribution and the field distribution due to the induced currents in the Nb tube should be reproducible from run to run. The temperature dependent portion of χ_{MT} associated with the temperature dependence of λ in the Nb tube and in the secondary coils is thus expected to be reproducible from run to run. Hence, the ac susceptibility thermometer is expected to give the best performance in the 1-4 K region and this was indeed the case (see Sec. IX A).

Although the CMN sample holders had, in general, the weakly temperature dependent susceptibilities desired (compared to CMN) and the epoxy CMN holder in particular reproduced well from run to run, the

possibility of an anomalous shift in χ_{MT} between an empty CMN holder run and a CMN calibration run cannot be ruled out. There are, however, tests that can be made on the CMN data which yield information about the reasonableness of the representations used for the CMN holders. In the crucial 1.3-3.5 K region, after subtracting χ_{MT} from χ_{TOTAL} to get χ_{CMN}, the χ_{CMN} versus T_{2776}^{-1} data may be fit to a Curie law (the of the Curie-Weiss law is too small to be detected in this temperature interval with our signal/noise ratio). A good fit is anticipated since χ_{CMN} is known to obey a Curie law in this region and the integrity of the GE2776 scale is known to be excellent. Hence, good fits in this region preclude any substantial χ_{MT} misrepresentation. In the 0.05-1.0 K range, the situation is different in that the temperature scales on the GE1751 and the GE2345 do not necessarily have the integrity of the GE2776. However, since the ac and the dc susceptibility thermometers were run simultaneously and were assumed to be in good equilibrium, the two thermometer outputs are expected to bear a linear relationship to each other if the CMN follows a Curie-Weiss law with similar values of Δ for the two thermometers. Verification of this relationship precludes any χ_{MT} misrepresentation in this region.

In addition to calibrating the epoxy holder at 16 Hz and 160 Hz, the holder was also calibrated in the dc susceptibility mode by shutting off the bridge and using the bridge secondary as a flux transformer. The static field for the measurement was the component of the earth's magnetic field trapped in the Nb tube. Since this field was quite small, the sensitivity of the thermometer in this configuration

was marginal. As shown in Figs. 25 and 26, the calibration consisted only of data points at 16 mK relative to a series of data points in the 0.1-1.0 K range. The calibration was done in this fashion for two reasons: (1) Intermediate data in the 0.016-0.1 K range were felt to be unnecessary (and were the most difficult to obtain) since the ac susceptibility measurements indicated that χ_{MT} was frequency independent and linear in T^{-1}. (2) The main reason for operating this thermometer in a dc mode was to double check the 16 Hz and the 160 Hz magnetic temperatures--a test best done at the lowest temperatures where the spin-lattice relaxation time of the CMN is the longest.

During the calibration of the epoxy holder in the dc mode, the fringe field of the heat switch coil was found to adversely affect the measurements. This effect was first observed as a large change in the SQUID output due to the opening of the heat switch when preparing to warm from 16 mK to 0.1 K. The change in the SQUID output was not due to the temperature dependence of χ_{MT} but rather to a change in the ambient magnetic flux in the flux transformer of the epoxy holder (in spite of the fact that the transformer was composed of an astatic pair of coils which should have cancelled a uniform perturbation to first order). Subsequently, the effect was also demonstrated to exist by holding the thermometer bus at a convenient constant temperature (as determined by a GRT) and ramping the current in the heat switch coil up and down. The SQUID output was observed to follow the heat switch ramping. When the epoxy holder was returned to ac operation, similar tests failed to detect any influence of the heat switch coil on the

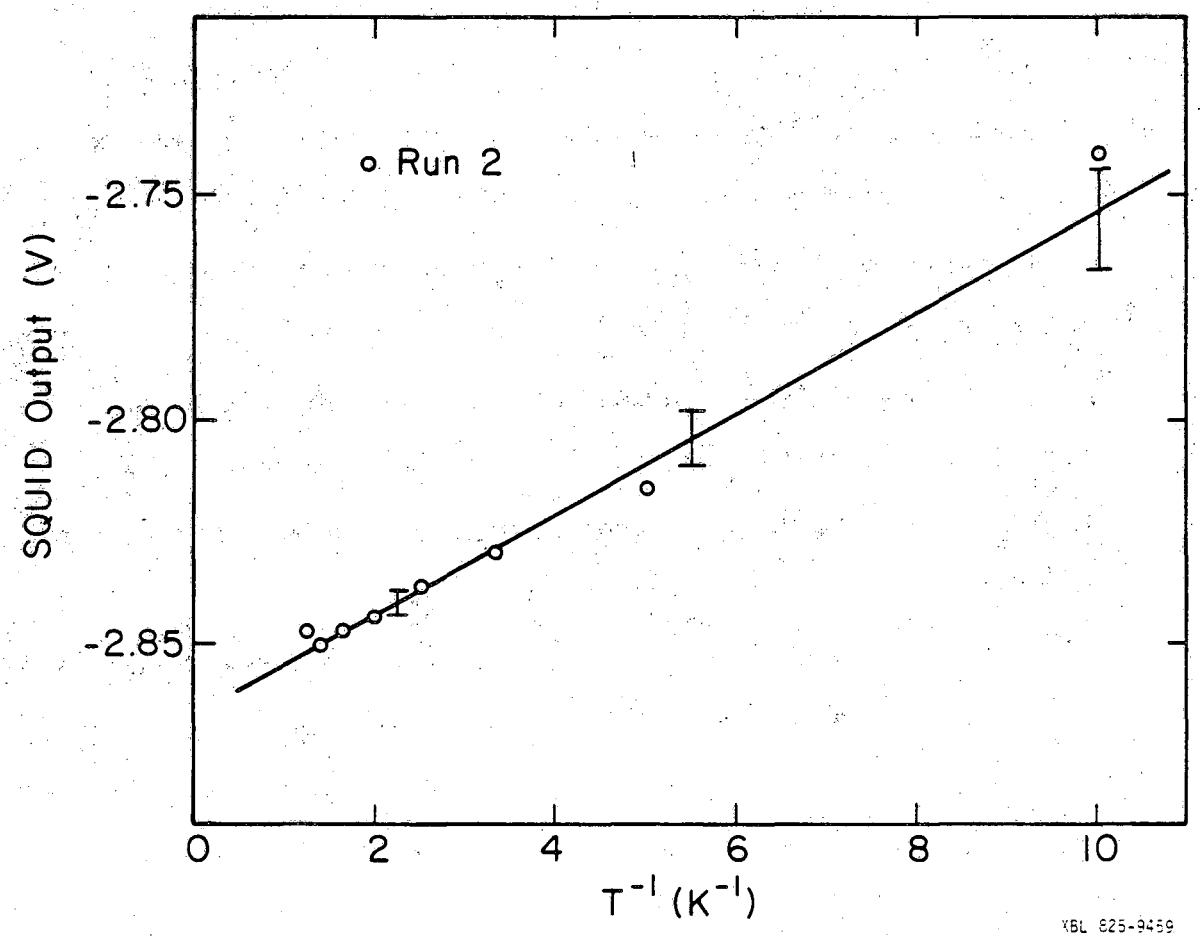

Fig. 25. The dc susceptibility of the epoxy CMN holder, expressed in units of the SQUID output voltage versus inverse temperature in the 0.1-1.0K region. The solid line represents a paramagnetic temperature dependence (the same as that in Fig. 26) while the bars correspond to 0.02 percent in CMN temperature as explained in the text.

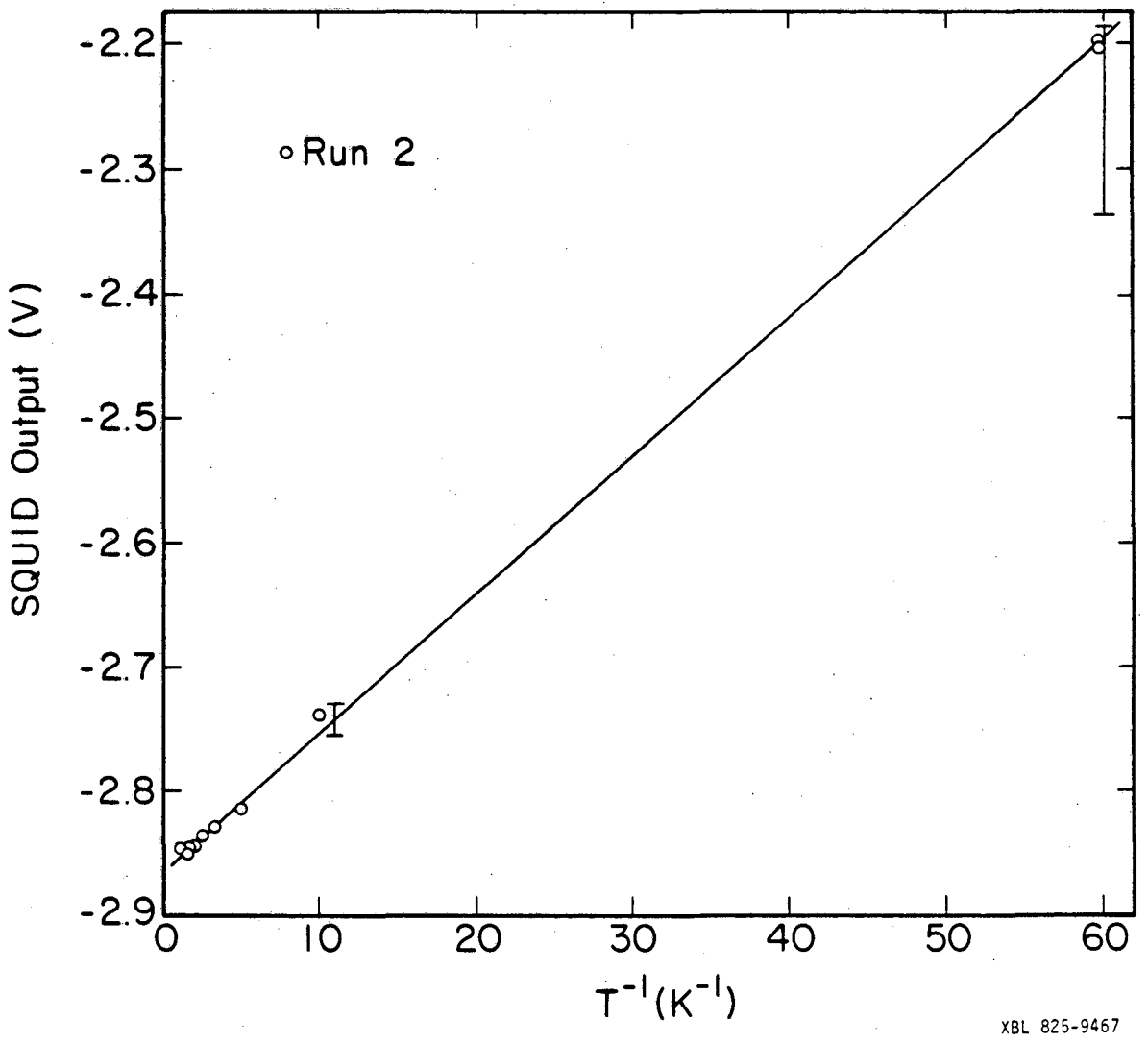

Fig. 26. The dc susceptibility of the epoxy CMN holder, expressed in units of the SQUID output voltage versus inverse temperature in the 0.017-1.0K region. The solid line represents a paramagnetic temperature dependence while the bars correspond to 0.02 percent in CMN temperature as explained in the text.

bridge balance or performance. This was expected since the ambient field changes were essentially a dc effect. More importantly, tests on the copper holder also failed to detect any adverse effects associated with changes in the fringe field of the heat switch coil. The immunity of this thermometer to changes in the ambient magnetic field was due to the much more favorable aspect ratio of its Nb shielding tube. The shielding capability of a superconducting tube (assumed to be an ideal diamagnet) has an exponential dependence on this ratio.[69] The leading term in the expressions for the attenuation of axial and radial perturbing fields is $\exp(-3.4\ z/r)$ and $\exp(-1.8\ z/r)$, respectively, where r is the tube radius and z is the on-axis distance into the tube at which the attenuation is calculated. Since the susceptibility thermometers were located in essentially the same plane as the heat switch coil, symmetry considerations suggest that the axial attenuation factor was the most important. In addition, the CMN coils of the flux transformers had axial symmetry which indicates that, to first order, the thermometer outputs were only sensitive to axial components of the CMN magnetization. For the ac susceptibility thermometer, $r = 0.385$ in. and the pickup coils were located at a distance $z = 0.75$ in. from the end of the tube. For the dc susceptibility thermometer, these dimensions were $r = 0.095$ in. and $z = 0.50$ in. The axial attenuation factors were thus 1.2×10^{-3} and 1.7×10^{-8} for the ac and dc susceptibility thermometers, respectively. Clearly, the shielding offered by the Nb tube on the copper holder was superior to that for the epoxy holder. In either case, the best test for any parasitic influence of the fringe field may be made with CMN in the hold-

er to accentuate the size of the effect. These tests will be described in Sec. IX B. Thus, the susceptibility of the copper holder and that of the epoxy holder in the ac mode was determined without any difficulty since these results were independent of the position of the superconducting heat switch. Although the heat switch was generally opened at ~0.1 K to minimize the regulation power, for the epoxy holder in the dc mode, the calibration data shown in Figs. 25 and 26 were taken with the heat switch closed (coil energized). This procedure ensured a constant measuring field for the epoxy holder over the entire calibration range.

A final point related to the χ_{MT} measurements concerns equilibrium times. For T > 0.5 K, both the copper and epoxy holders had such short relaxation times that equilibrium was attained as rapidly as the temperature could be regulated. It was for this reason that the reference temperatures used to normalize various sets of data were chosen to be at high temperatures. As the temperature was lowered, increasingly long relaxation times were observed for both CMN holders. Although the copper holder might have been expected to have short equilibrium times at low temperatures, it was in fact observed to respond to temperature changes with both a large and fast component of χ_{MT} as well as a small and slow component of χ_{MT}--the two contributions affecting the SQUID output in the opposite sense. The fast component is believed to be due to the metallic parts of the sensor while the slow component was presumably due to dielectric materials. In response to temperature changes, the epoxy holder simply became monotonically slower at low temperatures. At 16 mK, for both CMN holders, 6-8 hours

were needed to attain substantial equilibrium. The long term equilibrium values of χ_{MT} were determined by allowing the holders to equilibrate for 17 hours at 16 mK. Small errors in χ_{MT}, which were insignificant compared to the CMN sensitivity (susceptibility errors corresponding to CMN temperature errors of less than 0.05 percent), were made when ~3 hour equilibration times were used. The best way to determine χ_{MT} unambiguously at low temperatures is to measure χ_{MT} at a given temperature twice, once approaching the desired temperature from higher temperatures and finally approaching the desired temperature from lower temperatures after having been cold for an extended period. In this way, upper and lower limits on χ_{MT} may be established at any temperature. This procedure was followed in the second calibration run on the CMN holders (labeled as Run 2 in the figures) and is generally indicated by having two calibration points at essentially the same temperature.

In conclusion, with the possible exception of the copper holder in the 1-4 K region, the susceptibilities of the CMN holders are believed to be well defined relative to the susceptibility of CMN.

IX. SUSCEPTIBILITY OF CMN AND THE MAGNETIC TEMPERATURE SCALE

A. Calibration of the Susceptibility of CMN Against the Helium Vapor Pressure Scale

The primary objective of this work was to extend the vapor pressure scale to temperatures below 1 K via magnetic thermometers. Thus, in the CMN experiments, an important procedure was to calibrate the susceptibility thermometers against the vapor pressure scale in the 1-4 K region as represented on the GE2776. To minimize any uncertainty in the representation of the vapor pressure scale, the temperatures used in these calibrations coincided with GE2776-GE897 calibration points where the GE897 is one of the principal laboratory standard GRT upon which the vapor pressure scale is maintained (see Sec. V). In Table X, the calibration points of the 16 Hz bridge data from Run 3 are given. To analyze the performance of the thermometer, both the total mutual inductance (as measured by the null reading of the in-phase ratio transformer) and that quantity corrected for the empty CMN holder have been fit against inverse temperature (since the Curie-Weiss constant is too small to be detected in this temperature interval). The quality of the fits is illustrated by the percentage deviations, Δ_{CMN} and Δ_{TOT}, which are defined in Table X. T_{2776} is the observed temperature of a given point on the GE2776 thermometer and T_{FIT} is the temperature calculated from the fit equation using the observed values of α_{CMN} or α_{TOT}. In the final column, the quantity Δ_N, which represents a percentage deviation calculated from the observed bridge noise level, is tabulated. The point here is that the

Table X. Calibration of the ac susceptibility thermometer in Run 3 at 16 Hz with the GE2776 GRT. Fits of the in-phase null bridge reading (α_{TOT}) and that reading corrected for the empty sample holder (α_{CMN}) versus inverse temperature are given as Fit 1 and Fit 2, respectively. Δ_{TOT} and Δ_{CMN} are percentage deviations from the fits while Δ_N is a percentage deviation calculated from the observed noise level as explained in the text.

Point	T_{2776}	α_{TOT}	$\alpha_{CMN}(\times 10^3)$	Δ_{TOT}	Δ_{CMN}	Δ_N
1	1.37367	0.8944716	-10.1155	-0.146	-0.037	0.012
2	1.51556	0.8953038	- 9.2814	-0.068	-0.010	0.013
3	1.68062	0.8960942	- 8.4893	+0.035	+0.036	0.015
4	1.85549	0.8967814	- 7.8008	+0.095	+0.038	0.016
5	2.04926	0.8974072	- 7.1741	+0.140	+0.023	0.018
6	2.25810	0.8979624	- 6.6185	+0.171	-0.003	0.020
7	2.48680	0.8984638	- 6.1184	+0.197	-0.007	0.022
8	2.73742	0.8989183	- 5.6671	+0.197	+0.007	0.024
9	3.01974	0.8993425	- 5.2493	+0.134	+0.043	0.027
10	3.33496	0.8997420	- 4.8608	-0.226	-0.068	0.030
11	3.68375	0.9001072	- 4.5133	-0.709	-0.045	0.033

$$\text{Fit 1:}\quad \alpha_{TOT} = \frac{-1.23216\times10^{-2}}{T_{2776}} + 0.903428$$

$$\text{Fit 2:}\quad \alpha_{CMN} = \frac{-1.22757\times10^{-2}}{T_{2776}} - 1.1824\times10^{-3}$$

$$\Delta_{TOT} \text{ and } \Delta_{CMN} = \frac{T_{2776} - T_{FIT}}{T_{FIT}}\, 10^2 \qquad \Delta_N = \frac{\Delta\alpha_N \times T}{1.228\times10^{-2}}\, 10^2 = 8.88\times10^{-3}T$$

quality of the CMN fit cannot be expected to be better than the noise level of either the T_{2776} or the α_{TOT} measurement. In this particular case, the T_{2776} noise level is lower than that of the bridge, so it is the bridge noise level with which the fit quality should be compared. To calculate Δ_N, the fit equation is differentiated $|d\alpha/dT| = 1.228 \times 10^{-2}/T$ and rearranged so that $\Delta_N = 100\ \Delta T/T = 100(\Delta\alpha_N)T(1.228 \times 10^{-2})^{-1}$. The bridge noise level was observed to be $\Delta\alpha_N \sim 1 \times 10^{-6}$ when averaging the lock-in amplifier output for 100 seconds. This comparison of fit deviations and thermometer noise level will be used for all tables of data in this section. An inspection of Table X reveals several interesting points. The fit of α_{CMN} is clearly superior to that of α_{TOT}. For α_{CMN}, the deviations are small and oscillate in sign whereas for α_{TOT}, the deviations are much larger and have signs which indicate the data systematically deviate from Curie law behavior. The magnitude and sign of the deviations for α_{TOT} are consistent with the measurements of α_{MT}. Further, the Δ_N tabulation shows the α_{CMN} fit is close to the bridge noise level thus indicating the CMN follows a Curie law to within experimental error in Run 3. (It must also be true that the GE2776 scale is smooth to at least 5 parts in 10^4.) This result may be used to confirm that the temperature dependence of α_{MT} is the same in both the empty sample holder and CMN runs.

In Table XI, results for the bridge at 160 Hz in the same run are given, measurements having been made at every other temperature used in Table X. The results for 160 Hz are similar to those for 16 Hz--that

Table XI. Calibration of the ac susceptibility thermometer in Run 3 at 160 Hz with the GE2776 GRT. Compared with Table I, calibration data were taken at every other calibration point. Tabulated quantities are defined in Table I.

Point	T_{2776}	α_{TOT}	$\alpha_{CMN}(\times 10^3)$	Δ_{TOT}	Δ_{CMN}	Δ_N
1	1.37369	0.8938771	-10.1677	-0.099	-0.007	0.013
2	1.68039	0.8955057	- 8.5339	+0.009	+0.002	0.016
3	2.04921	0.8968173	- 7.2177	+0.160	+0.028	0.020
4	2.48685	0.8978746	- 6.1592	+0.225	-0.008	0.024
5	3.02000	0.8987555	- 5.2851	+0.134	-0.027	0.029
6	3.68434	0.8995151	- 4.5520	-0.537	+0.010	0.036

Fit 1: $$\alpha_{TOT} = \frac{-1.23294\times10^{-2}}{T_{2776}} + 0.902844$$

Fit 2: $$\alpha_{CMN} = \frac{-1.23025\times10^{-2}}{T_{2776}} - 1.2125\times10^{-3}$$

$$\Delta_{TOT} \text{ and } \Delta_{CMN} = \frac{T_{2776} - T_{FIT}}{T_{FIT}} 10^2 \qquad \Delta_N = \frac{\Delta\alpha_N \times T}{1.230\times10^{-2}} 10^2 = 9.67\times10^{-3}T$$

is, α_{CMN} yields a much better fit than α_{TOT} and the α_{CMN} fit is once again essentially limited by the bridge noise level. Note that the fit results for the 16 Hz and the 160 Hz α_{CMN} data have slopes which differ by only 0.22 percent. This indicates that the temperature dependence of the CMN susceptibility in the 1.4-3.7 K region is frequency independent from 16-160 Hz.

In Table XII, results for the dc susceptibility thermometer are reported. These data were taken simultaneously with the 16 Hz and 160 Hz data of Run 3 tabulated in Tables X and XI. Once again, the susceptibility thermometer output (the SQUID output in volts) and the output corrected for the empty CMN holder are fit versus inverse temperature with the respective percentage deviations tabulated as Δ_{TOT} and Δ_{CMN}. The dominant noise level in this calibration is also due to the CMN thermometer and the percentage temperature uncertainties associated with the noise level may be calculated in a fashion similar to that for the ac susceptibility thermometer. It follows that $|dV/dT| = 33.588/T^2$ and rearranging, $\Delta_N = 100\ \Delta T/T = 100(\Delta V_N)T(33.588)^{-1}$. It was observed in this experiment that ΔV_N, which is the uncertainty in the voltage output of the SQUID, was ~1 mV (when averaging the voltage output for 100 seconds). The results of this calibration are clearly poorer than those of the ac susceptibility thermometer even though, based upon the noise levels of the respective CMN thermometers, the dc susceptibility thermometer was expected to yield superior performance. (This expectation is largely due to the fact that this thermometer employed a static

Table XII. Calibration of the dc susceptibility thermometer in Run 3 with the GE2776 GRT. Fits of the SQUID output (V_{TOT}) and that reading corrected for the empty sample holder (V_{CMN}) versus inverse temperature are given as Fit 1 and Fit 2, respectively. The SQUID output is given in volts. Δ_{TOT} and Δ_{CMN} are percentage deviations from the fits while Δ_N is a percentage deviation calculated from the SQUID noise level as explained in the text.

Point	T_{2776}	V^a_{TOT}	V^a_{CMN}	Δ_{TOT}	Δ_{CMN}	Δ_N
1	1.37367	-10.313	-10.561	+1.01	+0.36	0.0041
2	1.51556	-12.487	-12.774	+0.22	+0.08	0.0045
3	1.68062	-14.519	-14.867	-0.50	-0.18	0.0050
4	1.85549	-16.233	-16.659	-0.99	-0.34	0.0055
5	2.04926	-17.745	-18.275	-1.20	-0.44	0.0061
6	2.25810	-19.035	-19.682	-1.06	-0.37	0.0067
7	2.48680	-20.148	-20.939	-0.47	-0.20	0.0074
8	2.73742	-21.092	-22.041	+0.76	+0.28	0.0081
9	3.01974	-21.904	-23.045	+2.79	+1.01	0.0090

Fit 1: $V_{TOT} = \frac{-31.895}{T_{2776}} + 29.351$

Fit 2: $V_{CMN} = \frac{-33.588}{T_{2776}} + 31.519$

Δ_{TOT} and $\Delta_{CMN} = \frac{T_{2776} - T_{FIT}}{T_{FIT}} 10^2$ $\qquad \Delta_N = \frac{\Delta V_N \times T}{33.588} 10^2 = 2.97 \times 10^{-3} T$

[a] The SQUID was used in the x100 sensitivity mode (1.958 volts = $1\phi_o$) for these measurements.

measuring field of 5 G whereas the ac susceptibility thermometer used a peak measuring field of only 0.1 G. The other relevant factor to consider is that the ac susceptibility thermometer had 4.6 times more CMN than the dc susceptibility thermometer.) The sign variation and the magnitude of the deviations from the fit for both V_{TOT} and V_{CMN} indicate that the data are not fit by a T^{-1} temperature dependence as well as in the case of the ac susceptibility thermometer. The most obvious explanation for this behavior lies in a lack of reproducibility of the trapped measuring field in this thermometer and its influence on the reproducibility of χ_{MT} from run to run (see Sec. VIII).

At this point, a comparison of the temperature dependence of the CMN thermometer outputs with theory may be made. For the ac susceptibility thermometer, the mutual inductance and the impedance of the CMN sensor may be written $M = M' + j\omega M''$ and $Z = j\omega (M'+j\omega M'')$, respectively. When the bridge is at null, $M' = \alpha\lambda m$ and $M'' = \beta\lambda RCm$ where α, β and λ are the ratio transformer settings (see Fig. 3), $m(=1.02\ \mu H)$ is the nulling mutual inductance, and $R(=10\ K\Omega)$ and $C(=0.10\ \mu F)$ are series bridge components in the nulling circuit. From Table X, the CMN fit yields $\alpha_{CMN} = -1.228\times10^{-2}/T - 1.182\times10^{-3}$ and since $\lambda = 0.3500$, $M' = -4.38\times10^{-9}/T + 4.22\times10^{-10}$ henries. The temperature independent term in the mutual inductance expression is due to secondary coil mismatch from run to run and is of no concern here. The magnitude of the observed temperature dependent term should be compared with the calculation in Sec. III. From Eq.(10), the predicted mutual inductance is $M = 4.32 \times 10^{-9}/T$ which is only 1.5 percent less than that observed. Considering that the absolute amount of CMN in the thermom-

eter is not known quite this well and considering the approximations involved in determining the flux threading the secondaries due to a nonuniformly magnetized sample of CMN in the shape of a right circular cylinder, the level of agreement is fortuitously good. In all other CMN experiments, the maximum deviation of experiment from theory has been 2.6 percent. For the dc susceptibility thermometer, the CMN fit in Table XII indicates a temperature dependent term $|V_{CMN}| = 33.59/T$ volts. The SQUID output voltage may be related to its input flux by a factor of 1.958 V/ϕ_0 when the SQUID is used on the x100 sensitivity scale. The temperature dependent term, in units of the flux quantum, is then $\phi_{sq} = 17.16\ \phi_0/T$. In Sec. II, a calculation based upon estimated circuit parameters and a trapped field of 5 G resulted in [see Eq. (4)] a predicted temperature dependence of $\phi_{sq} = 33.2\ \phi_0/T$. In a later experiment, M.C. Mayberry used the same thermometer with a completely different low-temperature experimental stage. Although the usual 8.9 mA was employed in the flux trapping coil in an attempt to trap 5 G, the observed thermometer temperature dependence was $\phi_{sq} = 28.1\ \phi_0/T$--a value much closer to that predicted by Eq. (4). Since the magnitude and direction of the earth's magnetic field are unknown in the cryostat and since the applied field and the earth's field may add or subtract depending upon the current direction in the trapping coil, the variation in the CMN sensitivity between these experiments and between theory and experiment is believed to be due primarily to an uncertainty in the measuring field. In any case, discrepancies between theory and experiment do not, of course, affect the usefulness of the thermometer once it has been calibrated.

To check the extent to which the results from Run 3 may be reproduced, similar data from Run 4 will be presented. To facilitate a straightforward comparison between the two runs, the CMN in the thermometers was not changed. As usual, an attempt was made in Run 4 to employ 5.00 G in the dc susceptibility thermometer. In Table XIII, the results of the 16 Hz calibration of the bridge are presented. The bridge data in the table have been corrected for χ_{MT}. In fitting the data to a Curie law, a heretofore unknown experimental difficulty became apparent. Between data points 5 and 6, a discontinuity in the α_{CMN} versus temperature data occurs and is associated with changing the most significant dial of the in-phase ratio transformer (the tenths dial). Fitting points 1 through 5 and 6 through 10 separately reveals that each data set is characterized by essentially the same slope but that the intercepts differ by $\sim 1 \times 10^{-4}$, an amount which is very large compared with the bridge noise level ($\sim 1 \times 10^{-6}$) or day-to-day reproducibility. (This is equivalent to saying that the readings 0.8X and 0.90, which are nominally the same, differ by $\sim 1 \times 10^{-4}$.) After this observation was made, an experimental examination of the ratio transformers was carried out and the difficulty described above was found to be present for each change of the tenths decade dial. The product of the shift in α times λ, which is a measure of the output voltage change of the in-phase transformer, was found to be roughly constant (to within a factor of two) for nominal values of α ranging from 0.1 to 1.0. Note that the size of this effect is substantially greater than the linearity specification of the ratio transformer so the discontinuity in the output voltage is presumably due to the design of the

Table XIII. Calibration of the ac susceptibility thermometer in Run 4 at 16 Hz with the GE2776 GRT. α_0 is the setting of the three step dials of the in-phase ratio transformer. The other tabulated quantities are defined in Table I. The difficulty associated with changing the tenths dial of the ratio transformer between points 5 and 6 is apparent in the first set of deviations. The second and third sets of deviations correspond to fitting points 1-5 and 6-10, respectively.

Point	T_{2776}	$\alpha_{TOT}(\times 10^3)$	α_0	Δ_1	Δ_2	Δ_3
1	1.37484	-8.2976	.896	+0.30	-0.004	
2	1.51648	-7.4653	.897	+0.06	-0.004	
3	1.68002	-6.6798	.898	-0.20	+0.011	
4	1.85527	-5.9911	.899	-0.05	+0.017	
5	2.04868	-5.3652	.899	-0.87	-0.020	
6	2.25694	-4.9170	.900	+0.73		+0.008
7	2.48598	-4.4151	.900	+0.50		-0.013
8	2.73728	-3.9629	.901	+0.29		+0.005
9	3.02034	-3.5425	.901	+0.02		-0.005
10	3.33701	-3.1575	.901	-0.25		+0.007

Fit 1: (1.3-3.3 K): $\alpha_{CMN} = \frac{-1.1936\times10^{-2}}{T_{2776}} + 4.104\times10^{-4}$

Fit 2: (1.3-2.0 K): $\alpha_{CMN} = \frac{-1.2254\times10^{-2}}{T_{2776}} + 6.150\times10^{-4}$

Fit 3: (2.2-3.3 K): $\alpha_{CMN} = \frac{-1.2268\times10^{-2}}{T_{2776}} + 5.190\times10^{-4}$

$$\Delta = \frac{T_{2776} - T_{FIT}}{T_{FIT}} 10^2$$

mutual inductance bridge. The consistency of the hundredths dial of the transformers was also carefully checked (e.g., 0.870 vs 0.86X) and although a slight shift was detected above the noise level, the shift was well within linearity specifications. A final observation associated with the step in the ratio transformer output is that the nulled quadrature channel was thrown significantly off null when the tenths dial of the in-phase channel was changed. No satisfactory explanation has been found to clarify these observations. Fortunately, from this point of view, the range of the bridge associated with one decade of the tenths dial is rather broad--a run can start with, for example, α = 0.8X at 4.2 K and not require a change in the tenths decade until 0.15 K. Also note that at lower temperatures, a fixed shift in α will correspond to a smaller apparent fractional temperature shift due to the rapidly increasing CMN sensitivity ($\Delta T/T = T(\Delta\alpha)/C$ where C is the CMN Curie law slope). As a result, the most undesirable temperature region in which this effect can occur is the 1-4 K region as illustrated in Table XIII.

Since this anomalous behavior of the bridge may be characterized, the data in Table XIII have been corrected by shifting the bridge readings for data points 6-10 by an amount determined in the ratio transformer tests described above. For λ = 0.3500 and α = 0.90 --> 0.8X, the appropriate correction is $\Delta\alpha = 1.047 \times 10^{-4}$. These data are tabulated in Table XIV along with a new Curie law fit and percentage deviations. The quality of the fit is seen to be excellent and once again essentially limited by the bridge noise level. The slope of the Curie law differs from the last experiment (Run 3 in Table I) by only 0.07 per-

Table XIV. Calibration of the ac susceptibility thermometer in Run 4 at 16 Hz with the GE2776 GRT. The data in Table IV have been corrected to compensate for the ratio transformer difficulty as discussed in the text. The corrected data are fit against the GE2776 in the usual fashion.

Point	T_{2776}	$\alpha_{CMN}(\times 10^3)$	Δ_{CMN}	Δ_N
1	1.37484	-8.2976	-0.018	0.012
2	1.51648	-7.4653	-0.008	0.014
3	1.68002	-6.6798	+0.017	0.015
4	1.85527	-5.9911	+0.034	0.016
5	2.04868	-5.3652	+0.009	0.018
6	2.25694	-4.8123	+0.003	0.020
7	2.48598	-4.3104	-0.020	0.022
8	2.73728	-3.8582	-0.004	0.024
9	3.02034	-3.4378	-0.016	0.027
10	3.33701	-3.0528	-0.006	0.030

Fit: $\alpha_{CMN} = \frac{-1.22664\times10^{-2}}{T_{2776}} + 6.228\times10^{-4}$

$\Delta_{CMN} = \frac{T_{2776} - T_{FIT}}{T_{FIT}} 10^2$ $\qquad$ $\Delta_N = \frac{\Delta\alpha_N \times T}{1.227\times10^{-2}} 10^2 = 8.88\times10^{-3}T$

cent thus illustrating the excellent reproducibility of the ac susceptibility thermometer in the 1.4-3.7 K range from run to run.

The data for the dc susceptibility thermometer from Run 4 are given in Table XV. As with the results from Run 3, the percentage deviations from the fit are systematic and large compared to the SQUID noise level. Note, however, that the sign variation of the deviations of these data is opposite to that in Run 3. Also, the slopes of the Curie law fits in the two experiments differ by ~8 percent in spite of the fact that the CMN was not changed between the two runs (thus ensuring a constant amount of CMN). Since the excellent reproducibility of the ac susceptibility thermometer results would seem to eliminate systematic problems like dehydration of the CMN, it is concluded that an uncertainty in χ_{MT} from run to run precludes achieving superior results with the dc susceptibility thermometer in the 1-3 K region. This conclusion is important since, if correct, it indicates that this thermometer is not well suited for extrapolating the vapor pressure scale to lower temperatures. In addition, it would also be a poor choice for a magnetic thermometer to interpolate between calibration points in a vapor pressure calibration experiment.

B. Effect of the Fringe Field of the Heat Switch on the CMN Thermometers

Before discussing the CMN results for $T < 1$ K, the influence of the heat switch coil on the CMN thermometer must be addressed. During the CMN holder experiments (see Sec. VIII), the operation of the superconducting heat switch coil was found to affect the epoxy CMN thermometer when operating in the dc mode. At that time, with no CMN in the

Table XV. Calibration of the dc susceptibility thermometer in Run 4 with the GE2776 GRT. These data were taken simultaneously with the ac susceptibility data in Table V. The SQUID output (corrected for the CMN holder) is fit versus inverse temperature.

Point	T_{2776}	V^{a}_{CMN}	Δ_{CMN}	Δ_N
1	1.37484	-7.9227	-0.17	0.0037
2	1.51648	-5.4575	-0.11	0.0041
3	1.68002	-3.1495	+0.06	0.0046
4	1.85527	-1.1248	+0.22	0.0051
5	2.04868	+0.7306	+0.27	0.0056
6	2.25694	+2.3801	+0.28	0.0062
7	2.48598	+3.8926	+0.17	0.0068
8	2.73728	+5.2804	-0.10	0.0075
9	3.02034	+6.6081	-0.74	0.0083

Fit: $V_{CMN} = \frac{-36.555}{T_{2776}} + 18.622$

$$\Delta_{CMN} = \frac{T_{2776} - T_{FIT}}{T_{FIT}} \, 10^2 \qquad \Delta_N = \frac{\Delta V_N \times T}{36.555} \, 10^2 = 2.74 \times 10^{-3} T$$

a The SQUID was used in the x100 sensitivity mode (1.958 volts = $1\phi_0$) for these measurements.

thermometers, the fringe field of the heat switch did not appear to affect either the epoxy CMN thermometer when operating in its usual ac mode or the dc susceptibility thermometer. Since the presence of CMN in the thermometers should enhance the size of any undesirable effect associated with changes in the ambient magnetic field, another test to examine fringe field effects was carried out during the CMN experiments. The idea behind the test was to try to measure directly a change in the output of either CMN thermometer due to a change in the heat switch coil fringe field while maintaining a constant temperature. The current in the heat switch coil was alternately ramped between zero and 1 A remembering that 2.5 A was required to actually close the switch. A temperature of 0.2 K was chosen for the test since this temperature was high enough to be maintainable with the heat switch open while simultaneously satisfying the desire for a low temperature to enhance the size of the effect (since $\Delta\phi_{sq} \propto \Delta H/T$). The temperature of the bus was monitored with a GRT and was regulated with the bus heater during the test. At the same time, the outputs of the CMN thermometers were carefully monitored. For the dc susceptibility thermometer, the maximum excursion of the output was 0.004 ϕ_o (scaled to the usual 2.5 A required for normal operation of the heat switch) in response to the applied fringe field. When this figure is used to calculate a change in the thermometer calibration slope, a change of only 0.004 percent is obtained. This implies that upon closing the heat switch at 0.1 K to initiate lower temperature work, the thermometer calibration slope (and hence the deduced magnetic temperatures) would change by 0.004 percent--an amount which is trivial.

However, since the 0.004 ϕ_0 figure at 0.2 K corresponded to a temperature uncertainty of 8.4×10^{-6} K and since the temperature regulation at 0.2 K as determined by the GRT was $\sim 1 \times 10^{-5}$ K, the effect cannot be considered to be real as it is at the uncertainty level of the measurement. Hence, the favorable aspect ratio of the Nb tube on the dc susceptibility thermometer adequately shielded the thermometer from the fringe field of the heat switch coil. For the ac susceptibility thermometer, at either 16 Hz or 160 Hz, the result is similar. Any effect associated with the fringe field of the heat switch coil is at or below the noise level of the experiment.

It thus appears that only the epoxy CMN thermometer, when operated in the dc mode, was affected by the fringe field of the heat switch coil (due to the inadequate aspect ratio of its Nb tube). The thermometer was used in that mode on an infrequent basis only and its integrity was preserved on those occasions by taking data with the heat switch closed thus keeping the dc measuring field constant.

C. The Determination of the Magnetic Temperature Scale for $T < 1$ K

In a preliminary calibration of the GE2345 and the GE1751, the first version of the epoxy CMN thermometer (whose χ_{MT} had a large anomaly at 1 K) was used to establish a temperature scale referred to as $T_\eta(8/77)$. (With the exception of these preliminary calibration data, all ac susceptibility thermometer data reported in this thesis utilized the final version of the epoxy CMN holder as described in detail in Sec. VIII.) The dc susceptibility thermometer was not included in this calibration. Unfortunately, due to a variety of experimental difficulties in that early experiment, the minimum temperature

achieved was only ~35 mK thus rendering accurate NOT temperatures difficult to obtain. The susceptibility data in the 1.3-3.0 K region were first fit to a Curie law (using the GE2776) to analyze the bridge performance in this temperature range and to define a magnetic temperature scale. It was then found that although the magnetic temperatures on this scale were in rough agreement with the original calibrations on the GE2345 and the GE1751 for $T > 0.15$ K, the magnetic temperatures diverged from the original calibrations as the temperature was lowered below this point. In addition, the magnetic temperatures ran ~7 percent higher than the NOT temperatures at ~35 mK. These two independent observations suggested that the ac susceptibility thermometer might be running hot at low temperatures. (To aid in examining this possibility, the dc susceptibility thermometer was included in all later experiments.) These discrepancies, as well as the unexplained difference between the on- and off-axis NOT temperatures (discussed in Sec. VII), precluded using the NOT to determine the Δ of the CMN Curie-Weiss law. Thus, the $T_\eta(8/77)$ scale was simply derived from the Curie law expression used to represent the 1-3 K bridge data on the GE2776, i.e., $\Delta \equiv 0$. The $T_\eta(8/77)$ scale is mentioned here because, in spite of its obvious limitations, it played a significant role in the subsequent calibration experiments.

If the ac and dc susceptibility thermometers each obey a Curie-Weiss law with similar values of Δ, the CMN contributions to the thermometer outputs should bear a linear relationship to one another. This is a test which may be used to detect a systematic problem with either thermometer <u>without</u> having a bona fide temperature scale in place in

the region of interest. In Fig. 27, the 16 Hz ac susceptibility thermometer data and the dc susceptibility thermometer data from Run 5 are plotted against each other. (Note that the steps in the bridge output associated with the ratio transformer difficulty described earlier were corrected before tabulating and analyzing these data.) The dc susceptibility data in Run 5 are in units of the flux quantum (not volts as in previous runs) since a commercial digital flux counter[25] was used in that experiment. This device affords the advantage of an experimental range of $\pm 10^5\ \phi_0$ while maintaining the high resolution associated with the x100 sensitivity scale. It is evident from Fig. 27 that while a linear relationship is observed at high temperatures, this relationship gradually breaks down for $T < 0.1$ K. This observation is put on a quantitative basis in Table XVI where the results of a least squares fit of the CMN thermometer data in the 0.21-0.85 K region are given. Percentage deviations from the fit are tabulated for all data points down to 38 mK, the lowest temperature of the GRT calibration data, and are compared with percentage deviations associated with the bridge noise level in the fit interval. The alternating sign and the magnitude of the fit deviations quantitatively demonstrate that the two CMN thermometer outputs are linearly related within experimental error in the 0.21-0.85 K region. Further, the deviations from the fit at lower temperatures indicate that this simple relationship breaks down in a monotonically increasing fashion. The magnitude of the discrepancy between the two CMN thermometers is perhaps best seen in terms of the percentage difference between their respective magnetic temperatures. It can be shown that, for $T \tilde{<} 0.1$ K, the entries in column 5

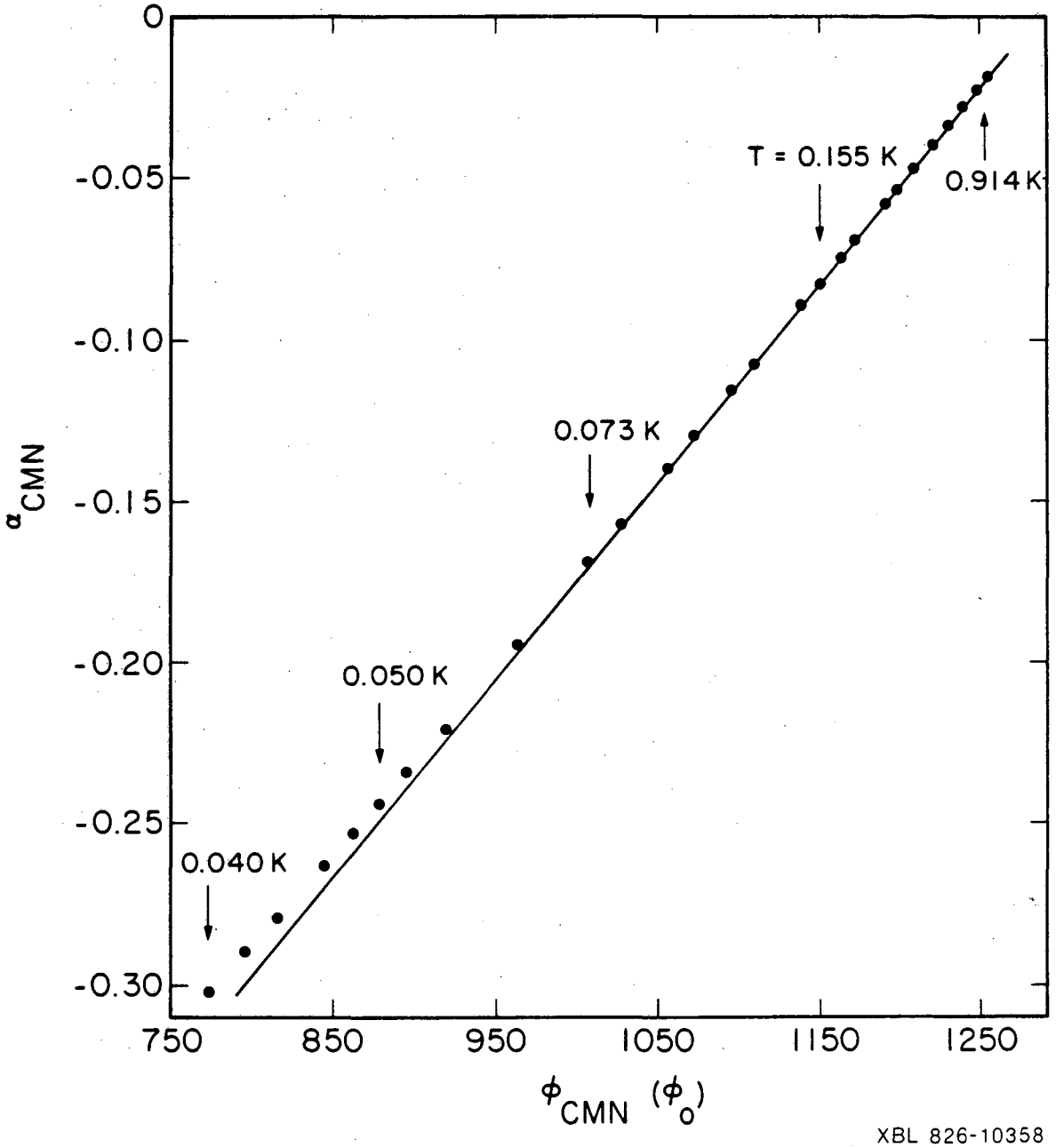

Fig. 27. The CMN output of the ac susceptibility thermometer versus that of the dc susceptibility thermometer for 0.04-0.85K. The solid line represents a linear fit of α_{CMN} versus ϕ_{CMN} in the 0.21-0.85K region. The deviation of the data from the fit at low temperatures is attributed to self-heating in the epoxy components of the ac susceptibility thermometer.

Table XVI. Comparison of the ac and the dc susceptibility thermometer outputs from Run 5 over the 0.04–0.85 K range. The 16 Hz bridge data are fit against the SQUID data in the 0.21–0.85 K region and the resulting percentage deviations are calculated for all temperatures. T^*_{2776} is the magnetic temperature derived from the vapor pressure scale in Run 5 and α_{CMN} and ϕ_{CMN} are the bridge and SQUID outputs corrected for the CMN holders. Δ_{CMN} and Δ_N, which represent the percentage deviations from the fit and the percentage deviations due to noise, respectively, are discussed in the text.

Point	T^*_{2776}	$\alpha_{CMN}(\times 10^2)$	ϕ^a_{CMN}	Δ^b_{CMN}	Δ_N
1	0.84581	−2.03390	1251.865	−0.0138	0.0054
2	0.78228	−2.14720	1250.020	−0.0120	0.0051
3	0.72136	−2.27457	1247.947	−0.0072	0.0048
4	0.61624	−2.55356	1243.402	−0.0087	0.0043
5	0.54736	−2.79449	1239.484	+0.0055	0.0039
6	0.48520	−3.07063	1234.992	+0.0162	0.0035
7	0.43196	−3.37033	1230.112	+0.0172	0.0032
8	0.38337	−3.71649	1224.464	−0.0008	0.0029
9	0.35433	−3.96873	1220.355	−0.0018	0.0027
10	0.31428	−4.39311	1213.446	+0.0027	0.0025
11	0.29077	−4.69663	1208.499	−0.0020	0.0023
12	0.25801	−5.21179	1200.111	+0.0013	0.0021
13	0.22888	−5.79377	1190.632	+0.0011	0.0019
14	0.21172	−6.21102	1183.829	−0.0059	0.0018
15	0.18639	−6.96802	1171.498	(−0.006)	
16	0.15507	−8.24462	1150.674	(−0.029)	
17	0.14153	−8.97078	1138.280	(−0.045)	
18	0.11678	−10.73199	1110.041	(−0.091)	
19	0.09538	−12.97916	1073.123	(−0.225)	
20	0.07795	−15.69899	1028.080	(−0.475)	
21	0.06199	−19.47138	946.628	(−1.01)	
22	0.05072	−23.46058	895.779	(−1.83)	
23	0.04669	−25.32422	863.024	(−2.25)	
24	0.04189	−27.92903	815.894	(−3.03)	
25	0.03831	−30.21535	772.991	(−3.88)	

Fit: $\phi_{CMN} = 1628.7435\ \alpha_{CMN} + 1284.9966$

$$\Delta_{CMN} = \frac{\alpha_{CMN} - \alpha_{FIT}}{\alpha_{FIT}} 10^2 \qquad \Delta_N = \frac{\Delta\alpha_N}{\alpha_{CMN}} 10^2 = \frac{1\times10^{-4}}{\alpha_{CMN}}$$

a The SQUID was used in conjunction with a commercial digital flux counter (DFC) in Run 5. The output is therefore in units of the flux quantum ϕ_0.

b Percentage deviations enclosed in parenthesis are for temperatures below the fit region.

of Table XVI (Δ_{CMN}) are just these percentage differences, each thermometer being calibrated in the 0.2-0.8 K region on $T_\eta(8/77)$. Hence, at 38 mK, the two CMN thermometers yield temperatures which disagree by 3.9 percent. To further illustrate the severity of the disagreement, lower temperature data reveal the ac susceptibility thermometer temperatures to be 9.7 and 27.3 percent higher than those of the dc susceptibility thermometer at 26.8 and 16.4 mK, respectively. The disparity is thus seen to increase very rapidly at lower temperatures and is <u>far</u> too large to be attributed to any uncertainty in the values of χ_{MT} for either thermometer (see Figs. 17 and 24).

In an attempt to resolve the above discrepancy, tests were conducted to determine if the high magnetic temperatures of the epoxy CMN thermometer were in some way related to the ac bridge measurement of the CMN susceptibility at low temperatures. Three independent magnetic temperature scales were formulated for this thermometer in the following way: In the 0.2-0.8 K region, the thermometer was calibrated versus the GE2345 on $T_\eta(8/77)$ at both 16 and 160 Hz (using a Curie law fit) thus defining two ac susceptibility scales. After cooling the bus to ~16 mK, bridge readings were taken (using various primary currents) at both 16 and 160 Hz to determine T^*_{16} and T^*_{160}. The bridge was then turned off to put the epoxy CMN thermometer into the dc mode (see Sec. III). The outputs of the SQUIDS monitoring the epoxy and copper CMN thermometers were recorded and the bus then warmed to the 0.2-0.8 K region where both thermometers were calibrated versus the GE2345 on $T_\eta(8/77)$. Subsequent extrapolation of the Curie law

calibrations back to the low-temperature SQUID readings yields the magnetic temperatures T^*_{EP} and T^*_{Cu} for the epoxy and copper CMN thermometers, respectively. (This particular technique of determining dc susceptibility temperatures was developed to minimize the time and hence the probability of flux jumps between low temperatures and the calibration region. Such a technique is unnecessary for ac operation as the SQUID serves only as a null detector for the bridge.) Typical results of the comparison from Run 4 are T^*_{Cu} = 16.19 mK, T^*_{16} = 20.96 mK, T^*_{160} = 20.96 mK, and T^*_{EP} = 21.00 mK. From Run 5, T^*_{Cu} = 16.27 mK, T^*_{16} = 20.68 mK, T^*_{160} = 20.67, and T^*_{EP} = 20.61 mK. Note that χ_{MT} for the epoxy CMN thermometer was measured at both 16 and 160 Hz as well as in the dc mode (see Sec. VIII) and appropriate corrections were made to the measured susceptibilities before calculating the magnetic temperatures. Also note that the 16 and 160 Hz temperatures were independent of the amplitude of the primary field ($\lesssim$ 0.12 G). Since the ac and dc susceptibility temperatures of the epoxy CMN thermometer were found to be in excellent agreement, it is clear that (1) the isothermal susceptibility of CMN was indeed measured under the conditions used in these experiments and (2) any non-ideal characteristics of the mutual inductance bridge (such as the small steps in the output of the ratio transformers discussed in Sec. IX A) cannot be responsible for the high magnetic temperatures of the epoxy CMN thermometer.

The final data which provide insight into the discrepancy between the two CMN thermometers are reported in Table XVII and concern the

Table XVII. A comparison of the temperatures from the ac susceptibility thermometer (T^*_{16}), the NOT (T_{NOT}) and the copper CMN thermometer (T^*_{Cu}) as a function of time in Run 5. The day of the run each comparison was made is given along with the magnetic tape tagword of each NOT spectrum. T^*_{16} and T^*_{CU} (in mK) are given on the T_η(8/77) temperature scale extrapolated below the 0.2-0.8 K calibration region with a Curie law fit. δ_{BR-NOT} and δ_{BR-Cu} (in mK) are the differences between the 16 Hz bridge temperatures and those of the NOT and the copper CMN thermometer, respectively.

Day	Spectrum	T^*_{16}	T_{NOT}	T^*_{Cu}	δ_{BR-NOT}	δ_{BR-Cu}
5	SE0027	23.65	19.23		4.42	
6	SE0028	23.00	18.50		4.50	
8	SE0034	21.82	18.07		3.75	
9	SE0035	21.85	18.05	16.92	3.80	4.93
10	SE0037	21.66	17.90		3.76	
11	SE0038	21.24	17.72	16.63	3.52	4.61
13	SE0040	21.31	17.66	16.72	3.65	4.59
15	SE0045	21.05	17.61		3.44	
17	SE0051	20.88	17.45	16.40	3.43	4.48
35		20.68		16.27		4.41

time dependence of the various low-temperature determinations over a period of about one month in Run 5. The important point to note here is that while the thermometer bus cooled slowly as a function of time, which was normal during an experiment, the epoxy CMN thermometer experienced a net cooling against both the NOT and the copper CMN thermometer. That is, between the 5th and 17th days of Run 5, the ac susceptibility thermometer cooled ~1 mK more than the NOT and between the 9th and 17th days of the run, a net cooling of 0.45 mK was observed relative to the dc susceptibility thermometer. These results appear to indicate that the temperature of the CMN-oil slurry in the ac susceptibility thermometer was adversely affected by a time-dependent heat leak.

In the preliminary calibration experiment used to define $T_n(8/77)$, it was observed that the magnetic temperatures from the first version of the epoxy CMN thermometer were higher than the NOT temperatures thus suggesting the possibility that the bridge temperatures were too high. Significantly, the results enumerated above, all of which are based on the final version of the epoxy CMN thermometer, are consistent with the hypothesis that the epoxy thermometers used in these calibrations ran hot for $T \lesssim 0.15$ K. The time dependence of the discrepancy in particular suggests that the heating was due to relaxation effects in the epoxies used to fabricate the thermometers. Similar heat leak difficulties in epoxy sample cells and nuclear cooling bundles potted with epoxies have been reported recently by a number of authors.[70] It is concluded that the ac susceptibility thermometers gradually entered a state of disequilibrium with the thermometer bus due to self-heating

effects and were thus unuseable in the temperature scale experiments for $T \tilde{<} 0.15$ K.

To demonstrate the reproducible behavior of the CMN thermometers in the 0.2-0.8 K region from run to run, results from Run 4 are presented in Table XVIII. Once again a linear fit is seen to yield small deviations with alternating signs which are indicative of an excellent fit when compared to the bridge noise level. Thus, the data in Runs 4 and 5 demonstrate that the two CMN thermometers, for $T > 0.2$ K, bear a linear relationship to each other to within experimental error--a result which certainly precludes the possibility of any serious misrepresentation of χ_{MT} for either thermometer in either experiment and demonstrates that the two CMN thermometers performed equally well in the 0.2-0.8 K region. This result for the dc susceptibility thermometer is a substantial improvement over that obtained in the 1-3 K region and is almost certainly due to the weak temperature dependence of χ_{MT} in the 0.1-1.0 K region.

Additional information about the physical law followed by the various CMN thermometers may be obtained by fitting the susceptibility data from the ac and dc susceptibility thermometers in Run 4 versus the provisional temperature scale $T_\eta(8/77)$ as represented on the GE2345. The results of these Curie law fits, which are presented in Tables XIX and XX, are seen to be excellent, yielding fractional temperature differences of only ~5 parts in 10^5. These results are typical of those seen in a number of CMN experiments and lead to the following conclusions: (1) The fit parameters from Tables XIX and XX may be compared with those from Tables XIV and XV which are derived

Table XVIII. Comparison of the ac and the dc susceptibility thermometer outputs from Run 4 over the 0.25–0.80 K range. The 16 Hz bridge data are fit against the SQUID data after correcting for the CMN holders. The T_{2345} temperatures are on the $T_n(8/77)$ provisional temperature scale.

Point	T_{2345}	$\alpha_{CMN}(\times 10^2)$	V^a_{CMN}	Δ_{CMN}	Δ_N
1	0.79891	-1.47241	15.8183	+0.0000	0.0074
2	0.75063	-1.57092	15.5307	-0.0120	0.0069
3	0.69880	-1.69209	15.1780	-0.0034	0.0064
4	0.64907	-1.82660	14.7862	-0.0003	0.0060
5	0.59926	-1.98358	14.3289	+0.0020	0.0055
6	0.55019	-2.16615	13.7970	+0.0033	0.0050
7	0.49973	-2.39105	13.1416	+0.0022	0.0046
8	0.44958	-2.66453	12.3445	-0.0006	0.0041
9	0.40140	-2.99163	11.3917	+0.0034	0.0036
10	0.35035	-3.43688	10.0943	+0.0032	0.0032
11	0.30005	-4.02342	8.3851	+0.0022	0.0027
12	0.25023	-4.83654	6.0149	-0.0041	0.0023

Fit: $V_{CMN} = 291.3926\ \alpha_{CMN} + 20.1088$

$$\Delta_{CMN} = \frac{\alpha_{CMN} - \alpha_{FIT}}{\alpha_{FIT}}\ 10^2 \qquad \Delta_N = \frac{\Delta\alpha_N}{\alpha_{CMN}}\ 10^2 = \frac{1\times10^{-4}}{\alpha_{CMN}}$$

a The SQUID was used in the x10 sensitivity mode (0.1953 volts = $1\phi_0$) for these measurements.

Table XIX. Comparison of the ac susceptibility thermometer output at 16 Hz with the provisional $T_\eta(8/77)$ temperature scale on the GE2345 in Run 4 over the 0.2–0.8 K region. The bridge output (corrected for the CMN holder) is fit against inverse temperature and the percentage deviations from the fit are compared with calculated deviations due to the observed bridge noise level. The superconducting heat switch was open during these measurements.

Point	T_{2345}	$\alpha_{CMN}(\times 10^2)$	Δ_{CMN}	Δ_N
1	0.20016	-6.06170	-0.0042	0.0018
2	0.25023	-4.83654	+0.0025	0.0022
3	0.30005	-4.02342	+0.0050	0.0027
4	0.35035	-3.43688	+0.0041	0.0031
5	0.40140	-2.99163	-0.0043	0.0036
6	0.44958	-2.66453	-0.0011	0.0040
7	0.49973	-2.39105	+0.0042	0.0044
8	0.55019	-2.16615	+0.0067	0.0049
9	0.59926	-1.98358	+0.0001	0.0053
10	0.64907	-1.82660	+0.0003	0.0058
11	0.69880	-1.69209	-0.0068	0.0062
12	0.75063	-1.57092	-0.0119	0.0067
13	0.79891	-1.47241	-0.0006	0.0071

Fit: $\alpha_{CMN} = \frac{-1.22570\times10^{-2}}{T_{2345}} + 6.179\times10^{-4}$

$\Delta_{CMN} = \frac{T_{2345} - T_{FIT}}{T_{FIT}} 10^2$ $\qquad$ $\Delta_N = \frac{\Delta\alpha_N \times T}{1.226\times10^{-2}} 10^2 = 8.88\times10^{-3}T$

Table XX. Comparison of the dc susceptibility thermometer output with the provisional $T_n(8/77)$ temperature scale on the GE2345 in Run 4 over the 0.2-0.8 K region. The SQUID output (corrected for the CMN holder) is fit against inverse temperature and the percentage deviations from the fit are compared with calculated deviations due to the observed SQUID noise level. The superconducting heat switch was open during these measurements.

Point	T_{2345}	V^a_{CMN}	Δ_{CMN}	Δ_N
1	0.20016	2.4427	+0.0033	0.0028
2	0.25023	6.0149	-0.0002	0.0035
3	0.30005	8.3851	-0.0027	0.0042
4	0.35035	10.0943	-0.0033	0.0049
5	0.40140	11.3917	-0.0106	0.0056
6	0.44958	12.3445	-0.0023	0.0063
7	0.49973	13.1416	+0.0016	0.0070
8	0.55019	13.7970	+0.0042	0.0077
9	0.59926	14.3289	+0.0001	0.0084
10	0.64907	14.7862	+0.0037	0.0091
11	0.69880	15.1780	+0.0009	0.0098
12	0.75063	15.5307	+0.0054	0.0105
13	0.79891	15.8183	+0.0062	0.0112

Fit: $V_{CMN} = \frac{-3.5720}{T_{2345}} + 20.2897$

$$\Delta_{CMN} = \frac{T_{2345} - T_{FIT}}{T_{FIT}} 10^2 \qquad \Delta_N = \frac{\Delta V_N \times T}{3.572} 10^2 = 0.0140\ T$$

a The SQUID was used in the x10 sensitivity mode (0.1953 volts = $1\phi_0$) for these measurements.

from GE2776 data in the 1.3-3.3 K region in the same experiment. After converting between the two SQUID sensitivity scales, the two slopes from the dc susceptibility thermometer fits are seen to differ by ~2.1 percent--a significant discrepancy which is attributed to the χ_{MT} reproducibility difficulty in the 1-4 K region as discussed in Secs. VIII and IX A. On the other hand, the two Curie law expressions for the ac susceptibility thermometer are essentially identical since the magnetic temperatures derived from them differ by no more than 0.08 percent at any temperature. This result is very important as it utilizes the final version of the epoxy CMN thermometer to verify independently the integrity of the provisional $T_\eta(8/77)$ temperature scale (within the $\Delta \equiv 0$ context) in the 0.2-0.8 K region. (2) Superficially, the fit results in Tables XIX and XX appear to demonstrate that the CMN in both thermometers follows a Curie law in the 0.2-0.8 K region to within experimental error. However, the $T_\eta(8/77)$ temperature scale almost certainly contains a systematic error since the scale was derived with the assumption that the Curie-Weiss constant (Δ) was zero (due to the inability to adequately define Δ at low temperatures with the NOT). Thus, it is likely that the $T_\eta(8/77)$ scale deviates from the thermodynamic scale in a well defined way which depends only upon the value of Δ. It then turns out that two considerations, namely the use of a Curie law fit instead of a Curie-Weiss relation and the lack of a Δ in the $T_\eta(8/77)$ scale, compensate one another to yield the high quality fits. The important result to be extracted from the fits in Tables XIX and XX is that the Curie-Weiss constants of the three susceptibility thermometers in question (the first epoxy CMN thermometer used to define

$T_\eta(8/77)$, the final version of the epoxy CMN thermometer fit versus $T_\eta(8/77)$ in Table XIX and the copper CMN thermometer fit versus $T_\eta(8/77)$ in Table XX) must be essentially the same (but, in general, not zero). The magnitude of the deviations from the fits ($\sim 5 \times 10^{-5}$) may in fact be used to calculate an upper limit on the difference between the Δ's of the various thermometers. Such a calculation reveals that the Curie-Weiss constants of the three thermometers must be the same to within ~0.1 mK. Although all three thermometers employed right circular cylinder salt pills with the diameter equal to the height, the relative geometries of the salt pills and pickup coils of the thermometers were rather different (see Table XXI). Since Betts[5] has emphasized the influence of these geometrical considerations on the Curie-Weiss constant of such thermometers, it might be expected that the Δ's of the various CMN thermometers should be significantly different. The results reported above, however, indicate that such geometrical considerations are not important for the powdered CMN thermometers used in these experiments.

In Sec. I, a brief summary of the evidence which indicates that the susceptibility of powdered CMN obeys a Curie-Weiss law down to at least 10 mK was presented. Significantly, the CMN results reported above support this contention since (1) the CMN susceptibility may be fit with a Curie law to within experimental error using the $^3He/^4He$ vapor pressure scale in the 1-4 K region (Δ not being determined here due to an inadequate signal to noise ratio at these temperatures) and (2) the linear relationship between the susceptibilities of the ac

Table XXI. Dimensions of the CMN slurries as well as the secondary and flux transformer coils used in the ac and dc susceptibility thermometers, respectively. All dimensions are in inches.

	First ac Thermometer	Final ac Thermometer	dc Thermometer
CMN Slurry Diameter[a]	0.088	0.088	0.053
Pickup Coil Length	0.040	0.060	0.053
Pickup Coil Diameter	0.246	0.246	0.131
Ratio of Coil Volume to Slurry Volume	3.55	5.33	6.10

[a] For the CMN slurries, the length is equal to the diameter of the right circular cylinders.

and dc susceptibility thermometers in the 0.2-0.8 K region is consistent with Curie-Weiss behavior if each thermometer has the same Δ. Thus, to define an accurate magnetic temperature scale for the CMN thermometers used in these experiments, the absolute value of Δ must be determined with the NOT.

The value of Δ was determined several times in both Runs 4 and 5. The general procedure for each measurement required ~2 days of run time and was as follows: The thermometer bus was cooled to a low temperature, generally ~17 mK, where NOT data were accumulated for an extended period of time to obtain good statistics. At the end of that period, the output of the dc susceptibility thermometer was recorded and the thermometer bus was warmed immediately to the 0.2-0.8 K region where the CMN thermometer was calibrated against the GE2345 or GE1751 on $T_\eta(8/77)$. The accumulation of high-temperature normalization data commenced as soon as the thermometer bus reached 0.5 K and continued for 15-20 hours. The NOT temperature is calculated using the FWHM regions of interest as discussed in Sec. VII and only the on-axis result is quoted owing to its higher precision. The dc susceptibility thermometer temperature is calculated by fitting the 0.2-0.8 K calibration data to a Curie law and extrapolating the resulting fit to low temperatures where the initial SQUID reading then yields T^*_{Cu}. The reason for fitting the data to a Curie law using the $T_\eta(8/77)$ temperature scale is that this procedure effectively extrapolates the 1-4 K Curie law calibration, which was used to define $T_\eta(8/77)$, to millikelvin temperatures. It is then easy to show that the difference between the magnetic temperature (T^*_{Cu}) and the absolute temperature

(T_{NOT}) is equal to Δ in the low-temperature limit. Before tabulating the results, one additional point must be addressed. The $^3He/^4He$ (T_{62}/T_{58}) vapor pressure scale used to calibrate the CMN in the 1-4 K region is known[71] to yield temperatures which are ~0.25 percent below the thermodynamic temperature scale for $T < 3.5$ K. Although an updated scale for $0.5 < T < 30$ K, referred to as T_{EPT-76},[71] corrects for this error (as well as others at higher temperatures), this scale has not been officially accepted on an international basis. The magnetic scale defined by these experiments is thus designed to extrapolate the T_{62}/T_{58} scale to low temperatures and hence, the NOT temperatures, which are assumed to be absolute, must be decreased by 0.25 percent to be consistent with the vapor pressure scale. Having made this correction, the various determinations of Δ are reported in Table XXII. Whereas the results in the 17-18 mK region yield an average value for Δ of 0.97 mK with a standard deviation of 0.09 mK, the higher temperature determinations appear to require a larger value of Δ. It is at this point that the comments in Sec. VII concerning the nonstatistical performance of the γ-ray spectrometer are particularly relevant. At 17 mK, spectrometer instabilities equivalent to 2 or even $3\sigma_{NOT}$ do not substantially exceed the uncertainty in the determination of Δ nor do they affect the final magnetic temperature scale in a significant way (a goal of this calibration being to determine absolute temperatures at ~17 mK to better than one percent). The same cannot be said of the determinations at higher temperatures, however, since the statistical uncertainties there are much greater than those at ~17 mK. On the other hand, if nonstatistical spectrometer performance

Table XXII. A tabulation of the data upon which the determination of the Curie-Weiss constant (Δ) is based. The run number and NOT spectrum label are given for each determination. (The NOT determinations without a spectrum label were not stored on magnetic tape.) T_{NOT} is the FWHM on-axis temperature while $1\sigma_{NOT}$ represents one standard deviation unit of uncertainty in that temperature. T^*_{Cu} is the extrapolated dc susceptibility thermometer temperature on $T_\eta(8/77)$ and $\Delta \equiv T_{NOT} - T^*_{Cu}$. Note that the listed values of T_{NOT} are 0.25 percent below those determined experimentally thus yielding consistency with the known deviation between the helium vapor pressure scale and the thermodynamic scale. All entries are in millikelvins.

Run	Spectrum	T_{NOT}	T^*_{Cu}	Δ	$1\sigma_{NOT}$
4	------	17.13	16.19	0.94	0.08
4	SE0005	17.76	16.90	0.86	0.03
5	SE0035	18.00	16.92	1.08	0.05
5	SE0038	17.68	16.63	1.05	0.05
5	SE0040	17.62	16.72	0.90	0.05
5	SE0051	17.41	16.40	1.01	0.04
5	SE0055	28.56	27.17	1.39	0.21
5	------	28.16	26.79	1.37	0.10
5	SE0057	40.80	38.80	2.00	0.35
5	SE0053	53.50	51.59	1.91	0.79
5	SE0060	53.31	51.33	1.98	0.60

is responsible for the larger values of Δ in the 25-55 mK region, it is somewhat disconcerting that Δ is in all cases greater than the 17 mK value (random spectrometer instabilities are expected to result in randomly high and low NOT temperatures). Although more data in the 25-50 mK region with better spectrometer stability are clearly desirable, similar data at lower temperatures than those achieved in these experiments, whereby the NOT sensitivity would be improved, would be even more useful. This would effectively allow the temperature dependence of the susceptibility of CMN to be examined in a region where it is sensitive to any temperature dependence of Δ. In any case, since the experiments outlined in Sec. I indicate that powdered CMN exhibits Curie-Weiss behavior down to 10 mK and since the results of the experiments in the 0.2-3.8 K region reported here are clearly consistent with Curie-Weiss behavior, the magnetic temperature scale derived from the above results is taken to be defined by a Curie-Weiss law with $\Delta = 0.97$ mK. Evidence which further supports this choice will be presented in Sec. X. Finally, note that this value of Δ is rather large compared to those enumerated in Sec. I. This indicates that Δ may indeed vary significantly from one thermometer to another, depending perhaps on the source or quality of the CMN and the particle size. (Strictly speaking, the quantity which has been determined above is not Δ but rather $[\Delta - C\lambda]$ where $C\lambda$ is the factor arising from the induced currents in the flux transformer and the Nb tube [see Sec. II]. Since $C\lambda$ was estimated to be 0.08 mK, the correct value of Δ for the CMN slurries used in these experiments is 1.05 mK. Insofar as cali-

brating the GRT is concerned, the proper susceptibility relationship employs the 0.97 mK figure since $T^* = T_{NOT}-[\Delta-C\lambda]$.)

A comment is in order concerning the 0.2 mK variation in the determination of Δ at ~17 mK. This variation appears rather large when compared to the dc susceptibility thermometer sensitivity (~10 nK) and the NOT statistical uncertainty (~0.04 mK) at 17 mK and is believed to be due to the inability to regulate the bus temperature adequately over the long periods required for NOT data acquisition. Since the bus temperature has generally been observed to drift about by several tenths of a millikelvin when the dilution refrigerator was running at its minimum temperature, the NOT temperature is then an average of the bus temperature over 10-15 hours whereas the dc susceptibility thermometer temperature reflects only that value of the bus temperature immediately before warming up to the calibration region. Thus, a high quality temperature regulation capability on the thermometer bus might well reduce the uncertainty in Δ to a value limited by the NOT statistical uncertainty. In any case, the 0.09 mK standard deviation in Δ is only 0.5 percent of the temperature at 17.5 mK and represents a significant contribution to the determination of Δ and, as a result, to the determination of absolute temperatures in the millikelvin region.

To define the magnetic temperature scale based on these experiments, and to recalibrate the GE2345 and GE1751 thermometers on that scale, the $\Delta = 0.97$ mK figure is incorporated into the calibration data of the ac susceptibility thermometer versus the GE2776 in Run 5 as illustrated in Table XXIII. As usual, an excellent fit is obtained

Table XXIII. Calibration of the ac susceptibility thermometer in Run 5 at 16 Hz with the GE2776 thermometer assuming a Curie-Weiss constant of 0.97 mK as determined by nuclear orientation thermometry (see text). The in-phase null bridge reading has been corrected for the susceptibility of the empty CMN holder. Δ_{CMN} is the percentage deviation from the fit while Δ_N is a percentage deviation calculated from the observed noise level of the bridge.

Point	T_{2776}	α_{CMN} ($\times 10^2$)	Δ_{CMN}	Δ_N
1	1.37346	-1.49580	-0.008	0.012
2	1.44359	-1.45405	-0.009	0.012
3	1.51488	-1.41561	-0.006	0.013
4	1.68034	-1.33914	+0.027	0.014
5	1.85598	-1.27280	+0.048	0.016
6	2.04849	-1.21285	+0.016	0.017
7	2.37019	-1.13447	-0.025	0.020
8	2.73996	-1.06732	-0.027	0.023
9	3.17717	-1.00822	+0.005	0.027
10	3.50319	-0.97366	+0.001	0.030

Fit: $\alpha_{CMN} = \frac{-1.17863\times10^{-2}}{T_{2776}-0.00097} - 6.3712 \times 10^{-3}$

$\Delta_{CMN} = \frac{T_{2776} - T_{FIT}}{T_{FIT}} 10^2$ $\qquad$ $\Delta_N = \frac{\Delta\alpha_N \times T}{1.179\times10^{-2}} 10^2 = 8.48\times10^{-3}T$

with deviations on the order of the bridge noise level. Note that a fit using a Curie law yields similar deviations and a slope which differs from that in Table XXIII by only 0.1 percent--an amount which is insignificant insofar as extrapolated temperatures are concerned. Hence, the difference between the Curie and Curie-Weiss law extrapolations at very low temperatures is just Δ, as expected. To extrapolate the Curie-Weiss scale to lower temperatures, the dc susceptibility thermometer was calibrated against the ac susceptibility thermometer temperature scale from Table XXIII in the 0.2-0.8 K range where both CMN thermometers functioned well. The resulting calibration on the dc susceptibility thermometer was then used down to 17 mK. The calibration of the GE2345 and GE1751 thermometers took place over a period of four days, the ac and dc susceptibility thermometers being used above and below 0.2 K, respectively. (The bridge was used whenever possible owing to its more convenient operation--the dc susceptibility thermometer had to be recalibrated versus the ac susceptibility thermometer periodically to properly account for possible flux jumps in the SQUID.) The calibration data were obtained by first stabilizing the bus at a desired temperature with the bus heater and then recording the currents and voltages of the GRT and the outputs of the CMN thermometers simultaneously. The bus temperature was subsequently incremented, typically by ~T/20, and the process repeated. The data sets from the four days of calibrations were overlapped to ensure continuity and to check for day-to-day inconsistencies. The current and voltage data on the GE2345 and GE1751 were used to calculate thermometer resistances for each data point while the CMN thermometer data were used to calculate

magnetic temperatures (referred to as T^*_{2776}) on the temperature scale defined in Table XXIII. The resulting resistance-temperature data were fit by a power series of the form (for the GE2345, for example)

$$(T^*_{2776})^{-1} = \sum_n A_n(\log_{10}R_{2345})^n \qquad (32)$$

to find the coefficients A_n. Difference tables of $(T^*_{2776}-T_{fit})/T_{fit}$ were generated to allow for systematic deviations from the fits. The fit coefficients and the accompanying difference tables then completely define the new magnetic temperature scale on the GE2345 and GE1751 thermometers in the 0.05-1.0 K region.

X. VERIFICATION OF THE MAGNETIC TEMPERATURE SCALE

In an attempt to gain insight into the quality of the magnetic temperature scale defined in Sec. IX C, two different tests have been employed. The first test compares the magnetic temperature scale with a NBS temperature scale while the second test examines the temperature dependence of the specific heat of high purity copper. Each of these procedures will be described in turn.

NBS has developed a temperature scale below 1 K, referred to as CTS-1 (cryogenic temperature scale-version 1),[12] which is based on NOT and Johnson noise thermometry in the 10-50 mK region and solely on Johnson noise thermometry from 50-500 mK. The stated accuracy of the scale is 0.5 percent for 10-50 mK and 0.2 percent for 50-500 mK. This scale is presently distributed by NBS via SRM 768 fixed point devices[72]--that is, units which contain five superconducting materials ($AuIn_2$, $AuAl_2$, Ir, Be, and W) whose transition temperatures (T_c's) have been measured on CTS-1. In three experiments conducted by M.C. Mayberry and E. W. Hornung, the magnetic temperature scale, as represented by the GE2345 thermometer, has been used to measure the T_c's of SRM 768 unit No. 44 (the T_c's of Be and W were not determined with the GE2345 as they lie below 50 mK, the lowest temperature of the GE2345 calibration). (A preliminary account of this work has been published,[73] and the results will be described in detail in Mayberry's thesis.) To make a proper comparison between the two temperature scales, since the GE2345 scale reflects the extrapolation of the helium vapor pressure scale and the CTS-1 scale is believed to represent the

thermodynamic temperature scale, the T_c's, as measured on the GE2345 scale, must be increased by 0.25 percent (see Sec. IX C). Having made this correction, the results are presented in Table XXIV. The agreement between the two temperature scales, at least at these temperatures, is extremely good--indeed, it is at the level of the stated uncertainty in the NBS CTS-1 scale (~0.2 percent). Further, the NBS scale may be used to gain insight into the reasonableness of the Curie-Weiss constant used in defining the magnetic temperature scale in the following way: A number of magnetic scales may be defined, each scale using a <u>different</u> value of Δ in conjunction with the CMN-GE2776 calibration data from Table XXIII. The NBS scale may then be compared with each of these magnetic scales and a "best" value of Δ determined according to the criterion of minimizing the sum of the squares of the deviations of the three NBS T_c's from the various magnetic scales. The best value of Δ turns out to be 1.02 ± 0.05 mK. Significantly, this result is comfortably within experimental error of Δ = 0.97 ± 0.09 mK, the value determined by the NOT data in Sec. IX C. (Note that using Δ = 0.0, as indicated by Wheatley's experiments,[9] leads to fractional differences of -0.60%, -0.59%, and -0.56% for the $AuIn_2$, $AuAl_2$, and Ir T_c's--results which are significantly poorer than those for $\Delta \sim 1$ mK.) The fact that the NBS temperature scale in the 100-200 mK region independently supports the <u>same</u> value of Δ as that determined by the 17 mK NOT data indicates that Δ was indeed temperature independent in these experiments and thus, the susceptibility of the powdered CMN obeyed a Curie-Weiss law at all

Table XXIV. Comparison of the T_c's of the upper three fixed points on the NBS SRM 768 unit No. 44 as measured on the NBS CTS-1 temperature scale versus the GE2345 temperature scale. The GE2345 results from three runs, their averages and the percentage differences from the NBS results (δ) are reported. Note the GE2345 temperatures have been increased by 0.25 percent over those determined experimentally to compensate for the discrepancy between the helium vapor pressure scale and the absolute temperature scale.

	T_c^{2345}					
Sample	Run 1	Run 2	Run 3	Average	T_c^{NBS}	δ
$AuIn_2$	205.12	205.19	205.13	205.15	205.57	-0.21
$AuAl_2$	162.47	162.45	162.42	162.45	162.57	-0.08
Ir	99.21	99.28	99.21	99.23	98.88	+0.35

temperatures. Consequently, the magnetic temperature scale defined in Sec. IX C is believed to be accurate over the entire 0.017-3.8 K range.

The second test of the quality of the magnetic temperature scale consists of examining the temperature dependence of the specific heat of pure copper. It has long been recognized that the simple temperature dependence of the specific heat of copper makes it an excellent calorimetry standard[74] and provides, at least indirectly, a basis by which various laboratories may intercompare their temperature scales. More importantly, from the point of view of these experiments, the simple temperature dependence of the specific heat observed in the 1-4 K region, where the temperature scale is well known, may be extrapolated to lower temperatures and compared with experimental data to test the accuracy of the temperature scale for $T < 1$ K. Such a test presupposes, of course, that the $C = \gamma T + AT^3$ temperature dependence found for copper in the 1-4 K region is valid for $T < 1$ K.

In Fig. 28, the specific heat of high purity copper (99.9999%), as measured on the GE2345, is reported. The specific heat results have been calculated using two temperature scales--the "old" magnetic scale which is based upon a blind $^3He/^4He$ vapor pressure scale extrapolation with single crystal CMN and the "new" magnetic scale which is described in Sec. IX C. The solid line in the figure represents a two term polynomial fit of the pure copper data in the 1.0-2.5 K region. Several interesting observations may be made concerning these results: (1) The heat capacities, when calculated on the two scales, disagree in the 0.70-0.85 K region and, most conspicuously, for $T < 0.4$ K. The

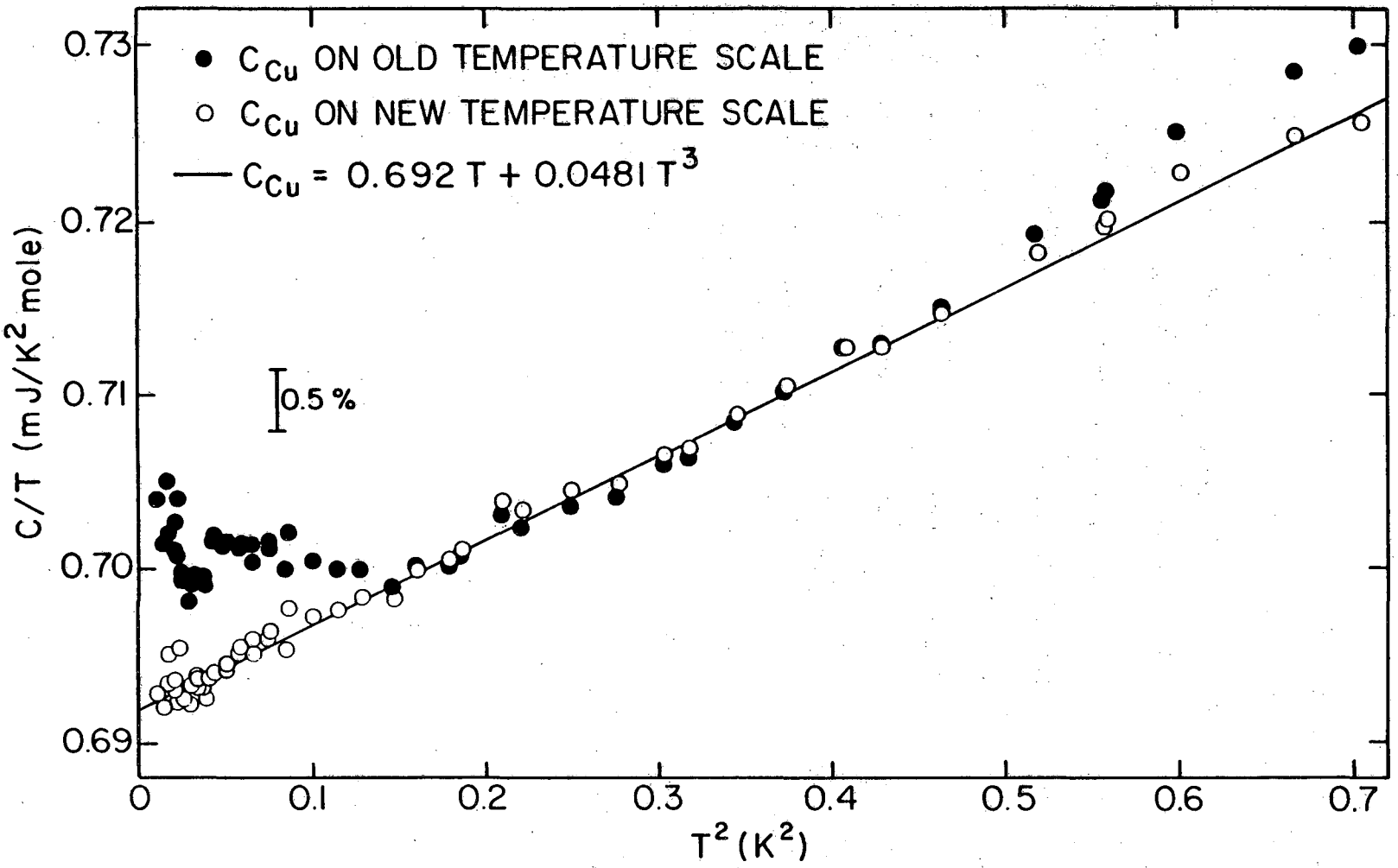

Fig. 28. The specific heat of high purity copper plotted as C/T versus T^2. The data have been calculated using both the old and new GE2345 temperature scales as discussed in the text. The solid line represents the extrapolation of the 1.0-2.5K polynomial fit results of the copper specific heat as calculated on the $^3He/^4He$ vapor pressure scale.

commencing of the divergence at 0.4 K is not surprising since the old GE2345 calibration was carried out in two steps--the first in a pumped ^{3}He apparatus which was refrigerated to ~0.3 K and the second in an adiabatic demagnetization cryostat which extended the calibration to $T < 0.3$ K. Thus, the most significant errors in the old calibration are clearly associated with the second step in the calibration procedure. (2) In the old calibration, there is an obvious discontinuity in the specific heat data at $T = 0.2$ K. This problem is associated with a thermometer current change at this temperature and results from the GE2345 running hot at low temperatures. To compensate for this problem, the new calibration overlaps each temperature at which current changes occur with both of the relevant thermometer currents. The temperature scale is then defined using a family of difference curves, one for each current used with the thermometer. The smoothness of the data as calculated on the new magnetic scale indicates that the heating problem in the GE2345 has been taken into account properly. (3) The agreement between the extrapolation of the 1.0-2.5 K temperature dependence and the measurements for $T < 1$ K is seen to be excellent. This result is an affirmation of the accuracy of the GE2345 temperature scale in the 0.10-0.85 K region.

In conclusion, the above tests provide an excellent verification of the accuracy of the magnetic temperature scale as defined in Sec. IX C. In addition, the test results indicate that this scale was successfully transferred to the GRT. The GRT scale thus provides a convenient basis for the accurate measurement of low-temperature heat capacities.

ACKNOWLEDGMENTS

I would like to thank Professor Norman E. Phillips for the advice, guidance and, in particular, the freedom he offered me during my tenure as a graduate student. I also want to thank Dr. Robert Fisher for many interesting discussions on various topics of low-temperature physics and for providing the CMN used in these experiments. Thanks are also due to Dr. Samuel Bader, Dr. James Boyer, Dr. Gary Brodale, Dr. Erwin Hornung, Mike Mayberry, Dr. Gary Schwartz and John Van Curen for useful discussions and assistance with various experiments.

I would like to thank George Gabor for his guidance in setting up the gain stabilizers for the γ-ray spectrometer and Paul Salz for designing some of the instrumentation used in these experiments. Thanks are also due to Dr. Stephen Rosenblum and Professor Ken Krane for enlightening discussions on the influence of angular correlations on nuclear orientation thermometry.

Finally, I would like to express my sincere appreciaton for the support afforded me by my wife, Marilyn, and by my parents. Their patience and encouragement were essential to the completion of this work.

This work was supported by the Director, Office of Energy Research, Office of Basic Energy Sciences, Materials Sciences Division of the U. S. Department of Energy under Contract No. DE-AC03-76SF00098.

REFERENCES

1. C. D. Amarasekara and P. H. Keesom, Phys. Rev. Lett. 48, 1506 (1982); Phys. Rev. B 26, 2720 (1982); Norman E. Phillips, Phys. Rev. Lett. 48, 1504 (1982); John van Curen, E. W. Hornung, J. C. Lasjaunias, and Norman E. Phillips, Phys. Rev. Lett., to be published.

2. A. C. Anderson, W. Reese, and J. C. Wheatley, Phys. Rev. 130, 495 (1963); W. R. Abel, A. C. Anderson, W. C. Black, and J. C. Wheatley, Phys. Rev. 147, 111 (1966); A. C. Mota, R. P. Platzeck, R. Rapp, and J. C. Wheatley, Phys. Rev. 177, 266 (1969); T. A. Alvesalo, T. Haavasoja, M. T. Manninen, and A. T. Soinne, Phys. Rev. Lett. 44, 1076 (1980); D. S. Greywall and P. A. Busch, Phys. Rev. Lett. 49, 146 (1982).

3. R. P. Hudson, Principles and Application of Magnetic Cooling (North-Holland, Amsterdam, 1972), p. 97.

4. R. P. Hudson, H. Marshak, R. J. Soulen, and D. B. Utton, J. Low Temp. Phys. 20, 1 (1975).

5. D. S. Betts, Refrigeration and Thermometry Below One Kelvin (Sussex University Press, London, 1976), p. 193.

6. G. J. Butterworth, C. B. P. Finn, and K. Kiymac, J. Low Temp. Phys. 15, 537 (1974).

7. J. E. Graebner, Rev. Sci. Instrum. 46, 571 (1975).

8. R. A. Fisher, E. W. Hornung, G. E. Brodale, and W. F. Giauque, J. Chem. Phys. 58, 5584 (1973).

9. J. C. Wheatley, Ann. Acad. Sci. Fennicae A. VI. 210, 15 (1966).

10. R. A. Webb, R. P. Giffard, and J. C. Wheatley, J. Low Temp. Phys. 13, 383 (1973).

11. R. J. Soulen, Jr. (private communication).

12. R. J. Soulen, Jr. and H. Marshak, Cryogenics 22, 408 (1980).

13. D. S. Greywall and P. A. Busch, J. Low Temp. Phys. 46, 451 (1982).

14. R. A. Erickson, L. D. Roberts, and J. W. T. Dabbs, Rev. Sci. Instrum. 25, 1178 (1954).

15. A. H. Silver and J. E. Zimmerman, Phys. Rev. 157, 317 (1967); J. E. Zimmerman, P. Thiene, and J. T. Harding, J. Appl. Phys. 41, 1572 (1970).

16. J. Bardeen, L. N. Cooper, and J. R. Schrieffer, Phys. Rev. 108, 1175 (1957).

17. B. D. Josephson, Phys. Lett. 1, 251 (1962).

18. R. P. Giffard, R. A. Webb, and J. C. Wheatley, J. Low Temp. Phys. 6, 533 (1972).

19. O. V. Lounasmaa, Experimental Principles and Methods Below 1 K (Academic Press, London, 1974), p. 176.

20. Cominco American, East 15128 Euclid, Spokane, Washington 99216.

21. Supercon, Inc., 9 Erie Drive, Natick, Massachusetts 01760.

22. R. A. Fisher, Rev. Sci. Instrum. 43, 386 (1972).

23. Dow Corning Corporation, Midland, Michigan.

24. Teledyne Wah Chang Albany, P. O. Box 460, Albany, Oregon 97321.

25. S. H. E. Corporation, 4174 Sorrento Valley Boulevard, San Diego, California 92121.

26. Electro Scientific Industries, 13900 N. W. Science Park Drive, Portland, Oregon 97229.

27. Princeton Applied Research Corporation, P. O. Box 2565, Princeton, New Jersey 08540.

28. Hewlett-Packard, 3003 Scott Boulevard, Santa Clara, California 95050.

29. Furane Plastics, Inc., 4516 Brazil Street, Los Angeles, California 90039.

30. Emerson and Cuming, Inc., Canton, Massachusetts 02021.

31. R. J. Commander and C. B. P. Finn, J. Phys. E 3, 78 (1970).

32. B. L. Berman, R. P. Madding, and J. R. Dillinger, Rev. Sci. Instrum. 39, 1214 (1968).

33. W. R. Abel, A. C. Anderson, and J. C. Wheatley, Rev. Sci. Instrum. 35, 444 (1964).

34. R. J. Blin-Stoyle and M. A. Grace, in Handbuch der Physik, edited by S. Flugge (Springer Verlar, Berlin, 1957), Vol. 42, pp. 555-610; S. R. deGroot, H. A. Tolhoek, and W. J. Huiskamp, in Alpha-, Beta-, and Gamma-Ray Spectroscopy, edited by Kai Siegbahn (North-Holland, Amsterdam, 1965), Vol. 2, pp. 1199-1261.

35. M. E. Rose, Phys. Rev. 91, 610 (1953).

36. M. J. L. Yates, in Perturbed Angular Correlations, edited by E. Karlsson, E. Matthias, and K. Kiegbahn (North-Holland, Amsterdam, 1964), pp. 453-466.

37. P. M. Berglund, H. K. Collan, G. J. Ehnholm, R. G. Gylling, and O. V. Lounasmaa, J. Low Temp. Phys. 6, 357 (1972).

38. W. D. Brewer, D. A. Shirley, and J. E. Templeton, Phys. Lett. 27A, 81 (1968).

39. H. Marshak and R. J. Soulen, Jr., in Proceedings of the 13th International Conference on Low Temperature Physics, edited by K. D. Timmerhaus, W. J. O'Sullivan, and E. F. Hammel (Plenum Press, New York, 1974), Vol. 4, p. 498.

40. S. Chikazumi, in Physics of Magnetism (Wiley, New York, 1964), p. 228.

41. D. J. Craik and R. S. Tebble, in Ferromagnetism and Ferromagnetic Domains, Selected Topics in Solid State Physics, edited by E. P. Wohlfarth (North-Holland, Amsterdam, 1965), Vol. 4, p. 116.

42. P. W. Nicholson, Nuclear Electronics (Wiley, New York, 1974), p. 103.

43. R. L. Caldwell and S. E. Turner, Nucleonics 12, 47 (1954); H. de Waard, Nucleonics 13, 36 (1955); R. A. Dudley and R. Scarpatetti, Nucl. Instrum. Methods 25, 297 (1964).

44. R. L. Heath, U.S. AEC Report IDO-16880-1, 1964.

45. V. I. Goldanskii, A. V. Kutsenko, and M. I. Podgoretskii, Counting Statistics of Nuclear Particles (Hindustan Publishing Corporation (India), Delhi, 1962), p. 22.

46. CryoCal, Inc., 2457 University Avenue, St. Paul, Minnesota 55114.

47. C. A. Swenson, Critical Reviews in Solid State Physics 1, 99 (1970); L. G. Rubin, Cryogenics 10, 14 (1970).

48. Leeds and Northrup, North Wales, Pennsylvania 19454.

49. Keithley Instruments, Inc., 28775 Aurora Road, Cleveland, Ohio 44139.

50. M. Suomi, A. C. Anderson, and B. Holmstrom, Physica 38, 67 (1968).

51. D. O. Edwards, R. E. Sarwinski, P. Seligmann, and J. T. Tough, Cryogenics 8, 392 (1968).

52. R. H. March and O. G. Symko, Proc. Grenoble Conf. Int. Institute of Refrigeration, Annexe 2, 57 (1965).

53. W. Reese and W. A. Steyert, Jr., Rev. Sci. Instrum. 33, 43 (1962).

54. A. Dupre, A. Van Itterbeek, and L. Michiels, Phys. Lett. 8, 99 (1964).

55. S. S. Markowitz (private communication).

56. R. L. Heath, Nucl. Instrum. Methods 43, 209 (1966).

57. R. G. Helmer, R. L. Heath, Marie Putnam, and D. H. Gipson, U.S. AEC Report IDO-17016, 1964.

58. R. H. Moore and R. K. Zeigler, Los Alamos Report 2367, 1959.

59. G. Chandra and T. S. Radhakrishnan, in Proceedings of the 14th International Conference on Low Temperature Physics, edited by M. Krusius and M. Vuorio (North-Holland, Amsterdam, 1975), Vol. 4, pp. 41-43.

60. V. I. Goldanskii, A. V. Kutsenko, and M. I. Podgoretskii, Counting Statistics of Nuclear Particles (Hindustan Publishing Corporation (India), Delhi, 1962), p. 306.

61. R. M. Steffen and K. Alder, in The Electromagnetic Interaction in Nuclear Spectroscopy, edited by W. D. Hamilton (North-Holland, Amsterdam, 1975), Chap. 12, pp. 505-582; K. S. Krane, R. M. Steffen, and R. M. Wheeler, Nucl. Data Tables 11, 351 (1973).

62. E. L. Brady and M. Deutsch, Phys. Rev. 78, 558 (1950).

63. H. Frauenfelder and R. M. Steffen, in Alpha-, Beta-, and Gamma-Ray Spectroscopy, edited by Kai Siegbahn (North-Holland, Amsterdam, 1965), Chap. 19, pp. 997-1198.

64. J. B. Garg and N. H. Gale, Nuovo Cimento 16, 1014 (1960); P. S. Jastrum, R. C. Sapp, and J. G. Daunt, Phys. Rev. 101, 1381 (1956).

65. H. Appel, H. Behrens, K. Burk, H.-W. Muller, L. Szybisz, and R. Wischhusen, Z. Phys. 268, 347 (1974).

66. K. S. Krane (private communication).

67. E. A. Wolicki, R. Jastrow, and F. Brooks, NRL Report 4833.

68. J. A. M. Cox and H. A. Tolhoek, Physica 19, 1178 (1953).

69. K. Grohmann and D. Hechtfischer, Cryogenics 17, 579 (1977).

70. J. A. Konter, R. Hunik, and W. J. Huiskamp, Cryogenics 17, 145 (1977); O. V. Lounasmaa, in Proceedings of the 1977 Hakone Symposium on Ultralow Temperatures, edited by T. Sugawara (The Japanese Physical Society, Tokyo, 1978), pp. 246-262; E. Varoquaux, J. Phys. (Paris) 39, C6-1605 (1978).

71. Bureau International des Poids et Mesures, Metrologia 15, 65 (1979); M. Durieux, D. N. Astrov, W. R. G. Kemp, and C. A. Swenson, Metrologia 15, 57 (1979).

72. R. J. Soulen, Jr. and R. B. Dove, NBS Special Publication 260-62 (1979) [U.S. GPO, Washington, DC 20402].

73. W. E. Fogle, E. W. Hornung, M. C. Mayberry, and N. E. Phillips, Physics 109 & 110B, 2129 (1982).

74. D. W. Osborne, H. E. Flotow, and F. Schreiner, Rev. Sci. Instrum. 38, 159 (1967); D. L. Martin, to be published.